Forschungszentrum Jülich
in der Helmholtz-Gemeinschaft

50 Jahre / Zukunft

Measurement of Peroxy Radicals using Laser-Induced Fluorescence Technique

Hendrik Fuchs

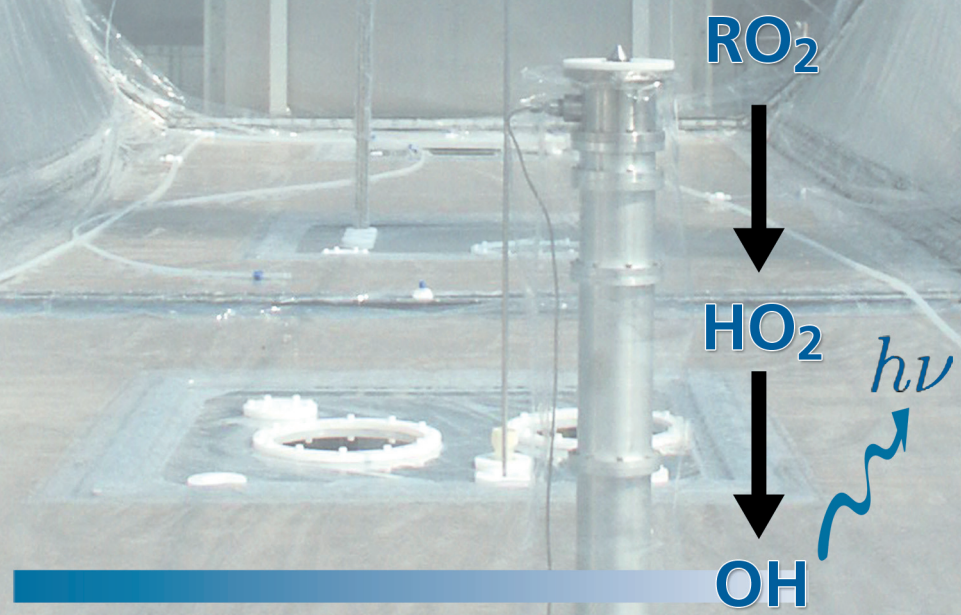

Umwelt
Environment

Schriften des Forschungszentrums Jülich
Reihe Umwelt/Environment Band/Volume 72

Forschungszentrum Jülich GmbH
Institut für Chemie und Dynamik der Geosphäre II: Troposphäre

Measurement of Peroxy Radicals using Laser-Induced Fluorescence Technique

Hendrik Fuchs

Schriften des Forschungszentrums Jülich
Reihe Umwelt/Environment Band/Volume 72

ISSN 1433-5530 ISBN 3-89336-467-6

Bibliographic information published by the Deutsche Nationalbibliothek.
The Deutsche Nationalbibliothek lists this publication in the Deutsche Nationalbibliografie; detailed bibliographic data are available in the Internet at http://dnb.d-nb.de.

Publisher and Distributor: Forschungszentrum Jülich GmbH
Zentralbibliothek, Verlag
52425 Jülich
Phone +49 (0)2461 61-5368 · Fax +49 (0)2461 61-6103
e-mail: zb-publikation@fz-juelich.de
Internet: http://www.fz-juelich.de/zb

Cover Design: Grafische Medien, Forschungszentrum Jülich GmbH

Printer: Grafische Medien, Forschungszentrum Jülich GmbH

Schriften des Forschungszentrums Jülich
Reihe Umwelt/Environment Band/Volume 72

D 11 (Diss., Berlin, Humboldt-Univ., 2006)

ISSN 1433-5530
ISBN-10: 3-89336-467-6
ISBN-13: 978-3-89336-467-1

Abstract

Peroxy radicals are produced during the photochemical degradation of volatile organic compounds (VOCs) in the atmosphere. They are part of the catalytic radical cycle initiated by hydroxyl radicals (OH) in which hydrocarbons are oxidized leading to the removal of pollutants. The reaction of peroxy radicals with nitrogen monoxide (NO) in conjunction with the photochemical cycling of nitrogen dioxide (NO_2) and nitrogen monoxide leads to the formation of ozone (O_3). This process is the major photochemical source for ozone in the troposphere concerning the local as well as the global ozone budget.

A new method for the measurement of atmospheric hydroperoxy and organic peroxy radical concentrations (HO_2 and RO_2) was developed using the successive conversion of RO_2 and HO_2 to OH radicals which are detected by laser-induced fluorescence (LIF). The detection system consists of two differentially pumped chambers. Ambient air is sampled through a nozzle into the first chamber in which the pressure is reduced from atmospheric pressure to $25\,hPa$. An excess of NO and CO is added downstream of the inlet, leading to the conversion of RO_2 to HO_2 radicals. The pressure is further reduced in the second chamber to $3.5\,hPa$. HO_2 is transformed to OH by the reaction with a further excess of NO. The detection of OH radicals is achieved by time delayed gated photon counting after resonant excitation of the OH-fluorescence at $308\,nm$ ($A^2\Sigma^+$ - $X^2\Pi$). The sensitivity of the system is calibrated using a radical source in which OH and HO_2 radicals are produced by water photolysis. In order to calibrate the RO_2 sensitivity, a hydrocarbon is mixed to the calibration gas. OH reacts quantitatively with the hydrocarbon resulting in the formation of RO_2 radicals. The typical detection limit of the LIF system for peroxy radicals is $2{\cdot}10^6\,cm^{-3}$ to $7{\cdot}10^6\,cm^{-3}$ ($0.1\,pptv$ to $0.3\,pptv$) for an integration time of $30\,s$ and for a signal-to-noise-ratio of two. The estimated accuracy is 10 % which is mainly determined by the uncertainty of the calibration. Unlike in peroxy radical amplifier (PERCA) instruments which are used for measuring HO_2+RO_2-radical concentrations, only a weak dependence of the sensitivity on the water vapor content in the sampled air is found which can be explained by humidity dependent quenching of the OH fluorescence.

The instrument was characterized in laboratory measurements. The results agree with analytic and numerical calculations investigating the reaction kinetics of the RO_2 conversion process.

Measurements of peroxy radicals were validated by simultaneous measurements of the new LIF instrument and an established measurement technique (Matrix Isolation and Electron Spin Resonance, MIESR) in experiments at the atmosphere simulation chamber SAPHIR. The SAPHIR chamber allows to investigate chemical processes under controlled atmospheric conditions. First ambient air measurements of peroxy radicals were performed during the international field campaign HOxCOMP in July 2005 showing reasonable diurnal profiles.

Zusammenfassung

Peroxyradikale entstehen in der Atmosphäre beim fotochemischen Abbau flüchtiger, organischer Verbindungen (volatile organic compounds, VOCs). Sie sind Teil eines von OH Radikalen initiierten, katalytischen Kreisprozesses, in dem Kohlenwasserstoffverbindungen oxidiert werden. Dieser begründet die Selbstreinigung der Atmosphäre. Die Reaktion von Peroxyradikalen mit Stickstoffmonoxid (NO) in Verbindung mit dem fotochemischen Kreisprozess zwischen Stickstoffdioxid (NO_2) and -monoxid führt zur Bildung von Ozon (O_3). Dieser Prozess stellt die wichtigste fotochemische Ozonquelle in der Troposphäre dar. Dies gilt sowohl für die lokale als auch für globale Ozonverteilung.

Eine neue Methode zur Konzentrationsmessung von Hydroperoxyradikal und organischen Peroxyradikalen (HO_2 und RO_2) wurde entwickelt. Sie besteht aus der zweistufigen Umwandlung von RO_2 und HO_2 zu OH Radikalen, die mit Hilfe laser-induzierter Fluoreszenz (LIF) nachgewiesen werden. Das Nachweissystem verwendet zwei differentiell gepumpte Kammern. Außenluft wird durch eine Düse in die erste Kammer gesogen, in der der Druck auf 25 hPa erniedrigt ist. Ein Überschuss NO und CO, der hinter der Düse in die Kammer gegeben wird, sorgt für die Umwandlung von RO_2 zu HO_2. Die umgewandelten Radikale werden in eine zweite Kammer überführt, in welcher der Druck auf 3.5 hPa reduziert ist. In dieser werden die HO_2 Radikale in OH umgewandelt, indem sie mit einem weiteren Überschuss NO reagieren. OH-Fluoreszenz, die durch resonante Laseranregung bei 308 nm erzeugt wird ($A^2\Sigma^+$ - $X^2\Pi$), wird durch zeitverzögerte Einzelphotonenzählung detektiert. Die Empfindlichkeit des Systems wird mit Hilfe einer Radikalquelle kalibriert, in der OH und HO_2 Radikale durch Wasserphotolyse erzeugt werden. Um die RO_2 Empfindlichkeit zu kalibrieren, wird ein Kohlenwasserstoff zu dem Kalibrationsgas gemischt. OH reagiert vollständig mit dem Kohlenwasserstoff, so dass RO_2 Radikale entstehen. Das typische Detektionslimit des Messsystems für Peroxyradikale liegt bei $2{\cdot}10^6\,cm^{-3}$ bis $7{\cdot}10^6\,cm^{-3}$ (0.1 $pptv$ bis 0.3 $pptv$) bei einer Integrationszeit von 30 s und einem Signal-zu-Rausch Verhältnis von zwei. Die Absolutgenauigkeit beträgt etwa 10 %, die im Wesentlichen durch die Unsicherheit der Kalibration bestimmt ist. Im Gegensatz zu chemischen Verstärkern (PERCA), die auch in der Lage sind, HO_2+RO_2-Konzentrationen zu messen, ist nur eine leichte Abhängigkeit der Empfindlichkeit vom Wassergehalt der Luft zu beobachten. Diese kann vollständig durch Löschen der OH-Fluoreszenz erklärt werden.

Das Instrument wurde in Labormessungen charakterisiert. Die Ergebnisse konnten mit analytischen und numerischen Modellrechnungen des chemischen Konversionprozesses von RO_2 Radikalen bestätigt werden.

Die Messungen von Peroxyradikalen wurden durch Experimente an der Atmosphärensimulationskammer SAPHIR validiert, bei denen gleichzeitig auch Messungen eines Referenzinstruments stattfanden (Matrix Isolation and Electron Spin Resonance, MIESR). Die SAPHIR Kammer ermöglicht die Untersuchung chemischer Prozesse unter kontrollierten, atmosphärischen Bedingungen. Erste Außenluftmessungen von Peroxyradikalen wurden während der internationalen Messkampagne HOxCOMP im Juli 2005 durchgeführt. Dabei wurden plausible Tagesgänge gemessen.

Contents

1 Introduction

The lower part of the Earth's atmosphere where we live and in that we breathe is called the troposphere. Its depth is about $9\,km$ to $15\,km$ and it is well mixed. Chemical compounds are released permanently by biogenic sources and anthropogenic activities (*Atkinson* (2000); *Atkinson and Arey* (2003a,b) and ref. therein). The worldwide interest to investigate atmospheric chemistry has been increased during the last decades. Environmental pollution by emissions affects the quality of life because it contributes to smog conditions, acid rain, the stratospheric ozone depletion and the global warming. A detailed understanding of the chemistry of pollutants should help to develop optimum strategies to deal with these worldwide challenges.

Our atmosphere has the ability to remove most pollutants by means of oxidation processes initiated by OH radicals which are highly reactive. They play a key role for the self-cleaning capacity of the atmosphere (*Ehhalt*, 1999). Enormous amounts of volatile organic compounds (VOCs) are emitted permanently into the troposphere. The major part of emissions originates from biogenic sources (about 1150 million tons per year, *Guenther et al.* (1995, 2000)). Furthermore, about 60 million to 140 million tons per year (*Guenther et al.*, 1995) of organic compounds are emitted by anthropogenic activities, such as combustion (vehicle and fossil-fueled power plant emissions), fuel storage and transport, solvent usage, emissions from industrial operations, landfills, and hazardous waste facilities (*Saywer et al.*, 2000; *Placet et al.*, 2000).

OH radicals are mainly produced by the photolysis of ozone. The lifetime of most pollutants in the troposphere is determined by their reaction with OH. Although atmospheric concentrations of highly reactive OH are usually small, they evolve an outstanding role in chemical mechanisms in the atmosphere because a catalytic radical reaction cycle is initiated which includes the production of organic peroxy (RO_2) and hydroperoxy radicals (HO_2). HO_2 and RO_2 radicals serve as a reservoir for OH which is formed back by a reaction sequence of RO_2 and HO_2 radicals with nitrogen monoxide (NO). Therefore, peroxy radicals are key species for the oxidation ability of our atmosphere.

This radical cycle is the most prominent oxidation process during which pollutants are transformed to products which can be removed easily by rain or by dry deposition on surfaces. One OH radical can initiate the degradation of several trace gas molecules before it is finally removed from the atmosphere by radical recombination reactions. The most important one is the reaction of OH with NO_2 leading to the formation of nitric acid (HNO_3) which is a major compound of acid rain.

Beside the role in the degradation of pollutants, the radical reaction cycle drives the production of tropospheric ozone. Ozone is not emitted directly in the atmosphere but is produced photochemically by the degradation of pollutants. Tropospheric ozone is

known as a toxic gas which is harmful for animals and plants. In addition, ozone is a greenhouse gas which contributes to the global warming. A high ozone concentration is the major component of the photochemical smog which is the most perceptible impact of anthropogenic emissions on people living in urban and industrial areas. Anthropogenic emissions often consist of a mix of hydrocarbons, carbon monoxide and nitrogen oxides. All together favor the formation of ozone during daytime. This is a self-energizing process because a higher ozone concentration leads to an increasing OH production and therefore a faster oxidation of VOCs. It is notable that the regional distribution of ozone as well as other harmful trace gases is not only determined by regional emissions but also by intercontinental plumes in which ozone is produced during the chemical aging of air masses containing long-lived VOCs.

The investigation of the degradation of different VOCs and of the ozone production in the atmosphere has been the subject of many kinetic and field measurement studies (*Atkinson and Arey*, 2003b). OH as well as peroxy radicals are involved in many of the chemical mechanisms. Therefore, various instruments using different experimental approaches were developed in the last decades to measure atmospheric radical concentrations (*Heard and Pilling*, 2003). Highly sensitive, contact-free, *in-situ* measurements are required because of the high reactivity and small atmospheric concentrations of radicals. Thus, direct methods like fluorescence and absorption spectroscopy for OH and electron spin resonance spectroscopy for peroxy radicals are used. A second class of methods makes use of indirect techniques in which radicals are converted to less reactive species chemically. However, most of the organic peroxy radical measurements are limited with respect to their accuracy or their temporal resolution. Therefore, improvements of organic peroxy radical measurements are desired for field measurements as well as for kinetic studies of atmospheric reaction mechanisms.

The aim of this work was to develop a new instrument for the detection of peroxy radicals which is based on the experiences with the laser-induced fluorescence (LIF) technique used for the measurement of OH and HO_2 radical concentrations. Peroxy radicals cannot be detected by fluorescence directly but they can be converted to OH chemically which is then detected by fluorescence. Therefore, this instrument belongs to the class of indirect methods. It is expected that the high sensitivity of the LIF detection allows to measure peroxy radical concentrations with a high precision and with a high temporal resolution.

This work is subdivided into two main parts. The first part deals with laboratory investigations. A short overview about the motivation for this work is given in Chapter 2 by discussing the role of peroxy radicals in the photochemistry of the troposphere. Existing techniques which are used for peroxy radical detection are described briefly in Chapter 3.

The new instrument is discussed in detail in Chapter 4. The principle of this technique is explained in conjunction with investigations of the reaction kinetic of the chemical conversion of peroxy radicals by means of analytic and numerical calculations. Results of the instrument's characterization in laboratory measurements are shown and compared to results of the theoretical investigations.

The instrument requires a calibration of its detection sensitivity. A calibration pro-

cedure was developed which makes use of an artificial radical source (Chapter 5).

First applications of the instrument are presented in the second main part of this work. Measurements of the new instrument were performed in kinetic studies under controlled conditions at the atmosphere simulation chamber SAPHIR at the Forschungszentrum Jülich (Chapter 6) and in ambient air measurements during the international field measurement campaign HOxComp in July 2005 in Jülich (Chapter 7). Radical measurements of the new instrument were validated by comparing them to measurements of a reference instrument for the SAPHIR experiments. In addition, expected radical concentrations were calculated by using a near-explicit numerical model of the chemical mechanism.

2 Radical photochemistry in the troposphere

Peroxy radicals are products of the oxidation process of pollutants in the atmosphere. One of the simplest oxidation mechanisms leading to the formation of peroxy radicals is the reaction of OH radicals with CO which generates hydroperoxy radicals (HO_2). Reactions of hydrocarbons with OH in which organic peroxy radicals (RO_2) are formed are more complex. OH, HO_2 and RO_2 radicals form a catalytic reaction cycle. This cycle is connected to the photochemically driven equilibrium between NO_2 and NO. Both together are responsible for the production of ozone in the atmosphere.

Reactions of nitrate radicals (NO_3) with hydrocarbons belong to another important class of oxidation reactions leading to the formation of organic peroxy radicals. However, the reactivity of NO_3 towards most pollutants is considerably smaller than that of OH. NO_3 is photolyzed easily whereas OH is produced by photolysis reactions. Therefore, NO_3 reactions typically play a minor role in the daytime chemistry but they can become dominant during nighttime.

Organic peroxy radicals are also formed by the ozonolysis of alkenes. The lifetime of ozone is longer than that of radicals so that the contribution of ozonolysis reactions to the entire oxidation processes is not limited to either daytime or nighttime.

In this work, the main focus of investigated mechanisms is on the photochemically initiated formation of peroxy radicals because of the dominance of the daytime chemistry. Figure 2.1 summarizes the reaction mechanisms discussed in this chapter in which VOCs are oxidized and ozone is produced. A more detailed description of the atmospheric chemistry can be found e.g. in *Finlayson-Pitts and Pitts, Jr.* (2000).

2.1 Oxidation of volatile organic compounds

OH radicals are highly reactive towards most pollutants and other trace gases so that their lifetime in the atmosphere is less than one second. One of the most important reactions is the oxidation of CO to CO_2 whereby HO_2 radicals are formed:

$$\mathrm{OH + CO} \rightarrow \mathrm{H + CO_2} \tag{R2.1}$$

$$\mathrm{H + O_2 + M} \rightarrow \mathrm{HO_2 + M} \tag{R2.2}$$

In regions where NO is in the order of 100 *pptv* (*pptv*: part per trillion per volume) or higher the following reaction of HO_2 with NO establishes a reaction cycle which regenerates OH:

$$\mathrm{HO_2 + NO \rightarrow OH + NO_2} \tag{R2.3}$$

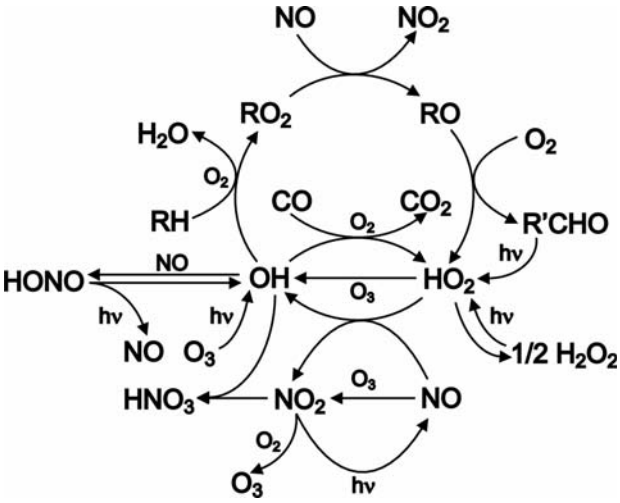

Figure 2.1: Schematic of the radical photochemistry in the troposphere. Some reactions are simplified. Refer to the text for details.

The cycling between OH and HO_2 radicals in polluted environments is fast. Therefore, concentrations are in an equilibrium and OH and HO_2 radical concentrations are often summed up as $[HO_x] = [OH] + [HO_2]$.

The most abundant atmospheric VOC is methane which is a long-lived species with a chemical lifetime in the order of eight years. Therefore, a relatively homogeneous spatial distribution of methane in the whole troposphere can be found. A radical chain reaction is initiated by the attack of OH leading to the formation of methylperoxy radicals (CH_3O_2). Similar to HO_2 radicals they are further processed in the reaction with NO in polluted environments. This leads to the formation of methoxy radicals (CH_3O). Due to the high concentration of oxygen, present in the atmosphere, alkoxy radicals react rapidly to HO_2 and formaldehyde (HCHO):

$$\mathrm{OH + CH_4} \rightarrow \mathrm{CH_3 + H_2O} \quad \text{(R2.4)}$$

$$\mathrm{CH_3 + O_2 + M} \rightarrow \mathrm{CH_3O_2 + M} \quad \text{(R2.5)}$$

$$\mathrm{CH_3O_2 + NO} \rightarrow \mathrm{CH_3O + NO_2} \quad \text{(R2.6)}$$

$$\mathrm{CH_3O + O_2} \rightarrow \mathrm{HCHO + HO_2} \quad \text{(R2.7)}$$

The reaction cycle back to OH is closed by Reaction R2.3.

Other VOCs are oxidized in a similar reaction chain as methane, resulting in the formation of organic peroxy (RO_2) and alkoxy (RO) radicals where R is an organic

group:

$$\mathrm{RH + OH} \rightarrow \mathrm{R + H_2O} \quad \text{(R2.8)}$$
$$\mathrm{R + O_2 + M} \rightarrow \mathrm{RO_2 + M} \quad \text{(R2.9)}$$
$$\mathrm{RO_2 + NO} \rightarrow \mathrm{RO + NO_2} \quad \text{(R2.10)}$$
$$\mathrm{RO + O_2} \rightarrow \mathrm{R'CHO + HO_2} \quad \text{(R2.11)}$$

Important examples of organic radicals are alkyl radicals with R=C_nH_{2n+1}, acetyl radicals with R=CH_3CO and radicals formed in the reaction of isoprene with OH (R=C_5H_7OH in RO_2). Different RO_2 radicals are often not treated separately because of the similarity of their reactions and their reaction rate constants. Therefore, in this work RO_2 and RO denote the sum of different peroxy radicals $RO_2 = \sum_i R_iO_2$ and alkoxy radicals $RO = \sum_i R_iO$.

OH, HO_2, RO and RO_2 radicals are often summarized as $[RO_x]$=[OH] + $[HO_2]$ + [RO] + $[RO_2]$ because they are interconverted in the above mentioned radical cycle. Peroxy radicals are less reactive than OH radicals. Therefore, their concentrations usually exceed the concentration of OH radicals up to two order of magnitudes. The RO radical concentration is small and does not contribute considerably to the entire RO_x concentration because RO radicals react rapidly with atmospheric oxygen.

Sources and sinks of OH radicals affect the entire RO_x concentration because of the interconversion between OH, HO_2 and RO_2 radicals. They are the key sources and sinks in the radical reaction cycle.

The most important global OH radical source is the photolysis of ozone. Photolysis of ozone by radiation at wavelengths shorter than 1180 *nm* leads to oxygen atoms in the ground state $O(^3P)$ which are of no importance for the radical production because they recombine with oxygen to form ozone. However, oxygen atoms in the excited state $O(^1D)$ can also be produced by the photolysis of ozone. This requires higher energetic photons in the UV region. The quantum yield of $O(^1D)$ production becomes dominant over the production of $O(^3P)$ for wavelengths shorter than 330 *nm* (*Matsumi et al.*, 2002):

$$\mathrm{O_3} + h\nu \rightarrow \mathrm{O(^3P) + O_2} \qquad (\lambda < 1180\mathrm{nm}) \quad \text{(R2.12)}$$
$$\mathrm{O_3} + h\nu \rightarrow \mathrm{O(^1D) + O_2} \qquad (\lambda < 330\mathrm{nm}) \quad \text{(R2.13)}$$

$O(^1D)$ is metastable (radiative lifetime about 148 *s*, *Matsumi et al.* (2002)) because the transition between the excited singlet state to the triplet ground state is spin-forbidden. Most $O(^1D)$ atoms are quenched by collisions with other molecules M, mainly nitrogen and oxygen,

$$\mathrm{O(^1D) + M \rightarrow O(^3P) + M.} \quad \text{(R2.14)}$$

This deactivation channel competes with the deactivation by chemical reactions. In the lower troposphere the water vapor concentration is that high (mixing ratio in the order of 1 %) that about 10 % of the produced $O(^1D)$ reacts with H_2O to form two OH radicals:

$$\mathrm{O(^1D) + H_2O \rightarrow 2\ OH} \quad \text{(R2.15)}$$

In addition to the photolysis of ozone, photolysis of nitrous acid (HONO) at wavelengths shorter than 390 nm can contribute considerably to the OH budget (see e.g. *Kleffmann et al.* (2003, 2005)). OH recombines with NO in the reverse reaction:

$$\mathrm{HONO} + h\nu \rightarrow \mathrm{OH} + \mathrm{NO} \qquad (\lambda < 390nm) \tag{R2.16}$$
$$\mathrm{OH} + \mathrm{NO} + \mathrm{M} \rightarrow \mathrm{HONO} + \mathrm{M} \tag{R2.17}$$

HONO is accumulated during nighttime in the presence of high NO_2 levels so that the photolysis of HONO can become the dominant OH source in the early morning hours when short-wavelength UV-B radiation, necessary for the ozone photolysis (Reaction R2.13), cannot penetrate the atmosphere.

Although there is no net production of radicals in the radical reaction chain (Reaction R2.1 to R2.3 and R2.8 to R2.11), further reactions of products can serve as sources of radicals. For example, the photolysis of formaldehyde (HCHO) which is produced in the oxidation process of methane and of other carbonyl compounds are important sources of peroxy radicals. HCHO can either react with OH leading to an interconversion of OH to HO_2 or can be photolyzed. Products of the photolysis can include the subsequent production of HO_2 radicals (*Karl*, 2004):

$$\mathrm{HCHO} + \mathrm{OH} \rightarrow \mathrm{HCO} + \mathrm{H_2O} \tag{R2.18}$$
$$\mathrm{HCHO} + h\nu \rightarrow \mathrm{H_2} + \mathrm{CO} \qquad (\lambda < 360nm) \tag{R2.19}$$
$$\mathrm{HCHO} + h\nu \rightarrow \mathrm{H} + \mathrm{HCO} \qquad (\lambda < 335\mathrm{nm}) \tag{R2.20}$$
$$\mathrm{H} + \mathrm{O_2} + \mathrm{M} \rightarrow \mathrm{HO_2} + \mathrm{M} \tag{R2.21}$$
$$\mathrm{HCO} + \mathrm{O_2} \rightarrow \mathrm{HO_2} + \mathrm{CO} \tag{R2.22}$$

The chain of atmospheric radical reactions which involve OH, HO_2, RO and RO_2 radicals is terminated by radical recombination reactions. The most important sink process in polluted environments is the reaction of OH with NO_2, resulting in the production of nitric acid (HNO_3):

$$\mathrm{OH} + \mathrm{NO_2} + \mathrm{M} \rightarrow \mathrm{HNO_3} + \mathrm{M}. \tag{R2.23}$$

RO_x radical self reactions are the dominant loss processes in less polluted air where NO concentrations are small:

$$\mathrm{HO_2} + \mathrm{HO_2} \rightarrow \mathrm{H_2O_2} + \mathrm{O_2} \tag{R2.24}$$
$$\mathrm{HO_2} + \mathrm{RO_2} \rightarrow \mathrm{ROOH} + \mathrm{O_2} \tag{R2.25}$$
$$\mathrm{RO_2} + \mathrm{RO_2} \rightarrow \text{products} \tag{R2.26}$$

2.2 Ozone formation

Beside their role in the oxidation process of pollutants, peroxy radicals are involved in the production of ozone. Ozone is mainly produced and destroyed in the photochemical

cycle between NO and NO_2:

$$NO_2 + h\nu \rightarrow NO + O(^3P) \qquad (\lambda < 420nm) \qquad \text{(R2.27)}$$

$$O_2 + O(^3P) + M \rightarrow O_3 + M \qquad \text{(R2.28)}$$

$$NO + O_3 \rightarrow NO_2 + O_2 \qquad \text{(R2.29)}$$

The NO and NO_2 concentrations are usually in a quasi-stationary equilibrium because of the fast cycling. This is called the photo stationary state (PSS). Concentrations are often summed up as $[NO_x]$=[NO]+$[NO_2]$.

In addition to the photochemical cycling in Reaction R2.27 to R2.29, the ratio of NO and NO_2 is influenced by the consumption of NO in the reaction with peroxy radicals (Reaction R2.10, R2.3). Although the effect on the resulting NO and NO_2 concentrations is small during daytime, these reactions have a large effect on the ozone concentration. During the cycling between NO and NO_2 in Reaction R2.27 to R2.29 the ozone concentration does not change ("null cycle"). Ozone formed after the photolysis of NO_2 (Reaction R2.27, R2.28) is destroyed in the reverse reaction with NO (Reaction R2.29). However, if NO_2 is produced in the reaction between NO and peroxy radicals, ozone is not consumed, leading to a net ozone production in the photolysis of NO_2.

Whereas ozone is produced in radical reactions in polluted environments, ozone is destroyed by radicals in very clean air masses. If the NO concentration is low and the ozone concentration is sufficiently high, the reaction of HO_2 with ozone becomes dominant over the reaction with NO leading to the destruction of ozone:

$$HO_2 + O_3 \rightarrow OH + 2O_2 \qquad \text{(R2.30)}$$

The radical mechanism of ozone production is the major ozone source in the polluted troposphere. It is worthwhile to note that anthropogenic emissions include often simultaneous emissions of NO, CO and VOCs. All together favor ozone production because organic peroxy radicals are formed in the reaction of VOCs with OH radicals. Net ozone production follows in conjunction with the high NO concentration. This is a self-energizing process because a higher ozone concentration leads to an increasing OH concentration and therefore a faster oxidation of VOCs.

3 Techniques for peroxy radical measurements

Measurements of radicals are technically difficult because of their high reactivity towards surfaces and trace gases. Highly sensitive detection systems are required to measure the small concentrations of peroxy radicals which are typically in the order of $10^8\,cm^{-3}$ during the day.

There are three direct measurement methods for peroxy radicals available. Matrix Isolation Electron Spin Resonance Spectroscopy (MIESR) is an established method for field measurements. Two other direct methods are Proton Transfer Reaction Mass Spectrometry (PTR-MS) and Cavity Ringdown Spectroscopy (CRDS) which are new techniques and have not been used in field measurements so far. In contrast to OH radicals, no direct optical method exists for field measurements of peroxy radicals in the troposphere because they do not show a distinctive UV-absorption spectrum like OH radicals. Moreover, conventional, infrared (IR) absorption spectroscopy is generally not sensitive enough.

Two other methods, namely laser-induced fluorescence (LIF) and chemical amplification, are established for field measurements. They are indirect methods and a technically difficult calibration is required which limits the accuracy of the measurements. The LIF method is based on the conversion of HO_2 to OH radicals which are measured by laser-induced fluorescence. In chemical amplifier systems the sum of peroxy radical concentration (RO_x) is converted to a less reactive species with a product yield greater than one. Therefore, a less sensitive detection system can be used for the measurement.

Differences between these techniques exist with respect to their ability to discrimination between different peroxy radicals. The typical specification of instruments available for field measurements of peroxy radicals are summarized in Table 3.1.

3.1 Devices for laboratory studies

3.1.1 Proton Transfer Reaction Mass Spectrometry

Proton Transfer Reaction Mass Spectrometry (PTR-MS) is widely used for quantification of organic compounds (*Lindinger et al.* (1998) and ref. therein). The measurement principle of PTR-MS combines chemical ionization with mass spectrometric detection. Therefore, PTR-MS can be regarded as a special case of Chemical Ionization Mass Spectrometry (CIMS) methods in which chemical ionization is accomplished by using

Table 3.1: Comparison of instruments which perform ambient air measurements of HO_2 and RO_2 radicals.

Instrument		Time Res. $[s]$	Det. Limit $[10^6 cm^{-3}]$	2σ Accuracy [%]	Chain Length	
LIF (Tokyo)	HO_2	60	4	24	-	*Kanaya et al.* (2001)
LIF (Leeds)	HO_2	150	0.5	56	-	*Creasey et al.* (2003)
LIF (Penn State)	HO_2	10	2.5	32	-	*Faloona et al.* (2004)
LIF (Jülich)	HO_2	10	10	20	-	*Holland et al.* (2003)
ROxMas (Heidelberg)	HO_2, RO_2	120	13	30	10-15	*Hanke et al.* (2002)
PerCIMS (Boulder)	HO_2, RO_2	15	10	41, 35	10	*Edwards et al.* (2003)
LIF PERCA (Tokyo)	RO_x	60	75	20	190	*Sadanaga et al.* (2004b)
dual-channel PERCA (Leicester)	RO_x	60	25	42	200-250	*Green et al.* (2006)
PERCA (Bremen) [a]	RO_x	60	100	48	140-180	*Andrés Hermandéz et al.* (2001)
MIESR (Jülich)	HO_2, RO_2	1800	50	5	-	*Mihelcic et al.* (2003)
LIF (Jülich)	HO_2, RO_2	60	2, 7	20	1-2	this work

[a] The PERCA instrument of the group in Bremen should be seen as example for standard PERCA instruments.
$RO_x = RO_2 + RO + HO_2 + OH$
$RO_2 = \sum_i R_iO_2$
$RO = \sum_i R_iO$

H_3O^+ ions to transfer a proton to the analyst. One major advantage of this method is the ability to detect specific organic peroxy radicals.

With respect to peroxy radicals, PTR-MS has only been used for kinetic laboratory studies so far (*Scholtens et al.*, 1995; *Ranschaert et al.*, 2000; *Elrod et al.*, 2001; *Chow et al.*, 2003). The most critical point is the formation of water clusters with protons. A significant water vapor dependence of the sensitivity is reported by *Hanson et al.* (2004). In the conclusion it is figured out that this may be a problem if the method is applied in ambient air measurement because of the variability of ambient water vapor concentrations. Expected detection limits are not specified in the kinetic studies. However, this method has the potential of becoming an important tool after further development because of its high sensitivity and the capability to measure specific organic peroxy radicals.

3.1.2 Cavity Ringdown Spectroscopy

Another technique, used for detection of specific organic peroxy radicals, is Cavity Ringdown Spectroscopy (*Pushkarsky et al.*, 2000; *Zalyubovsky et al.*, 2001, 2003; *Just et al.*, 2006). Like PTR-MS this technique has only been applied in laboratory kinetics studies so far (*Zalyubovsky et al.*, 2005; *Glover and Miller*, 2005).

Cavity Ringdown Spectroscopy is a specific kind of long path absorption spectroscopy. The transient absorption in a resonator is observed following Lambert-Beer's law. The sensitivity of this technique is higher than that of conventional absorption spectroscopy (*Pushkarsky et al.*, 2000).

Until now, only few studies are reported using Cavity Ringdown Spectroscopy. Absorption spectra of organic peroxy radicals in the infrared region (around $1.3\,\mu m$) are observed (*Pushkarsky et al.*, 2000; *Zalyubovsky et al.*, 2001, 2003; *Glover and Miller*, 2005; *Just et al.*, 2006). IR light is generated by stimulated Raman scattering of dye laser radiation. Most studies only show the principle of measurement or first rudimentary kinetic studies. Although the importance of peroxy radicals with respect to atmospheric chemistry is emphasized in all studies, neither a possible application of Cavity Ringdown Spectroscopy in field measurement nor expected detection limits are discussed. However, it is assumed that an identification of different organic peroxy radicals in a mixture can be achieved because of the specific structures in their absorption spectra (*Pushkarsky et al.*, 2000).

3.2 Matrix Isolation Electron Spin Resonance Spectroscopy (MIESR)

Measurement of atmospheric peroxy radicals with Matrix Isolation and Electron Spin Resonance Spectroscopy was developed by *Mihelcic et al.* (1985, 1990). So far, only one instrument of this kind exists in the world at the Forschungszentrum Jülich. It has the capability to measure the concentrations of HO_2, RO_2, $CH_3C(O)O_2$, NO_3 and NO_2 simultaneously in one sample.

This technique is an offline method. The measurement is accomplished by electron spin resonance (ESR) spectroscopy in the laboratory after cryogenically sampling of ambient air in the field. The samples are taken by expanding air through a nozzle into a chamber with reduced pressure (about $10^{-4}\,hPa$). The radicals are frozen out in a matrix formed by D_2O molecules on a sampling finger which is cooled with liquid nitrogen in order to avoid further chemical interactions between reactive molecules. A sampling time of about 30 minutes is required to collect a sufficient number of radicals in the matrix for the detection. The typical detection limit is about $1 \cdot 10^7\,cm^{-3}$ for peroxy radicals for these conditions.

The samples are analyzed with ESR spectroscopy. Electronic states are degenerated because of the coupling of the spin (electron and nucleus) and the angular momentum of the molecule. They are separated in a strong magnetic field. A specific absorption microwave spectrum is measured. This method is an absolute measurement technique and does not require a calibration. However, spectra of most atmospheric organic peroxy radicals are overlapping because of the similarities in their electronic structure. Therefore, it is not possible to distinguish between them, except for acetyl peroxy radicals. HO_2 and RO_2 spectra can be separated.

Only small data sets with a relatively low time resolution are available. The number of samples is limited because of the necessity to store them cryogenically and because of the relatively long sampling time of $30\,min$. The time for the analysis of each sample takes about one day. However, the main advantage of this method is that no calibration of the instrument is required. This allows to use this technique as a reference method for intercomparison to other instruments like chemical amplifier systems (*Platt et al.*, 2002) or the instrument developed in this work (Chapter 6).

3.3 Chemical amplifier systems

Beside the MIESR instrument, chemical amplifier systems are the only instruments available to detect organic peroxy radical concentrations in field campaigns so far. A higher time resolution (in the order of one minute) than for data of the MIESR instrument can be achieved because of fast online detection systems. Here, radicals are not measured directly but the concentration of a molecule which is produced in a chemical chain reaction. The reaction chain is similar for the two different approaches, Peroxy Radical Chemical Amplifier (PERCA) and Peroxy Radical Chemical Ionization Mass Spectrometry (PerCIMS, ROxMas), that have been developed so far (Table 3.1). An overview of the chemical systems is shown in Figure 3.1 and details are discussed in the following sections. The new instrument described in this work makes also use of the chemical conversion of RO_2 radicals. Nevertheless, it does not belong to the class of chemical amplifiers. It is also denoted in Figure 3.1 because a similar reaction system is used as discussed in detail in Chapter 4.

The sum of HO_2 and RO_2 radical concentrations is measured by chemical amplifier systems since organic peroxy radicals are converted to HO_2 in a chemical reaction sequence at atmospheric conditions (Figure 3.1). Like in the atmosphere, RO_2 radicals

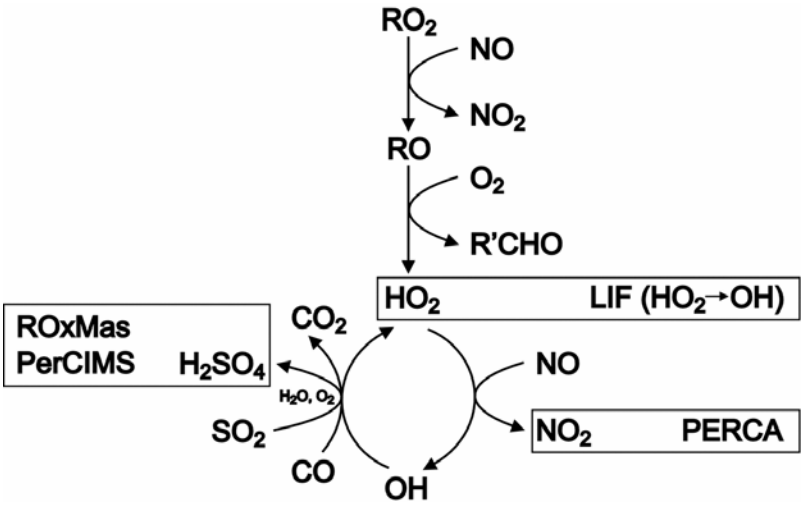

Figure 3.1: Chemical principle of indirect techniques (LIF, PERCA, PerCIMS, ROxMas) for the measurement of peroxy radical concentrations. The detected species is framed together with the detection technique.

react with NO of which an excess is added into a reaction tube. This leads to the formation of RO radicals which react subsequently with atmospheric oxygen forming HO_2 radicals:

$$RO_2 + NO \rightarrow RO + NO_2 \quad \text{(R2.10)}$$
$$RO + O_2 \rightarrow R'CHO + HO_2 \quad \text{(R2.11)}$$

Therefore, the converted RO_2 radical concentration adds to the HO_x concentration which has been sampled from ambient air. Discrimination between different organic peroxy radicals is not possible because of the similar reaction rates of the reaction of RO_2 radicals with NO.

A reaction cycle between HO_2 and OH radicals is initiated in the next step. Once NO is added for the conversion of RO_2 to HO_2 radicals, HO_2 further reacts to form OH. The reverse reaction from OH back to HO_2 is accomplished by the reaction of OH with another added reagent which is either CO or SO_2, depending on the desired products which are detected by the amplifier system. The products of interest (NO_2 or H_2SO_4) accumulate with each completed reaction cycle which can passed through many times. By choosing appropriate chemical conditions, the product concentration is multiplied in the reaction cycle that concentration values are well above the detection limit of the detection systems. The number of turnarounds in the HO_x cycle is equivalent to the amplification factor (or chain length) because one product molecule is formed during one cycling between OH and HO_2. This is limited by chain terminating reactions like wall loss or gas phase loss reactions. The competition between the chain terminating

HONO formation (Reaction R2.17) and the chain driving reactions with NO determines the optimum NO concentration to about 2 *ppmv* to 3 *ppmv*. The exact chain length and the sensitivity of the instrument with respect to the detected species must be known accurately for the determination of radical concentrations. This is accomplished in a calibration process using a radical source.

3.3.1 Peroxy Radical Chemical Amplifier (PERCA)

The first Peroxy Radical Chemical Amplifier (PERCA) instrument was explored by *Cantrell et al.* (1984). Today, PERCA systems are used by various groups for field measurements (*Hastie et al.*, 1991; *Hu and Stedman*, 1994; *Mihele and Hastie*, 1999; *Burkert et al.*, 2001; *Andrés Hermandéz et al.*, 2001; *Green et al.*, 2003, 2006).

The reaction cycle between OH and HO_2 which is initiated by the reaction of HO_2 with NO (Reaction R2.3) is closed by the addition of CO to convert OH to HO_2:

$$\begin{aligned} OH + CO &\rightarrow H + CO_2 && \text{(R2.1)} \\ H + O_2 + M &\rightarrow HO_2 + M && \text{(R2.2)} \\ HO_2 + NO &\rightarrow OH + NO_2 && \text{(R2.3)} \end{aligned}$$

NO_2 is formed in Reaction R2.3 and amplified in the HO_x cycle (Figure 3.1). The NO_2 concentration is usually measured by a chemiluminescence detector (using Luminol). The cycling between OH and HO_2 radicals is fast because of the high CO mixing ratio (10 %) in the reaction tube. This allows an amplification of the NO_2 concentration by a factor of 50 to 150 compared to the initial radical concentration. The reaction time of about 0.7 *s* to 1 *s* is chosen such that nearly all radicals are consumed by loss reactions in the end. The detection limit for RO_x concentrations is in the range of $2.5 \cdot 10^7\, cm^{-3}$ to $10 \cdot 10^7 cm^{-3}$ for PERCA instruments (see Table 3.1 for details).

The signal caused by NO_2 present in ambient air has to be subtracted from the signal caused by the NO_2 concentration produced in the amplification process. This background can be determined by either alternate modulation of the chemical regime in the reactor (*Hastie et al.*, 1991) or by simultaneous measurements as done in the dual channel PERCA instrument (*Green et al.*, 2006).

PERCA instruments measure the sum of RO_2, RO, HO_2 and OH radical concentrations because all of these species become part of the HO_x cycling in which the amplification process takes place. Discrimination between different radical species especially HO_2 and RO_2 is not done. This is a general limitation which may lead to difficulties in the interpretation and modeling of measured data.

The most problematic issue concerning PERCA instruments is the fact that the chain length and therefore the sensitivity of the instrument changes considerably with the relative water vapor content of the sampled air. This was reported firstly by *Mihele and Hastie* (1999) and confirmed by all other groups using PERCA instruments (see e.g. *Reichert et al.* (2003)). The reduction of the sensitivity can be in the order of a factor of 5 if the relative humidity changes about 50 %. An accurate determination of the water dependence is necessary because of the high variability of the relative

water vapor content in ambient air. Though measurements can be corrected, the exact mechanism of the water dependence is still unknown.

Sadanaga et al. (2004b) reports a new instrument of a PERCA system. The same chemical system as in common PERCA instruments is used but the NO_2 concentration is measured by laser-induced fluorescence. Although the sensitivity of this instrument is higher than that of previous PERCA instruments, the principle limitations are the same. The sensitivity depends considerably on the relative water vapor content of the sampled air and only the sum of RO_x radicals is detected.

3.3.2 Peroxy Radical Chemical Ionization Mass Spectrometry (PerCIMS, ROxMas)

A different kind of chemical amplifier system was developed by *Reiner et al.* (1997) and by *Cantrell et al.* (2003a). In contrast to PERCA instruments, a different reaction partner is used for the conversion of OH back to HO_2 radicals. SO_2 is added instead of CO. H_2SO_4 and HO_2 radicals are formed in reactions between atmospheric oxygen, water and the added SO_2 (Figure 3.1):

$$OH + SO_2 + M \rightarrow HSO_3 + M \quad \text{(R3.1)}$$

$$HSO_3 + O_2 \rightarrow SO_3 + HO_2 \quad \text{(R3.2)}$$

$$SO_3 + 2H_2O \rightarrow H_2SO_4 + H_2O \quad \text{(R3.3)}$$

During each cycle one H_2SO_4 molecule is formed. The amplified H_2SO_4 concentration is measured by Chemical Ion Mass Spectrometry (CIMS) which is an established method for indirect OH radical concentration measurements (*Eisele and Tanner*, 1991; *Berresheim et al.*, 2001, 2003). This technique is much more sensitive than the chemiluminescence detector with Luminol used in PERCA systems in order to measure the amplified NO_2 concentration. For this reason, a chain length, respectively an amplification factor, of about 10 is sufficient for peroxy radical measurements. This different approach of PerCIMS and ROxMas has an important advantage over PERCA instruments: The detection sensitivity is independent of the water vapor content of the sampled air as will be discussed in more detail in Section 4.7.8. A detection limit in the range of $10 \cdot 10^6\, cm^{-3}$ to $13 \cdot 10^6\, cm^{-3}$ is reached at a temporal resolution of $10\, s$ to $120\, s$. This is lower than for PERCA instruments because of the higher sensitivity of the detection system.

Discrimination between H_2SO_4 from the amplification process and ambient H_2SO_4 is done in the same way as for the background measurement in PERCA systems. In contrast to PERCA systems, separation between RO_2 and HO_2 radical concentrations can be achieved by chemical modulation (*Hanke et al.*, 2002; *Edwards et al.*, 2003). By periodical variation of the amount of NO or O_2 in the reaction system, the yield of HO_2 from the RO_2 conversion is modulated and allows to distinguish between HO_x collected from ambient air and HO_x produced by RO_2 conversion. Discrimination of different organic peroxy radicals is not possible as discussed above.

3.4 Laser-induced fluorescence

Laser induced fluorescence (LIF) technique has been used for the indirect detection of HO_2 but not for RO_2 so far. HO_2 can be converted chemically to OH which is detected by highly sensitive LIF. This concept was realized firstly by *Hard et al.* (1984), who had also developed the FAGE (fluorescence assay by gas expansion) technique for atmospheric OH radical measurements. Today, the detection of HO_2 is a standard extension of all instruments measuring ambient OH by LIF (*Holland et al.*, 2003; *Faloona et al.*, 2004; *Creasey et al.*, 2003; *Kanaya et al.*, 1999; *Brune et al.*, 1995; *Bloss et al.*, 2003).

HO_2 radicals cannot be detected by laser-induced fluorescence directly. Like in chemical amplifier systems an excess of NO is added to the sampled gas leading to the conversion reaction

$$HO_2 + NO \rightarrow OH + NO_2. \qquad \text{(R2.3)}$$

OH radicals are detected by LIF as described in more detail in the next chapter. Air is expanded into a fluorescence cell at low pressure. Single photon counting is done after resonant excitation of OH ($A\Sigma^+, \nu' = 0$ - $X^2\Pi, \nu" = 0$). The fluorescence wavelength is similar to the excitation wavelength and cannot be separated from the excitation by using a wavelength filter. Therefore, the detection of the fluorescence is delayed to the excitation. Low pressure of $1\,hPa$ to $4\,hPa$ in the measurement cell is required for a sufficiently long fluorescence lifetime which depends strongly on collision fluorescence quenching. In addition, the product yield of HONO formation which limits the conversion efficiency of HO_2 to OH is reduced at low pressure:

$$OH + NO + M \rightarrow HONO + M. \qquad \text{(R2.17)}$$

Both the OH radicals present in the sampled air and the OH which results from the conversion of HO_2 radicals contribute to the fluorescence signal. This means that the sum of ambient OH and HO_2 concentrations is measured. In order to distinguish between OH and HO_2 radical concentrations, the OH concentration is determined simultaneously in a separate fluorescence cell in which HO_2 radicals are not converted to OH.

The HO_x radical measurement channel of the Jülich LIF instrument which can be seen as a starting point of this work was carefully characterized by *Weber* (1998); *Holland et al.* (2003). NO is injected into the gas expansion on the low pressure side (NO mixing ratio of 0.6 %). The reaction time between the addition of NO and the laser excitation of OH is estimated to $240\,\mu s$, resulting in a conversion efficiency of HO_2 to OH of about 70 %. The detection limit is $2 \cdot 10^7\,cm^{-3}$ for ambient HO_2 radical concentrations with a time resolution of $150\,s$.

In Table 3.1 specification of all LIF instruments which perform HO_2 measurements in field campaigns are compared.

So far the LIF-technique has only been applied for the detection of HO_2 radicals. In principle, organic peroxy radicals are also converted to OH by NO added to the sampled gas (Reaction R2.10, R2.11, R2.3, Figure 3.1). However, the time between

the addition of NO and detection of OH in the low pressure LIF-cell is too short for an efficient conversion of organic peroxy radicals to OH radicals. The instrument in this work is based on this general idea which has not been realized until now. It modifies the experimental conditions such that an efficient RO_2 to OH conversion becomes possible, allowing a high sensitivity of RO_2 detection by LIF. Details of this concept are described in the following.

4 RO_2 measurement using LIF-technique

4.1 Measurement principle

The idea to measure organic peroxy radicals using LIF is based on experiences with the measurement of HO_2 radicals using a similar approach. The combination of chemical conversion of HO_2 to OH radicals with following detection of OH by LIF has become an established method (Section 3.4). The possibility to convert RO_2 to OH radicals is known from the photochemical degradation of VOCs in the atmosphere (Chapter 2). However, the implementation as a reliable analytic technique for RO_2 measurements requires further development due to the complexity of the chemical system.

Organic peroxy radicals are converted to OH radicals in a two stage process. In the first step RO_2 is converted to HO_2 from which OH is formed in the second step (Figure 4.1). The two stage process is accomplished in two differentially pumped chambers in which the pressure and the chemical conditions differ significantly (Figure 4.2).

In the first reaction chamber which is kept at a pressure of $25\,hPa$ an excess of nitrogen monoxide is mixed to the flow of the sampled ambient air resulting in a mixing ratio of $0.7\,ppmv$ NO. RO_2 is mainly converted to RO by the reaction with NO at these conditions:

$$RO_2 + NO \rightarrow RO + NO_2 \tag{R2.10}$$

RO radicals react further with oxygen forming HO_2 and oxidized organic compounds (e.g. aldehydes):

$$RO + O_2 \rightarrow R'CHO + HO_2 \tag{R2.11}$$

The conversion of RO_2 to HO_2 by Reaction R2.10 and R2.11 is rate limited by the first reaction (Reaction R2.10) resulting in a chemical RO_2 lifetime of $0.3\,s$ at the given conditions. Thus, an almost complete conversion of RO_2 can be achieved for a residence time of one second in the chamber. However, the overall HO_2 yield can be diminished by several radical loss processes.

Firstly, RO_2 and RO radicals can be lost by competing reactions at the walls or by

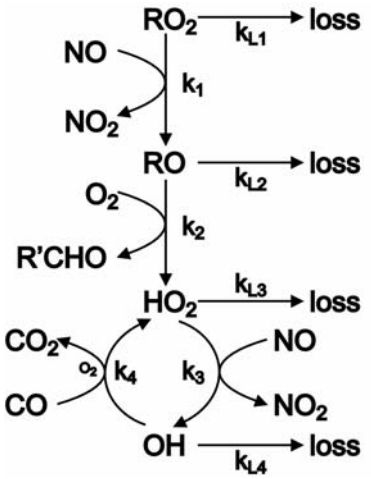

Figure 4.1: Principle reaction scheme of the chemical conversion of organic peroxy radicals in the developed system. k_i denotes the reaction rate constant of conversion reactions i and k_{Li} denotes the sum of reaction rate constants of gas phase and wall loss reactions competing with the conversion reaction i.

gas phase formation of organic nitrates and nitrites, respectively:

$$\mathrm{RO_2 + NO + M} \rightarrow \mathrm{RONO_2 + M} \quad \text{(R4.1)}$$
$$\mathrm{RO + NO + M} \rightarrow \mathrm{RONO + M} \quad \text{(R4.2)}$$
$$\mathrm{RO_2 + wall} \rightarrow \mathrm{products} \quad \text{(R4.3)}$$
$$\mathrm{RO + wall} \rightarrow \mathrm{products.} \quad \text{(R4.4)}$$

In order to suppress the formation of $RONO_2$ and RONO the total pressure is reduced to $25\,hP$ in the first chamber. The reaction rates of nitrate and nitrite formation are decreased with decreasing pressure because the product formation requires collision stabilization by a third molecule M.

Secondly, HO_2 may react at the wall or recombine in a pressure dependent reaction with NO:

$$\mathrm{HO_2 + NO + M} \rightarrow \mathrm{products} \quad \text{(R4.5)}$$
$$\mathrm{HO_2 + wall} \rightarrow \mathrm{products} \quad \text{(R4.6)}$$

Both reactions are relatively slow and cause only small HO_2 losses as will be shown later in Section 4.5.

Thirdly, HO_2 radicals can further react with excess NO and form OH via Reaction R2.3. The resulting OH is a highly reactive compound and can be easily lost by wall

collisions or formation of HONO in the presence of the high NO concentration added into the first chamber:

$$\begin{aligned} OH + NO + M &\rightarrow HONO + M && \text{(R2.17)} \\ OH + \text{wall} &\rightarrow \text{products.} && \text{(R4.7)} \end{aligned}$$

In order to avoid such radical losses by OH, a large amount of CO (mixing ratio 0.17 %) is added to the reaction chamber together with the NO. The high CO concentration converts essentially all OH back to HO_2 which is much less reactive than OH:

$$\begin{aligned} HO_2 + NO &\rightarrow OH + NO_2 && \text{(R2.3)} \\ OH + CO &\rightarrow H + CO_2 && \text{(R2.1)} \\ H + O_2 + M &\rightarrow HO_2 + M. && \text{(R2.2)} \end{aligned}$$

Thus, in the first chamber all RO_2, RO and HO_2 radicals are transformed to HO_2 which is sufficiently long-lived to reach the inlet of the second chamber.

The second chamber which serves for the radical detection is kept at much lower pressure ($3.5\,hPa$) than the conversion reactor. Part of the gas mixture is sampled from the first into the second chamber through another nozzle. More NO is injected into the sampled flow in the detection chamber raising the NO concentration to about $300\,ppmv$. This shifts the equilibrium between HO_2 and OH towards OH. OH is detected further downstream by LIF with high sensitivity.

The two chamber concept has the advantage that the conditions for the radical conversion and detection can be optimized independently in the two chambers. Conditions in the first chamber are chosen in order to minimize chemical losses during the conversion of radicals. In the second chamber conditions are chosen with the aim to maximize the quantum yield of fluorescence photons. This requires mainly pressure reduction to avoid fluorescence quenching. Conversion of HO_2 to OH is fast enough so that chemical loss processes (either gas phase or wall loss) are negligible. This is assisted by the low pressure because termolecular reactions like HONO formation are suppressed.

The described method is equally sensitive to ambient RO_2, HO_2 and OH radicals which are all converted to HO_2 in the conversion reactor. They are detected as OH in the fluorescence chamber. Therefore, the sum of all RO_x radical species is measured by the method.

If the reagent NO is switched off in the first chamber and is replaced by non-reactive nitrogen, organic peroxy radicals are not converted to HO_2. In this case, the method is only sensitive to HO_x radicals which have been sampled from ambient air.

The system can be operated alternately in two different modes to distinguish between RO_2 and HO_x radical concentrations. In the RO_x mode reactive gases NO and CO are added into the first chamber leading to the conversion of RO_2 radicals. In the second mode (HO_x mode) either only CO (HO_x mode I) is added or all reactive gases are replaced by non-reactive nitrogen (HO_x mode II, Table 4.1). The HO_x radical concentration is subtracted from the RO_x radical concentration to calculate the RO_2 radical concentration. HO_x mode I and II only differ in the OH radical sensitivity. If

Table 4.1: Measurement modes of the system.

Mode	Added Reagent Gas
RO_x mode	NO[a] + CO[b]
HO_x mode I	CO[b]
HO_x mode II	N_2

[a] $0.7\,ppmv$
[b] $0.17\,\%$

CO is added, OH radicals are converted to HO_2 in the reactor and are detected as HO_2 in the fluorescence cell. Therefore, their initial concentration is only reduced by smaller HO_2 loss processes. However, effective OH loss processes lead to a significantly smaller OH sensitivity of the system if no CO is added. Reactions between HO_2 and CO are not known. The sensitivity of the system to HO_2 is not expected to be affected by the addition of CO. HO_x mode I is the preferred measurement mode because the chemical system is more robust against interfering trace gases contained in ambient air as will be shown in Section 4.7.10. Therefore, the HO_x mode I is discussed in more detail and is the default HO_x mode in this work if it is not denoted otherwise.

4.2 Experimental setup

The radical detection system uses two differentially pumped chambers (Figure 4.2). The first chamber is an aluminum tube (length: $830\,mm$, inner diameter: $66\,mm$) which is covered internally with a teflon layer. A flow of $7\,slm$ (slm: liter per minute at $1\,atm$, $20\,°C$) of ambient air is expanded through a conically shaped nozzle (Beam Dynamics, nickel, opening angle: 70°, orifice $1\,mm$) from ambient pressure to a reduced pressure of $25\,hPa$. Reactive gases can be added $20\,mm$ downstream of the sampling nozzle through a $6\,mm$ (outer diameter) glass tube which ends in the center of the aluminium tube. The type of reagent gas depends on the measurement mode. NO/CO is added in the RO_x mode whereas CO or pure nitrogen is used in the HO_x mode I/II.

All flows of additional gases are controlled by mass flow controllers (Brooks, 5850 TR) and can be switched on and off by magnetic valves. An additional 3/2 way magnetic valve which is controlled by the operating software switches automatically between the kind of gases needed to change between the HO_x and RO_x mode of the system. Gases are provided by Linde AG and are of highest available purity (NO 2.5, CO 3.0, N_2 5.0). To achieve the desired mixing ratios, gas mixtures of reactive gases in nitrogen are used. Gas flows of $10\,sccm$ ($sccm$: cm^3 per minute at $1\,atm$, $20\,°C$) of a NO-mixture ($500\,ppmv$ NO in N_2) and of $120\,sccm$ of a CO-mixture ($10\,\%$ in N_2) are added in the first chamber for the RO_2 conversion leading to mixing ratios of $0.7\,ppmv$ NO and of $0.17\,\%$ CO, respectively.

The entire gas flow trough the conversion reactor is expected to be laminar (Reynolds number is about $RE \approx 75$). At the end of the reaction chamber half of the air flow

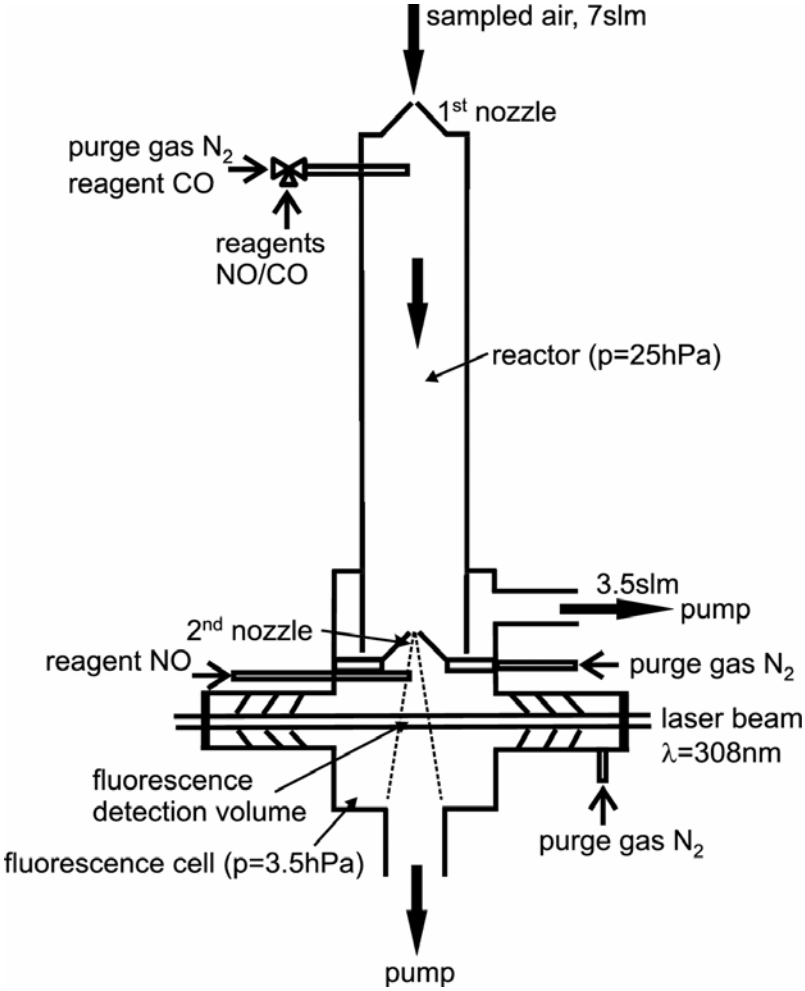

Figure 4.2: Schematic of the experimental setup for the two-stage conversion of RO_2 radicals to OH which is detected by LIF. The conversion of RO_2 to HO_2 is accomplished in the conversion reactor. HO_2 radicals are transformed to OH in the fluorescence cell which is excited resonantly by a $308\,nm$ laser. This system is part of the entire experimental setup as shown in Figure 4.3

($3.5\,slm$) is collected by another conically shaped inlet nozzle (home-made, stainless steel, opening angle 70°, orifice $4\,mm$) from the center flow of the first chamber into the second chamber. This avoids sampling of air which had wall contact and is depleted of radicals.

The sampling point into the second chamber is about $10\,mm$ above the bottom of the first chamber. The excess gas is pumped out laterally at the end of the aluminum tube using a rotary pump (Edwards, XDS35i). The outlet is placed at a similar height as the sampling nozzle of the fluorescence cell but is hidden by the inner teflon tube to avoid that the oncoming flow to the nozzle is influenced by turbulence. The pressure in the chamber is stabilized by a butterfly control valve (MKS, Type 153) in front of the pump. The pressure is monitored by a temperature stabilized, capacitance manometer (MKS, Baratron Type 127).

The second chamber (Figure 4.2) which serves for the radical detection is similar to the fluorescence cell of the LIF system used for OH detection described in detail by *Sedlacek* (2001). It consists of an aluminum block (base length $100\,mm$) with $70\,mm$-diameter bores from all three sides. The excitation laser beam crosses the cell perpendicular to the gas beam direction. Two baffle arms each containing three laser baffles are mounted in order to minimize stray light from the laser entrance and exit windows. To avoid build up of gaseous contaminations they are flushed with dry nitrogen ($200\,sccm$). The third axis is used for the detection of fluorescence photons (Figure 4.3). Opposite of the detector a concave mirror is mounted which nearly doubles the solid angle from which fluorescence photons are collected. An interference filter ($\lambda = 308\,nm$, $10\,nm$ FWHM) in front of the detector ensures that only photons matching the OH fluorescence wavelength range can reach the detector.

A sheath flow of pure nitrogen ($200\,sccm$) which is introduced $10\,mm$ downstream of the inlet nozzle flushes the space between the gas beam and the wall of the cell. This exchanges the background gas volume in order to avoid accumulation of trace gases which may cause artificial OH production (see Section 4.7.9). The inlet for pure NO (Linde AG, purity 2.5) needed to convert HO_2 to OH consists of a $6\,mm$ (outer diameter) glass tube which ends $15\,mm$ downstream of the nozzle in the center gas beam. The end of the tube narrows to an orifice of about $1\,mm$. The NO flow is $1\,sccm$, leading to a mixing ratio of $300\,ppmv$ NO in the fluorescence cell. The NO passes a cartridge filled with Ascerite (Sigma-Aldrich) before entering the chamber to remove impurities from the NO which may cause photolytical interferences (Section 4.7.9). Flows of NO and nitrogen are controlled by mass flow controllers (Brooks, 5850 TR) and can be switched on and off by magnetic valves.

In this work, OH radicals in the ground state ($X^2\Pi, \nu" = 0$) are excited to the state $A^2\Sigma^+, \nu' = 0$, using the transition of the $Q_{11}(3)$ absorption line at $308.155\,nm$ (see Appendix A). The laser pulses must be short ($20\,ns$) compared to the fluorescence lifetime in order to discriminate temporally between laser stray light and fluorescence photons. Due to the small radical concentrations, a high repetition rate of the excitation laser ($8.55\,kHz$) is required to obtain a sufficiently high rate of fluorescence photons. A higher rate of fluorescence photons could also be achieved by a higher photon flux (higher laser power) but this should be avoided to prevent depletion of the

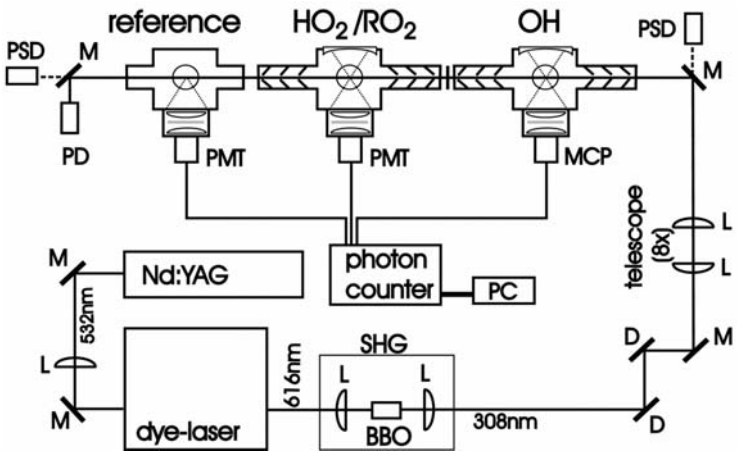

Figure 4.3: Schematic drawing of the "MobiLIF"-system (PSD: position sensitive photodiode, M: mirror, D: dichroitic mirror, L: lens, PD: photodiode, PMT: photomultiplier tube, MCP: micro channel plate photomultiplier, BBO: beta-bariumborate crystal, SHG: second harmonic generation).

Table 4.2: Specifications of the laser system and major differences in the detection systems of the "MobiLIF" and "SaphirLIF" instruments

	MobiLIF	SaphirLIF
Nd:YAG pump laser	Photonics, DS20	
dye laser	Laser Analytic Systems, Intradye	
laser power pump laser	$8\,W$	
max. UV laser power	$40\,mW$	
detector (HO_2/RO_2)	Perkin Elmer, PMT C 1943 P	Hamamatsu, MCP-PMT R2024U-06
detector gating	Photek, GM150-20C	standard switch
gating voltage	$250\,V$	$12\,V$
photon counter	Becker & Hickl, PMS 300	Stanford Research Systems, SR 400

OH population in the ground state leading to saturation of the signal. In addition, artificial production of OH radicals by laser photolysis of e.g. ozone is less probable at lower laser power (Section 4.7.9).

Two different detection systems are used in this work. All measurements described in this chapter and all ambient air measurements (Chapter 7) were done with the "MobiLIF" system (Figure 4.3) which is a mobile instrument for measurements of OH and HO_2 concentrations and can be used either for investigations in the laboratory or for ambient air measurements. The HO_2 detection cell was replaced by the assembly described above (Figure 4.2) for this work to allow RO_x and HO_x measurements simultaneously to the measurement of OH. The second system "SaphirLIF" is installed permanently at the atmosphere simulation chamber SAPHIR and is only used for measurements at SAPHIR (Chapter 6). The RO_x/HO_x converter was removed from the "MobiLIF" instrument and mounted in the "SaphirLIF" instrument for the experiments at SAPHIR. At the same time the laser system of the "MobiLIF" system was moved to the "SaphirLIF" system. Major differences between both systems and specifications of the laser system are summarized in Table 4.2.

The laser system consists of a diode pumped, frequency doubled Nd:YAG laser which provides pulsed laser light at its SHG (second harmonic generation) wavelength ($532\,nm$). The Nd:YAG laser pumps a tunable dye laser. The dye solution is $80\,mg$ of Rhodamine 101 (Radiant Dyes) solved in $1\,l$ ethanol (KMF, Ethanol 510 absolute). The wavelength is selected by angle tuning of a solid etalon inside the laser resonator. The light of the dye laser at wavelengths around $616.23\,nm$ is frequency doubled (SHG) by a beta-bariumborate (BBO) crystal to $308.155\,nm$ (laser band width about $6\,GHz$). The UV laser beam is expanded to a diameter of $8\,mm$ by a telescope (magnification factor about 8) and guided to the measurement cells by several mirrors in the "MobiLIF" system (Figure 4.3). Alternatively, the laser beam is coupled into a fiber (OZ Optics, QMMJ-5,5HP-UVVIS-200/240-3AS-6) in the "SaphirLIF" system and is collimated by a spherical lens (LINOS, $f = 40mm$). The laser power in both systems is measured permanently by a photodiode placed behind the measurement cells. The typical power of the UV laser light is about $20\,mW$ to $35\,mW$. The alignment of the laser beam through the detection cells is monitored by two position sensitive photodiodes (PSD).

Fluorescence photons are detected by gated single photon counting using a photomultiplier tube (PMT) or a micro channel plate photomultiplier (MCP) (Table 4.2). The detector's gain is gated so that photoelectrons are not amplified during the time window when the laser pulse crosses the fluorescence cell. If the detectors were not gated, the strong laser stray light would cause a high current of amplified photoelectrons which could damage the detectors and which could cause strong afterpulsing.

Photons are counted by a gated photon counter after the detector has been switched on again. A discriminator is used to separate photon signals from the electronic noise.

Three measurement cells are present in the system (Figure 4.3). One is used for OH radical detection and a second for HO_x respectively RO_x radical detection. The third cell is a reference cell in which a high concentration of OH radicals is produced by photolysis of water vapor in argon. Radiation at $185\,nm$ is provided by a low pressure discharge mercury lamp. OH radicals in the reference cell are excited by the

Table 4.3: Parameters of the standard experimental setup in this work.

	Parameter	Value
converter	nozzle orifice	$1.0\,mm$
	flow rate	$7\,slm$
	reagent gases	[NO]=$0.7\,ppmv$, [CO]=$0.17\,\%$
	NO flow ($500\,ppmv$ in N_2)	$10\,sccm$
	CO flow ($10\,\%$ in N_2)	$120\,sccm$
	length	$830\,mm$
	diameter	$66\,mm$
	volume	$2.8\,l$
	pressure	$25\,hPa$
	temperature	ambient
	residence time	$0.6\,s$
fluorescence cell	nozzle orifice	$4.0\,mm$
	sample flow	$3.5\,slm$
	reagent gas	[NO]=$300\,ppmv$
	NO flow ($100\,\%$)	$1\,sccm$
	pressure	$3.5\,hPa$
	distance NO addition - laser excitation	$65mm$
	typical laser power	(20 to 35) mW
	laser repetition rate	$8.55\,kHz$
	laser pulse length (FWHM)	$20\,ns$
	diameter of the laser beam	$8\,mm$
	photon counter time delay	$70\,ns$
	photon counter count gate	$500\,ns$

same laser beam as OH radicals in the two other detection cells. The fluorescence is detected by gated photon counting using a PMT (Hamamatsu, R212). The OH radical concentration is such high that the signal to noise ratio of the fluorescence signal is about 50:1. Laser generated background signals of the detector play only a small role and gating of the detector is not required. This allows to shorten the delay between the laser pulse and start of the photon counting (about $10\,ns$). Therefore, a shorter fluorescence lifetime about $16\,ns$ at a higher pressure of $100\,hPa$ is acceptable.

The parameters of the experimental setup are summarized in Table 4.3. These conditions are used for all experiments in this work if not noted elsewise.

4.3 Determination of the OH fluorescence signal

Photon counting of the OH fluorescence in the measurement cells starts about $70\,ns$ after the laser pulse has crossed the fluorescence cells. The delay between laser pulse

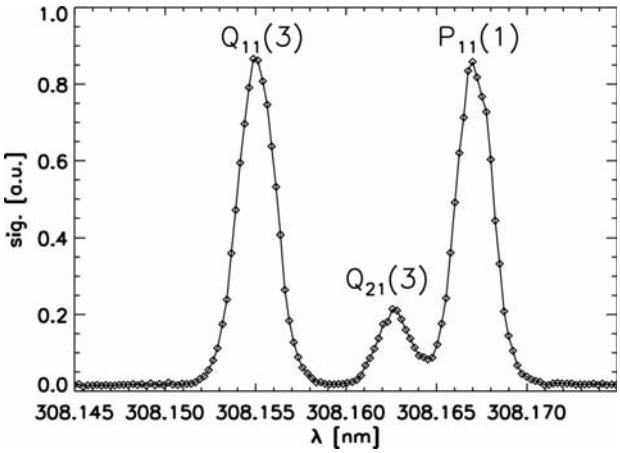

Figure 4.4: OH excitation spectrum, derived from measurements in the reference cell in the "MobiLIF"-instrument. OH radicals are produced by water photolysis at $185\,nm$ (humidified argon at room temperature, pressure $100\,hPa$).

and photon counting is necessary in order to discriminate between laser and fluorescence photons which are of similar wavelengths so that the fluorescence can not be discriminated by a wavelength filter. The rise time of the gating voltage applied to the detector and possible electronic noise associated with the switching require an additional delay between the end of the laser pulse and the beginning of the counter gate. Photon counting lasts $500\,ns$ (about 2.5 times longer than the fluorescence lifetime of OH in the measurement cell).

The detector signal is integrated over successive laser pulses for a certain integration time ($1\,s$ to $5\,s$) and is expressed as photon count rate S'_{det} ($[cts/s]$) which consists of different contributions:

$$S'_{det} = S'_{flu} + S'_{las} + S'_{dark}. \tag{4.1}$$

- S'_{flu}: OH fluorescence
- S'_{las}: laser generated background signal
- S'_{dark}: dark signal of the detector

Sunlight as possible source of photons entering the system through the first inlet nozzle does not play any role in this system because the detector is well shielded against sunlight by the second inlet nozzle.

The contribution of the detector's dark signal to the entire signal is measured by additional photon counting after each laser pulse with a time delay and integration time of $25\,\mu s$, each. At this time no more OH fluorescence can be expected. A long integration time of $25\,\mu s$ ensures a high precision of this measurement. Photon count

rates during both time windows are integrated separately and subtracted after the signals have been read out from the photon counter. This is done for every single measurement resulting in a signal which contains only the fluorescence signal and laser generated background. Both contributions depend on the laser power. Therefore, the signal S_{det} is normalized to the the power of the excitation laser beam P_{ex}:

$$S_{det} = P_{ex}^{-1}(S'_{flu} + S'_{las}) = S_{flu} + S_{las}.$$

The photon count rate is normalized by the laser power which is permanently monitored, leading to the normalized photon count rate S_{det} measured in $[cts(mWs)^{-1}]$.

In order to distinguish between the laser generated background signal and the fluorescence signal, the laser wavelength is tuned periodically between on-resonance and off-resonance wavelengths with respect to the OH excitation (Figure 4.4) using the $Q_{11}(3)$ absorption line. At each wavelength position the signal is integrated between one and five seconds. Off-resonance measurements are done at four different wavelengths, either smaller or greater than the absorption wavelength of OH radicals. These signals include only background signals. They are averaged and subtracted from the signal measured during the on-resonance measurements. In order to derive the fluorescence signal, the wavelength is scanned over six different wavelength positions across the absorption line. Scanning is necessary because the excitation wavelength can drift with time due to temperature changes which affect the laser. Changes of the spectral overlap between the OH absorption cross section and the excitation laser light lead to changes of the detection sensitivity. The drift can be observed in the excitation spectrum measured in the reference cell and is corrected automatically by the measurement software.

All on-resonance measurements of the fluorescence cell are normalized during one on-off cycle with respect to the relative signal measured by the reference cell. After normalization the shape of the signal becomes a rectangular function. This allows to average all on-resonance measurements in order to get a higher precision of the fluorescence measurement. This procedure is justified because the measured OH line profiles in the measurement and reference cell are very similar since they are dominated by the spectral profile of the laser.

4.4 Determination of the RO_x and HO_x concentrations

The new instrument is principally sensitive to the sum of RO_2, RO, HO_2 and OH radicals. However, it is desirable to distinguish between the different species because of their different role in atmospheric chemistry.

The OH radical concentration is measured in a separate fluorescence cell in the present setup. A simultaneous measurement of the OH concentration allows to determine the contribution of OH radicals to the signal of RO_x measurement. In principle, a simultaneous measurement of HO_x and RO_x is desirable but this has not been realized until now.

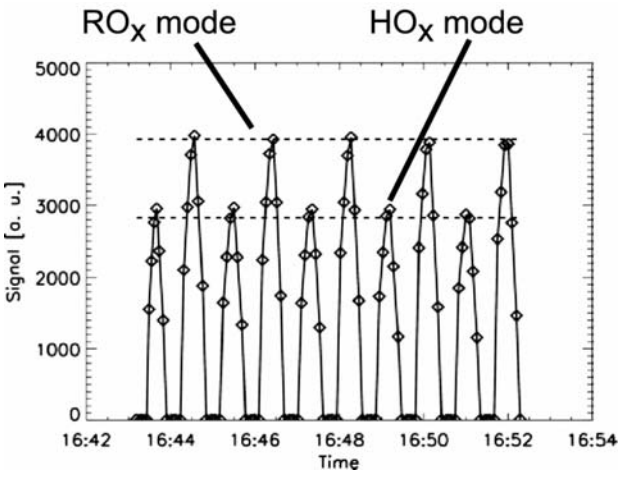

Figure 4.5: Alternating measurement in the HO_x and RO_x mode. Gas is sampled from the radical source providing equal concentrations of HO_2 and CH_3O_2 radicals (Chapter 5). The excitation wavelength is tuned periodically from on-resonance to off-resonance wavelengths. The chemical regime is changed by switching the addition of NO when the first off-resonance measurement is performed. Dashed lines refer to the mean values of the calculated fluorescence signals in each mode.

Therefore, the system is operated alternately in the HO_x mode I/II and the RO_x mode in order to discriminate between HO_x and RO_2 radical concentrations. The measured fluorescence signals in the different modes consist of contributions of different radical species which are detected with different sensitivities:

$$S_{\mathrm{HO_x-I}} = C_{\mathrm{OH}}^{\mathrm{CO}}[\mathrm{OH}] + C_{\mathrm{HO_2}}^{\mathrm{CO}}[\mathrm{HO_2}] \quad (4.2)$$

$$S_{\mathrm{HO_x-II}} = C_{\mathrm{OH}}[\mathrm{OH}] + C_{\mathrm{HO_2}}[\mathrm{HO_2}] \quad (4.3)$$

$$S_{\mathrm{RO_x}} = C_{\mathrm{OH}}^{\mathrm{NO+CO}}[\mathrm{OH}] + C_{\mathrm{HO_2}}^{\mathrm{NO+CO}}[\mathrm{HO_2}] + C_{\mathrm{RO_2}}[\mathrm{RO_2}] \quad (4.4)$$

- S_i: fluorescence signal in the measurement mode i in $[cts(mWs)^{-1}]$
- C_j^k: detection sensitivity for the radical species j if reagent gases k are added to the gas flow

The sensitivity of the measurement system describes the relation between the rate of detected photons normalized to the power of the excitation beam and the concentration of detected radicals in the sampled volume. The HO_2 concentration can be determined from Equation 4.2 or 4.3 if the corresponding detection sensitivities ($C_{\mathrm{OH}}^{\mathrm{CO}}$ and $C_{\mathrm{HO_2}}^{\mathrm{CO}}$) and the OH concentration are known:

$$[\mathrm{HO_2}] = (C_{\mathrm{HO_2}}^{\mathrm{CO}})^{-1}\left(S_{\mathrm{HO_x}} - C_{\mathrm{OH}}^{\mathrm{CO}}[\mathrm{OH}]\right) \quad (4.5)$$

Calculations are the same for HO_x mode I and II and are only shown for mode I. S_{HO_x} denotes the signal in HO_x mode I. The sensitivities are determined by the calibration of the system as described in Chapter 5 whereas the OH radical concentration is measured simultaneously in a separate fluorescence cell.

The RO_2 concentration can be calculated in a similar way if the OH and HO_2 concentrations are known:

$$[RO_2] = (C_{RO_2})^{-1} \left(S_{RO_x} - C_{HO_2}^{NO+CO}[HO_2] - C_{OH}^{NO+CO}[OH] \right) \tag{4.6}$$

In the present setup it is necessary to interpolate the HO_2 radical concentration because HO_x and RO_x radical concentration are not measured simultaneously. The minimum time resolution for a single radical measurement is about $1\,min$. This time span may exceed the time during which the HO_2 radical concentration may change but can be approximated by a linear interpolation. Figure 4.5 shows the fluorescence signal if gas is sampled from the radical source providing equal concentrations of HO_2 and CH_3O_2. The signal is modulated by tuning the excitation wavelength (on-resonance and off-resonance measurements) and by changing the chemical regime (HO_x and RO_x mode). The time dependent signal is nearly constant zero at off-resonance wavelengths and displays the central portion (∼FWHM) of the OH excitation line at each sequence of on-resonance wavelengths. The maximum of the fluorescence signal in the RO_x mode is higher than that in the HO_x mode. This can be seen as a proof of the system's potential to measure CH_3O_2 radicals. An increase of the signal in the RO_x mode compared to the signal in the HO_x mode must be caused by the conversion of CH_3O_2 to HO_2 radicals which contribute to the entire HO_2 radical concentration. The sum of HO_2 sampled from the radical source and HO_2 which results from the conversion of CH_3O_2 is measured in the fluorescence cell. A possible increase of the signal because of a higher HO_2 sensitivity in the RO_x mode compared to the HO_x mode can be excluded because the sensitivity for HO_2 radicals is reduced if reactive gases are added as discussed later (Section 4.5).

The procedure was tested with respect to a possible memory effect caused by NO which may be present in the HO_x mode after the NO which has been added in the RO_x mode has been switched off. This could lead to an unwanted conversion of RO_2 radicals in the HO_x mode. However, this could be excluded by comparing the signals derived in the alternating mode to the signals derived if the gases are not switched. No memory effects could be found. Measured signals in the alternating mode corresponded to the expected values.

The detection sensitivities C for the radical species defined in Equation 4.2 to 4.4 depend on many instrumental parameters (e.g. pressure, gas volume flow, concentration of reagent gases). The overall sensitivities of the instrument can be broken down to the yields of HO_2 radicals in the first chamber and the HO_2 detection in the second chamber including the HO_2 conversion to OH and the detection of OH with LIF

(fluorescence cell):

$$C^k_{\mathrm{OH}} = \epsilon^k_{\mathrm{OH}} \epsilon_F C_F \tag{4.7}$$
$$C^k_{\mathrm{HO_2}} = \epsilon^k_{\mathrm{HO_2}} \epsilon_F C_F \tag{4.8}$$
$$C_{\mathrm{RO_2}} = \epsilon_{\mathrm{RO_2}} \epsilon_F C_F \tag{4.9}$$

The first factors refer to the conversion reactor. They are defined by

$$\epsilon^k_{\mathrm{OH}} = \frac{[\mathrm{HO_2}]_{conv}}{[\mathrm{OH}]_0} \tag{4.10}$$
$$\epsilon^k_{\mathrm{HO_2}} = \frac{[\mathrm{HO_2}]_{conv}}{[\mathrm{HO_2}]_0} \tag{4.11}$$
$$\epsilon_{\mathrm{RO_2}} = \frac{[\mathrm{HO_2}]_{conv}}{[\mathrm{RO_2}]_0}. \tag{4.12}$$

Here, $[\mathrm{OH}]_0$, $[\mathrm{HO_2}]_0$ and $[\mathrm{RO_2}]_0$ denote the concentrations of the sampled radicals contained in the ambient air. $[\mathrm{HO_2}]_{conv}$ is the HO_2 concentration resulting from chemical processing when the gas reaches the inlet nozzle of the fluorescence cell. Accordingly, ϵ^k_i is the corresponding HO_2 yield of the radicals i (OH, HO_2 and RO_2) in the conversion reactor and k denotes the reagent gases (NO+CO or CO) which are added for chemical processing.

The other two factors in Equation 4.7 to 4.9 refer to the HO_2 detection in the fluorescence cell. ϵ_F is the conversion efficiency of HO_2 to OH and is defined by

$$\epsilon_F = \frac{[\mathrm{OH}]_{flu}}{[\mathrm{HO_2}]_{conv}}. \tag{4.13}$$

$[\mathrm{OH}]_{flu}$ is the OH concentration in the fluorescence cell at the point where OH is excited by the laser and $[\mathrm{HO_2}]_{conv}$ is the HO_2 concentration sampled from the conversion reactor. C_F is the OH fluorescence detection sensitivity in the fluorescence cell.

OH is converted quantitatively to HO_2 in the conversion reactor in the RO_x mode and HO_x mode I and no OH is sampled into the fluorescence cell as will be shown in Section 4.5.

The following sections of this chapter mainly deal with the experimental and theoretical investigation of the system's detection sensitivity. This allows to optimize the system with respect to a high detection sensitivity. In addition, a detailed understanding of the chemistry of the conversion mechanism helps to identify factors influencing the stability of the system like possible interference signals. The HO_2 yields in the conversion reactor (ϵ^k_{OH}, $\epsilon^k_{\mathrm{HO_2}}$, $\epsilon_{\mathrm{RO_2}}$) mainly depend on the chemical kinetics of the conversion process. This is investigated by analytical and numerical models in Section 4.5. The HO_2 conversion with the efficiency ϵ_F and OH detection with the sensitivity C_F in the fluorescence cell is discussed in Section 4.6. The characterization of the system with respect to the parameters which affect the overall sensitivities of the system is shown in Section 4.7.

4.5 Chemical model of the radical conversion

In this section, the kinetics of the radical conversion in the first chamber is investigated by model calculations. The results are used to describe the HO_2 yields (ϵ^k_{OH}, $\epsilon^k_{HO_2}$, ϵ_{RO_2}) as defined in Equation 4.7, 4.8 and 4.9. After discussion of the reaction mechanism, an analytic solution of a simplified mechanism is presented. This is compared with numerical calculations and measurements later in Section 4.7.

4.5.1 Reaction mechanism

The reaction mechanism as shown in Figure 4.1 consists of the RO_2 conversion propagating reactions which lead to the HO_x cycle and radical chain terminating reactions. Reaction rate constants are summarized in Table 4.4. A detailed analysis is required to determine the optimum chemical and physical parameters for a maximum conversion efficiency. The strategy is to minimize radical loss processes in order to maximize the HO_2 yield at the inlet of the fluorescence cell.

Firstly, RO_2 radicals are converted to RO radicals in the reaction with NO. Reactions with NO dominate the entire gas phase reactions of RO_2 radicals because of the high concentration of the added NO. Reactions of RO_2 radicals e.g. with NO_2 can be neglected. This also applies for sampled polluted air in which NO_2 mixing ratios may reach values about $100\,ppbv$. The lifetime of RO_2 radicals with respect to the reaction with $100\,ppbv$ NO_2 would be $27\,s$ which is large compared to the RO_2 lifetime with respect to the reaction with NO (about $0.3\,s$, calculated for CH_3O_2 radicals, *NASA* (2003)).

Although the RO_2 wall loss rate cannot be determined easily, it can be assumed that the wall loss rate for organic peroxy radicals is smaller than that for HO_2 because of their generally smaller reactivity. The lifetime of peroxy radicals with respect to the reaction with NO is also shorter than their lifetime resulting from the upper limit of the wall loss rate:

$$k^{wall}_{RO_2} < k^{wall}_{HO_2} = 0.5s^{-1} < k_1[\mathrm{NO}] = 3s^{-1}.$$

Formation of nitrates competes with the formation of alkoxy radicals in the reaction of peroxy radicals with NO:

$$\begin{array}{rcll} RO_2 + NO & \rightarrow & RO + NO_2 & \text{(R2.10)} \\ RO_2 + NO + M & \rightarrow & RONO_2 + M & \text{(R4.1)} \end{array}$$

Rate constants of these reactions are reviewed (*Atkinson and Arey*, 2003b) and included in the latest NASA (*NASA*, 2003) and IUPAC (*IUPAC*, 2005) evaluations for alkyl peroxy radicals up to R=C_4H_9. Rate constants of Reaction R2.10 are essentially identical within the range of $8 \cdot 10^{-12}\,s^{-1}$ to $9 \cdot 10^{-12}\,s^{-1}$ at $T = 298K$ for alkyl peroxy radicals with R=C_nH_{2n+1}, $n \geq 2$ (*Atkinson and Arey*, 2003b). The rate constants increase with higher carbon number of the peroxy radical (*Eberhard and Howart*, 1997). The value for methylperoxy radicals is slightly smaller with $k = 7.7 \cdot 10^{-12}\,s^{-1}$ (*NASA*, 2003).

Table 4.4: Reactions and reaction rate constants which are relevant during the conversion of different RO_2 radicals in the system. Values are given for the conditions in the conversion reactor ($p = 25hPa$, $T = 298K$).

		Reaction			k $[s^{-1}cm^3]$
†	(R2.6)	$CH_3O_2 + NO$	$\rightarrow$	$CH_3O + NO_2$	$7.7 \cdot 10^{-12}$ [a]
	(R2.10)	$C_nH_{2n+1}O_2 + NO$	$\rightarrow$	$C_nH_{2n+1}O + NO_2$	$9.0 \cdot 10^{-12}$ [dh]
	(R2.10)	$C_5H_8OHO_2 + NO$	$\rightarrow$	$C_5H_8OHO + NO_2$	$9 \cdot 10^{-12}$ [e]
†	(R2.7)	$CH_3O + O_2$	$\rightarrow$	$HCHO + HO_2$	$1.9 \cdot 10^{-15}$ [a]
	(R2.11)	$C_nH_{2n+1}O + O_2$	$\rightarrow$	$C_{n-1}H_{2n-1}CHO + HO_2$	7-8 $\cdot 10^{-15}$ [d]
†	(R2.3)	$HO_2 + NO$	$\rightarrow$	$OH + NO_2$	$8.1 \cdot 10^{-12}$ [a]
†	(R2.1)	$OH + CO$	$\rightarrow$	$H + CO_2$	$1.5 \cdot 10^{-13}$ [a]
†	(R2.2)	$H + O_2 + M$	$\rightarrow$	$HO_2 + M$	$3.4 \cdot 10^{-14}$ [a]
†	(R2.23)	$OH + NO_2 + M$	$\rightarrow$	$HNO_3 + M$	$9.8 \cdot 10^{-13}$ [a]
†		$HO_2 + NO_2 + M$	$\rightarrow$	$HO_2NO_2 + M$	$9.5 \cdot 10^{-14}$ [a]
†		$CH_3O + NO_2 + M$	$\rightarrow$	$CH_3ONO_2 + M$	$1.7 \cdot 10^{-11}$ [a]
†		$CH_3O_2 + NO_2 + M$	$\rightarrow$	$CH_3OONO_2 + M$	$6.1 \cdot 10^{-13}$ [a]
		$C_nH_{2n+1}O + NO_2 + M$	$\rightarrow$	$C_nH_{2n+1}ONO_2 + M$	$2.4 \cdot 10^{-11}$ [ag]
		$C_nH_{2n+1}O_2 + NO_2 + M$	$\rightarrow$	$C_nH_{2n+1}OONO_2 + M$	$2.5 \cdot 10^{-12}$ [ag]
†	(R2.17)	$OH + NO + M$	$\rightarrow$	$HONO + M$	$3.8 \cdot 10^{-13}$ [a]
†	(R4.2)	$CH_3O + NO + M$	$\rightarrow$	$CH_3ONO + M$	$4.9 \cdot 10^{-12}$ [a]
	(R4.2)	$C_nH_{2n+1}O + NO + M$	$\rightarrow$	$C_nH_{2n+1}ONO + M$	$4.2 \cdot 10^{-11}$ [ag]
	(R4.1)	$CH_3O_2 + NO + M$	$\rightarrow$	$CH_3ONO_2 + M$	0.0 [c]
	(R4.1)	$C_nH_{2n+1}O_2 + NO + M$	$\rightarrow$	$C_nH_{2n+1}ONO_2 + M$	$< 9.0 \cdot 10^{-13}$ [bi]
	(R4.1)	$C_5H_8OHO_2 + NO + M$	$\rightarrow$	$C_5H_8(OH)ONO_2 + M$	$1.1 \cdot 10^{-12}$ [ej]
†		$OH + O_3$	$\rightarrow$	$HO_2 + O_2$	$7.3 \cdot 10^{-14}$ [a]
†		$HO_2 + O_3$	$\rightarrow$	$OH + 2O_2$	$1.9 \cdot 10^{-15}$ [a]
†		$NO + O_3$	$\rightarrow$	$NO_2 + O_2$	$1.9 \cdot 10^{-14}$ [a]
†		$OH + HO_2$	$\rightarrow$	$H_2O + O_2$	$1.1 \cdot 10^{-10}$ [a]
†	(R2.24)	$HO_2 + HO_2$	$\rightarrow$	$H_2O_2 + O_2$	$2.7 \cdot 10^{-12}$ [ak]
†	(R2.25)	$HO_2 + CH_3O_2$	$\rightarrow$	$CH_3OOH + O_2$	$5.2 \cdot 10^{-12}$ [a]
†	(R2.26)	$CH_3O_2 + CH_3O_2$	$\rightarrow$	$CH_3OOH + O_2$	$3.5 \cdot 10^{-13}$ [a]
	(R2.25)	$HO_2 + C_nH_{2n+1}O_2$	$\rightarrow$	products	(7-17)$\cdot 10^{-12}$ [dh]
					k $[s^{-1}]$
†	(R4.7)	OH + wall	$\rightarrow$		5.4 [f]
†	(R4.6)	HO_2 + wall	$\rightarrow$		0.5 [f]
†	(R4.4)	RO + wall	$\rightarrow$		<5.4 [f]
†	(R4.3)	RO_2 + wall	$\rightarrow$		<0.5 [f]

[a] *NASA* (2003)
[b] *Atkinson et al.* (1983)
[c] *Bacak et al.* (2004)
[d] *Atkinson and Arey* (2003b)
[e] *Zhang et al.* (2003)
[f] this work
[g] $n = 2$
[h] $n \geq 2$
[i] $n = (5 - 8)$
[j] atmospheric pressure
[k] water concentration: 1 %
† used for model runs in Section 4.7

Less data are available for the branching ratio of Reaction R2.10 and R4.1. It is widely accepted that both channels share a common intermediate, the peroxy nitrite (ROONO) (*Zhang et al.*, 2004). Production of nitrates (Reaction R4.1) requires collision stabilization of the intermediate nitrite. The yield of alkyl nitrates increases with the complexity of the peroxy radical and with increasing pressure. *Atkinson et al.* (1983) investigated n-alkanes with carbon number between 5 and 8 and calculated an expression for the yield of nitrates which results in yields within the range of 2 % to 10 % at low pressure. *Bacak et al.* (2004) discusses the branching ratio for the reaction of methylperoxy radicals with NO in detail. No evidence for the formation of methyl nitrate was found within the temperature range of 193 K to 300 K and within a pressure range of 130 hPa to 260 hPa. This is also supported by quantum mechanical investigations (*Lesar et al.*, 2006).

Isoprene (2-methyl-1,3-butadiene, C_5H_8) is one of the most abundant biogenic hydrocarbons. Hydroxyalkyl peroxy radicals are formed in the reaction of OH with isoprene. *Zhang et al.* (2003) investigated the mechanism of the reaction between the hydroxyalkyl peroxy radical ($C_5H_8OHO_2$) with NO in detail. The observed reaction rate ($(9 \pm 3) \cdot 10^{-12}\, s^{-1} cm^3$) is similar to the values found for alkyl peroxy radicals. The branching ratio for the formation of the corresponding nitrate was not measured. It is assumed to be slightly higher than for alkyl nitrates.

Due to the similarities of the results found for the reaction of various peroxy radicals with NO, it is suggested that the rate constants may be applicable to other peroxy radicals for which experimental data are not available (*Atkinson et al.*, 1987; *Atkinson and Arey*, 2003b).

In the second step of the conversion process alkoxy radicals which are formed in the first step react further with oxygen forming HO_2 radicals. This reaction is mainly in competition with the formation of nitrites due to the high NO concentration present in the conversion reactor:

$$\mathrm{RO + O_2} \rightarrow \mathrm{R'CHO + HO_2} \quad \text{(R2.11)}$$

$$\mathrm{RO + NO + M} \rightarrow \mathrm{RONO + M} \quad \text{(R4.2)}$$

In principle, alkoxy radicals can also undergo unimolecular decomposition (Reaction R4.8) and unimolecular isomerization (Reaction R4.9):

$$\mathrm{RO + M} \rightarrow \mathrm{R' \cdot + R''CHO \quad (or \quad R'R''CO) + M} \quad \text{(R4.8)}$$

$$\mathrm{RO + M} \rightarrow \mathrm{R'(OH)CH_2 \cdot + M} \quad \text{(R4.9)}$$

Loss reactions which require collision stabilization like Reaction R4.2, R4.8 and R4.9 are generally expected to play a minor role because of the reduced pressure in the reactor. This is independent of the organic group of the alkoxy radical.

Only few studies treating simpler alkoxy radicals are available investigating the rate constants and branching ratios of these reactions. Most studies are concerned with atmospheric conditions. Isomerization and decomposition are negligible in the presence of oxygen for simple alkoxy radicals (*Atkinson*, 2003) whereas both become more

important for more complex species (*Atkinson et al.*, 1987). Measured rate constants of Reaction R2.11 and R4.2 are limited to a subset of alkoxy radicals derived from C1-C4 alkanes (*Orlando et al.*, 2003). However, the database is small and only values of methoxy and ethoxy radicals are assured (*NASA*, 2003). From these values it is expected that the yield of nitrite is less than 1 % at low pressure.

The reaction of RO with ambient NO_2 is another possible loss reaction if polluted air is sampled, leading to the formation of nitrates. Again, reaction constants are not well investigated. However, losses are expected to be small. Assuming a high mixing ratio about 100 *ppbv* NO_2, the lifetime of e.g. methoxy radicals can be calculated to 140 ms and of ethoxy radicals to 980 ms. This is long compared to their lifetime with respect to their reactions with oxygen which are within the range of a few milliseconds (4 ms for methoxy and 1 ms for ethoxy radicals).

The measured OH wall loss rate can be taken as an upper limit for the wall loss rate of RO radicals. However, this is small compared to the reaction of e.g. CH_3O with oxygen:

$$k_{\mathrm{RO}}^{wall} < k_{\mathrm{OH}}^{wall} = 5.4 s^{-1} \ll k_2[\mathrm{O_2}] = 250 s^{-1}.$$

This upper limit for the wall loss rate is justified because OH and RO radicals can be seen as part of a homologous series in which the reactivity decreases with the carbon number.

Once NO is added to the sampled gas, HO_2 radicals react further to OH:

$$\mathrm{HO_2 + NO \rightarrow OH + NO_2}. \qquad \text{(R2.3)}$$

The yields of the competing radical recombination reactions (Reaction R2.24, R2.25) are negligible because of the small radical concentrations expected under atmospheric conditions. This is assisted by the reduced pressure in the conversion reactor leading to the dilution of radical concentrations by a factor of 40.

If polluted air containing NO_2 is sampled, peroxynitric acid (PNA, HO_2NO_2) can serve as a reservoir for HO_2. Therefore, PNA may be responsible for artificial production of radicals which causes an interference signal. It is not expected that this reaction system is affected by PNA as discussed in Section 4.7.10. The formation of PNA as competing reaction to the reaction of HO_2 with NO is negligible because the HO_2 lifetime to the reaction with e.g. 100 *ppbv* NO_2 is much longer (160 s) than that to the reaction with NO (0.3 s).

The reaction of HO_2 with ozone is an alternative reaction to the reaction with NO leading to the production of OH (Reaction R2.30). Assuming highly polluted air with an ozone mixing the lifetime of HO_2 is again much longer than the HO_2 lifetime with respect to the reaction with NO. Therefore, this reaction path does not play any role in this system.

Investigations of the water dependence of the sensitivity in PERCA-systems suggest further chain terminating reactions in the HO_x cycle (*Mihele and Hastie*, 1998a; *Reichert et al.*, 2003; *Butkovskaya et al.*, 2005). *Butkovskaya et al.* (2005) investigates the formation of HNO_3 at room temperature and reduced pressure (230 hPa). It is suggested that HO_2 and NO form an intermediate which can decompose to OH and

NO_2 or can be stabilized by collisions to HNO_3. The yield of HNO_3 depends on the water vapor content in the sampled air. This is an agreement with the observation of the water vapor dependence of the sensitivity in PERCA systems (see Section 4.7.8). However, the yield of HNO_3 is expected to be less than 1 % for conditions in this work and should not influence the entire HO_2 yield.

A reaction cycle between OH and HO_2 radicals is initiated by the addition of CO:

$$\begin{aligned} OH + CO &\rightarrow H + CO_2 && \text{(R2.1)} \\ H + O_2 + M &\rightarrow HO_2 + M. && \text{(R2.2)} \end{aligned}$$

Due to the high NO concentration, the most important competing gas phase reaction is the formation of HONO which is a termolecular reaction like the formation of nitrites and nitrates:

$$OH + NO + M \rightarrow HONO + M. \qquad \text{(R2.17)}$$

The reaction of OH with NO_2 and ozone in polluted air can be neglected because of the fast reaction with CO. Assuming a high NO_2 mixing ratio of 100 *ppbv* the OH lifetime with respect to the reaction with NO_2 is 17 s and to the reaction with 300 *ppbv* ozone 75 s. Both OH lifetimes are large compared to the lifetime of 6 ms resulting from the OH reaction with the added CO.

Wall loss of both HO_2 and OH radicals (Reaction R4.6 and R4.7) are the main radical loss processes in the reaction system. This rate constants have been measured (Section 4.7.3).

The HO_x cycle is well investigated because of its importance for the daytime photochemistry in the troposphere (Chapter 2). Reaction constants and branching ratios are investigated in many studies (*NASA*, 2003). Values for model calculations in this work are taken from the recommendations in *NASA* (2003).

4.5.2 Analytical model

Concentrations of radicals can be calculated by analytically solving the differential equation system for the scheme shown in Figure 4.1. The derivation of the radical concentrations with respect to time is given by the production and destruction terms:

$$\begin{aligned} \frac{d[RO_2]}{dt} &= -k_1[NO][RO_2] - k_{L1}[RO_2] && (4.14) \\ \frac{d[RO]}{dt} &= k_1[NO][RO_2] - k_2[O_2][RO] - k_{L2}[RO] && (4.15) \\ \frac{d[HO_2]}{dt} &= k_2[O_2][RO] - k_3[NO][HO_2] + k_4[CO][OH] - k_{L3}[HO_2] && (4.16) \\ \frac{d[OH]}{dt} &= k_3[NO][HO_2] - k_4[CO][OH] - k_{L4}[OH]. && (4.17) \end{aligned}$$

Subscripts of reaction constants correspond to notations in Figure 4.1. Time constants of loss reactions are summarized as

$$k_{Li} = \sum_j k^i_{M_j}[M_j] + k^{wall}_i, \tag{4.18}$$

whereby $k^i_{M_j}$ is the reaction constant of the loss reaction between radical i with any species M_j and k^{wall}_i is the wall loss reaction constant of the radical i.

The differential equation system can be simplified by using the steady state approximation for the calculation of the radical concentrations of OH and RO in order to solve the differential equations for RO_2 and HO_2 radical concentrations.

The RO radical concentration is small and in equilibrium with the RO_2 radical concentration due to the fast reaction of RO with ambient oxygen (20.5 %) for conditions in the reactor. The lifetime of RO radicals with respect to this reaction is about $4\,ms$ and the lifetime of RO_2 radicals with respect to the reaction with the added NO ($0.7\,ppmv$) is about $0.3\,s$. This results in a much faster destruction than production of RO radicals. Therefore, the RO radical concentration becomes very small and the following approximation can be made:

$$\begin{aligned} \frac{d[\mathrm{RO}]}{dt} &= k_1[\mathrm{NO}][\mathrm{RO_2}] - k_2[\mathrm{O_2}][\mathrm{RO}] - k_{L2}[\mathrm{RO}] = 0 \\ \Rightarrow [\mathrm{RO}](t) &= \frac{k_1[\mathrm{NO}]}{k_2[\mathrm{O_2}] + k_{L2}}[\mathrm{RO_2}](t) = \alpha_1[\mathrm{RO_2}](t) \end{aligned} \tag{4.19}$$

where

$$\alpha_1 = \frac{k_1[\mathrm{NO}]}{k_2[\mathrm{O_2}] + k_{L2}}. \tag{4.20}$$

The OH radical concentration can also be calculated by using the steady state approximation because of the high CO concentration added in the conversion reactor. Like for RO radicals the concentration is determined by the slow production (reaction of HO_2 radicals with NO, lifetime about $0.3\,s$) because of the fast destruction of OH in the reaction with CO (lifetime about $6\,ms$). From steady state conditions follows:

$$\begin{aligned} \frac{d[\mathrm{OH}]}{dt} &= k_3[\mathrm{NO}][\mathrm{HO_2}] - k_4[\mathrm{CO}][\mathrm{OH}] - k_{L4}[\mathrm{OH}] = 0 \\ \Rightarrow [\mathrm{OH}](t) &= \frac{k_3[\mathrm{NO}]}{k_4[\mathrm{CO}] + k_{L4}}[\mathrm{HO_2}](t) = \alpha_2[\mathrm{HO_2}](t) \end{aligned} \tag{4.21}$$

where

$$\alpha_2 = \frac{k_3[\mathrm{NO}]}{k_4[\mathrm{CO}] + k_{L4}}. \tag{4.22}$$

The differential equation for the RO_2 radical concentration (Equation 4.14) can be solved directly because this equation is not coupled with any of the others:

$$\begin{aligned} \frac{d[\mathrm{RO_2}]}{dt} &= -k_1[\mathrm{NO}][\mathrm{RO_2}] - k_{L1}[\mathrm{RO_2}] \\ \Rightarrow [\mathrm{RO_2}](t) &= [\mathrm{RO_2}]_0 \exp(-(k_1[\mathrm{NO}] + k_{L1})t) = [\mathrm{RO_2}]_0 \exp(-\kappa_1 t) \end{aligned} \tag{4.23}$$

where

$$\kappa_1 = k_1[\mathrm{NO}] + k_{L1}. \tag{4.24}$$

The initial RO_2 concentration is reduced by the conversion to RO radicals and loss reactions in a mono-exponential decay.

The differential equation for the HO_2 radical concentration (Equation 4.16) can be solved by using the equilibrium RO and OH radical concentrations (Equation 4.19 and 4.21):

$$\begin{aligned} \frac{d[\mathrm{HO_2}]}{dt} &= \kappa_2[\mathrm{RO_2}]_0 \exp(-\kappa_1 t) - \kappa_3[\mathrm{HO_2}] \\ \Rightarrow [\mathrm{HO_2}](t) &= [\mathrm{RO_2}]_0 \frac{\kappa_2}{\kappa_3 - \kappa_1} \left(\exp(-\kappa_1 t) - \exp(-\kappa_3 t)\right) + C \exp(-\kappa_3 t) \end{aligned} \tag{4.25}$$

where

$$\kappa_2 = \alpha_1 k_2[\mathrm{O_2}] = k_1[\mathrm{NO}] \left(1 + \frac{k_{L2}}{k_2[\mathrm{O_2}]}\right)^{-1} \tag{4.26}$$

$$\kappa_3 = k_3[\mathrm{NO}] - k_4[\mathrm{CO}]\alpha_2 + k_{L3} = k_3[\mathrm{NO}] \left(1 - \frac{k_4[\mathrm{CO}]}{k_4[\mathrm{CO}] + k_{L4}}\right) + k_{L3}. \tag{4.27}$$

C is the HO_2 concentration after the equilibrium between initially present OH and HO_2 radicals has been reached. The value can be calculated by the initial concentrations of ambient OH and HO_2 radicals ($[\mathrm{OH}]_0$ and $[\mathrm{HO_2}]_0$):

$$\begin{aligned} [\mathrm{HO_2}]_0 + [\mathrm{OH}]_0 &= [\mathrm{HO_2}](t=0) + [\mathrm{OH}](t=0) = C + \alpha_2 C \\ \Rightarrow C &= \frac{[\mathrm{HO_2}]_0 + [\mathrm{OH}]_0}{1 + \alpha_2}. \end{aligned} \tag{4.28}$$

Equation 4.25 includes two processes. The first term refers to the HO_2 radicals which are produced by the conversion of organic peroxy radicals with the effective rate constant κ_1. They are destroyed by HO_2 and OH loss reactions (k_{L3}, k_{L4}) with the effective rate constant κ_3. The second term refers to the initial HO_x concentration sampled from ambient air which also decays effectively with the rate constant κ_3.

The analytic solutions can be further simplified by neglecting the reactions which are slow compared to the fastest production or destruction reactions.

The formation of nitrates in the reaction of organic peroxy radicals with NO is not significant compared to the formation of alkoxy radicals as discussed in section 4.5.1. The destruction of RO_2 radicals is only determined by the formation of alkoxy radicals:

$$[\mathrm{RO_2}](t) \approx [\mathrm{RO_2}]_0 \exp(-k_1[\mathrm{NO}]t) \tag{4.29}$$

$$\kappa_1 \approx k_1[\mathrm{NO}]. \tag{4.30}$$

α_1 in Equation 4.20 can be approximated by neglecting loss reactions of RO radicals because the reaction of RO with O_2 is fast and loss reactions are not expected to be significant as discussed in Section 4.5.1 ($k_2[\mathrm{O_2}] = 250 s^{-1} \gg k_{L2}$):

$$\alpha_1 = \frac{[\mathrm{RO}]}{[\mathrm{RO_2}]} \approx \frac{k_1[\mathrm{NO}]}{k_2[\mathrm{O_2}]} = 0.014 \tag{4.31}$$

From this follows that the RO radical concentration is much smaller compared to the RO_2 concentration.

Similar considerations apply to the OH radical concentration. The reactivity of the dominant destruction term ($k_4[\mathrm{CO}] \approx 170\,s^{-1}$, Reaction R2.1) dominates the overall destruction of OH radicals. Wall loss is expected to be the most important OH loss process ($k_{L4} \approx k_{\mathrm{OH}}^{wall} = 5.4\,s^{-1}$, see Table 4.4). As a result, the OH/HO_2 radical concentration ratio can be approximated as

$$\alpha_2 = \frac{[\mathrm{OH}]}{[\mathrm{HO_2}]} \approx \frac{k_3[\mathrm{NO}]}{k_4[\mathrm{CO}]} = 0.022 \tag{4.32}$$

This means that OH can not accumulate during the conversion process in the reactor.

The analytic solution for the HO_2 radical concentration (Equation 4.25) can be approximated using Equation 4.31 and 4.32. Assuming that wall loss is the dominant loss reaction, the terms in Equation 4.25 can be simplified (Table 4.4). The effective rate constant κ_3 (Equation 4.27) becomes:

$$\kappa_3 \approx k_{L3} \approx k_{\mathrm{HO_2}}^{wall}$$

because $k_4[\mathrm{CO}] \gg k_{L4}$. In addition, it is $k_{L2} \ll k_2[\mathrm{O_2}]$ so that the effective rate constant κ_2 (Equation 4.26) becomes

$$\kappa_2 \approx k_1[\mathrm{NO}].$$

Together with the simplified expression for the effective rate constant κ_1 (Equation 4.30) follows:

$$\begin{aligned}[\mathrm{HO_2}](t) &= [\mathrm{RO_2}]_0 \frac{k_1[\mathrm{NO}]}{k_{\mathrm{HO_2}}^{wall} - k_1[\mathrm{NO}]} \left(\exp(-k_1[\mathrm{NO}]t) - \exp(-k_{\mathrm{HO_2}}^{wall}t)\right) \\ &\quad + ([\mathrm{HO_2}]_0 + [\mathrm{OH}]_0)\exp(-k_{\mathrm{HO_2}}^{wall}t). \end{aligned} \tag{4.33}$$

The HO_2 radical concentration is mainly determined by the conversion of RO_2 radicals and the HO_2 wall loss.

Using Equation 4.33, the conversion efficiencies can be calculated as defined in Equation 4.10 to 4.12. HO_x yields for sampled ambient OH and HO_2 as defined by Equation 4.10 and 4.11 are identical in the HO_x mode I and the RO_x mode:

$$\epsilon_{\mathrm{OH}}^{k} = \epsilon_{\mathrm{HO_2}}^{k} = \exp(-k_{\mathrm{HO_2}}^{wall}T) = 0.74 \tag{4.34}$$

T=0.6 s is the mean residence time of the sampled air in the reactor and is assumed to be the reaction time for the conversion process. k denotes the added gases either in the HO_x ($k = \mathrm{CO}$) or RO_x ($k = \mathrm{CO} + \mathrm{NO}$) mode.

The conversion efficiency for RO_2 radicals (Equation 4.12) can be calculated using the similar approach:

$$\epsilon_{\mathrm{RO_2}} = \frac{k_1[\mathrm{NO}]}{k_{\mathrm{HO_2}}^{wall} - k_1[\mathrm{NO}]} \left(\exp(-k_1[\mathrm{NO}]t) - \exp(-k_{\mathrm{HO_2}}^{wall}t)\right) = 0.71 \tag{4.35}$$

The chain length of the reaction cycle between HO_2 and OH radicals can be calculated by investigating the yield of NO_2. One NO_2 molecule is formed during each cycling between HO_2 and OH. Therefore, the chain length CL can be defined by the ratio of the NO_2 concentration, produced in the HO_x cycle, and the initial radical concentration:

$$CL = \frac{[\mathrm{NO_2}](t=T)}{[\mathrm{RO_x}]_0}. \tag{4.36}$$

The build up of NO_2 can be calculated by solving the differential equation:

$$\frac{d}{dt}[\mathrm{NO_2}] = k_3[\mathrm{NO}][\mathrm{HO_2}](t). \tag{4.37}$$

Using Equation 4.33 and setting the initial NO_2 concentration to zero, the solution is:

$$\begin{aligned}[\mathrm{NO_2}](t) &= \frac{[\mathrm{RO_2}]_0 k_3[\mathrm{NO}]}{k^{wall}_{\mathrm{HO_2}} - k_1[\mathrm{NO}]}\left((1-\exp(-k_1[\mathrm{NO}]t)) - \frac{k_1[\mathrm{NO}]}{k^{wall}_{\mathrm{HO_2}}}(1-\exp(-k^{wall}_{\mathrm{HO_2}}t))\right) \\ &\quad +([\mathrm{HO_2}]_0 + [\mathrm{OH}]_0)\frac{k_3[\mathrm{NO}]}{k^{wall}_{\mathrm{HO_2}}}(1-\exp(-k^{wall}_{\mathrm{HO_2}}t)).\end{aligned} \tag{4.38}$$

The first term results from the production of NO_2 from sampled RO_2 radicals and the second results from the cycling of the sampled HO_x radical concentration. Therefore, one can distinguish between the chain length for RO_2 ($CL_{\mathrm{RO_2}}$) and HO_x radicals ($CL_{\mathrm{HO_2}}$). They are different because RO_2 radicals have to be converted firstly before they become part of the HO_x cycling in which the NO_2 is produced. The chain lengths are calculated as:

$$\begin{aligned}CL_{\mathrm{RO_2}} &= \frac{k_3[\mathrm{NO}]}{k^{wall}_{\mathrm{HO_2}} - k_1[\mathrm{NO}]}\left((1-\exp(-k_1[\mathrm{NO}]T)) - \frac{k_1[\mathrm{NO}]}{k^{wall}_{\mathrm{HO_2}}}\left(1-\exp(-k^{wall}_{\mathrm{HO_2}}T)\right)\right) \\ &= 1.0\end{aligned} \tag{4.39}$$

$$CL_{\mathrm{HO_x}} = \frac{k_3[\mathrm{NO}]}{k^{wall}_{\mathrm{HO_2}}}(1-\exp(-k^{wall}_{\mathrm{HO_2}}T)) = 1.8 \tag{4.40}$$

The chain length is shorter for RO_2 radicals than for HO_2 radicals as expected. However, the average number of cycles between OH and HO_2 and is small for both radicals. This supports the assumption that effects caused by a long chain length like the water effect in PERCA instruments (Section 4.7.8) do not play any role in this system.

4.5.3 Numerical model

Numerical model calculations serve as a second approach to investigate the chemical system in the conversion reactor. In contrast to the analytic solution, additional side reactions which may be relevant are included as noted in Table 4.4. Reactions which are neglected in the analytic solution may have some influence on the entire reaction kinetics. This may be difficult to see because of the complexity of the chemical system. A short description of the model is given in this section.

A time dependent, zero-dimensional box model is used for numerical model calculations. The gas phase in the reactor is assumed to be mixed homogeneously. The time dependence of the chemical development of air components traveling from the reactor inlet to the end of the reactor is modeled. The assumption of a homogeneously mixed gas phase may not be completely fulfilled, especially behind the inlet nozzle and in front of the outlet nozzle. Therefore, it is necessary to test the validity of the model results against experimental data. This is shown later in Chapter 4.7.

Reaction constants are taken from literature (Table 4.4) except for the wall loss rates which depend strongly on the special design of the reactor. They were measured for the reaction chamber used in this work (Section 4.7.3). Conditions like pressure and temperature as well as initial concentrations of reactants NO and CO were set to standard values used in this work (Table 4.3). Initial radical concentrations correspond to typical values provided by the radical source (about $1 \cdot 10^8\, cm^{-3}$, Chapter 5). All other initial trace gas concentrations are set to zero. Only values which differ from these standard conditions are denoted if results of numerical calculations are shown in this work.

Model calculations are done by solving the coupled differential equation system resulting from the production and destruction of all relevant molecules M_i numerically:

$$\frac{d}{dt}[\mathrm{M_i}] = \sum_{\mathrm{j}}^{\mathrm{j}\neq\mathrm{i}} \sum_{\mathrm{l}\leq\mathrm{j}}^{\mathrm{l}\neq\mathrm{i}} \mathrm{k_{jl}^P}[\mathrm{M_j}][\mathrm{M_l}] - \sum_{\mathrm{j}} \mathrm{k_j^D}[\mathrm{M_j}][\mathrm{M_i}] - \mathrm{k_i^{wall}}[\mathrm{M_i}] \tag{4.41}$$

- k_{jl}^P: reaction constant for production reactions of molecule M_i from the reaction of compound M_j with M_l
- k_j^D: reaction constant for destruction reactions of molecule M_i in its reaction with compound M_j
- k_i^{wall}: wall loss rate of molecule M_i

A standard differential equation solver provided by the mathematical programming package MATLAB was used.

4.6 Model description of the fluorescence detection sensitivity

The overall detection sensitivities as defined in Equation 4.7, 4.8 and 4.9 consist of the HO_2 radical yields in the conversion reactor as discussed in the last sections and the detection efficiency of HO_2 sampled into the fluorescence chamber. The latter is described briefly in this section.

Firstly, HO_2 is converted to OH in the reaction with NO. Therefore, the mixing ratio of NO is increased from $0.7\,ppmv$ in the conversion reactor to $300\,ppmv$ in the fluorescence cell. The reaction kinetics of this conversion was investigated theoretically

and experimentally in detail by *Weber* (1998); *Holland et al.* (2003). The residence time of the sampled gas between the addition of NO and the detection of OH by fluorescence is estimated to $240\,\mu s$ (*Weber*, 1998). This is sufficiently long for the conversion of HO_2 to OH but it is much shorter than the time needed for the formation of HONO at low pressure ($3.5\,hPa$, OH-lifetime $0.7\,s$) and it is also shorter than the OH lifetime with respect to the reaction with CO ($45\,ms$) sampled from the conversion reactor. Therefore, the conversion of HO_2 to OH can be described by a simple mono-exponential decay, leading to a conversion efficiency of about $70\,\%$ (*Weber*, 1998).

Secondly, the OH-fluorescence is detected with the sensitivity C_{OH}^{flu} which consists of several factors (*Stevens et al.*, 1994; *Holland et al.*, 1995):

$$C_F = \omega \cdot \alpha \cdot R \cdot V \cdot Q \cdot \eta \cdot \gamma. \tag{4.42}$$

- ω: ratio of densities inside and outside of the sampling chamber
- α: fraction of excited OH
- R: repetition rate of the laser excitation
- V: volume of the laser beam overlapping the ambient airstream and solid angle from which fluorescence photons are collected
- Q: quantum yield of the OH fluorescence
- η: efficiency of the photon detection
- γ: radical loss factor

Here, the detection in the fluorescence cell is similar to the HO_x detection using LIF technique as described by *Weber* (1998); *Holland et al.* (2003). Beside the quantum yield Q of the OH fluorescence and the efficiency of the photon detection η, Equation 4.42 is not needed to explain experimental results in this work. In addition, most of these factors are not accurately accessible in order to calculate the detection sensitivity from Equation 4.42. Therefore, only the quantum yield of the OH fluorescence and the photon detection efficiency is discussed in the following. Refer to *Stevens et al.* (1994); *Holland et al.* (1995); *Weber* (1998) for a detailed description of other factors contained in Equation 4.42.

The quantum yield of OH fluorescence is limited by fluorescence quenching. Fluorescence quenching is the non-radiative deactivation of the excited OH by collisions with other molecules. The probability of fluorescence quenching is specific for both the energetic state of the OH radical and the molecule with which OH collides. It is described by the quenching constant k_q. The population distribution within the rotational levels of the first excited state accords to the Boltzmann distribution after rotational relaxation which is faster than the delay between OH excitation and detection of the fluorescence.

Nitrogen, oxygen and water vapor are the most prominent collision partners (Table 4.5). The ratio of the fluorescence lifetime τ_{flu} and the natural radiative lifetime

Table 4.5: Quenching constants for OH radicals ($A^2\Sigma^+, \nu' = 0$) at room temperature.

	k_q $[10^{-10}\, cm^3 s^{-1}]$	mix. ratio	τ_q $[ns]$
N_2	0.32 [a]	0.78	460
O_2	1.18 [a]	0.21	490
H_2O [c]	7.9 [b]	≈ 0.01	≈ 1500
NO [d]	3.46 [a]	0.006	5600
CO [d]	3.2 [a]	0.005	7200

[a] *Kenner et al.* (1990)
[b] *Copeland et al.* (1985)
[c] variable under atmospheric conditions
[d] present in the conversion reactor

$\tau_{rad} = 1/k_{rad} = 688\, ns$ (*German*, 1975) represents the fraction of excited OH radicals which emit fluorescence photons:

$$Q = \frac{\tau_{flu}}{\tau_{rad}} = \frac{k_{rad}}{k_{rad} + \sum_i k_q^i [\mathrm{M}_i]} \tag{4.43}$$

($[\mathrm{M}_i]$: concentration of collision partner M_i). Fluorescence quenching at atmospheric pressure leads to a fluorescence lifetime which is comparable to the duration of the laser pulse. Discrimination between the fluorescence and the excitation laser pulse is only possible by starting fluorescence counting after the laser has been applied because fluorescence and laser wavelength are within the same range. Therefore, a longer fluorescence lifetime than the length of laser pulse is required for an efficient detection. This can be achieved by pressure reduction in the fluorescence cell. The detection sensitivity shows a maximum around a pressure value of $3.5\, hPa$. On the one hand, the temporal overlap between the fluorescence and the counting window which is delayed with respect to the start of the fluorescence decreases with increasing pressure. On the other hand, the concentration of OH radicals is reduced linearly with decreasing pressure.

Fluorescence quenching does not only influence the number of emitted fluorescence photons but also influences the efficiency of the detection. Photon counting starts to the time t_1 for Δt after the excitation to the time $t_0 = 0$:

$$\eta \propto \left[\exp\left(-\frac{t_1}{\tau_{flu}} \right) - \exp\left(-\frac{t_1 + \Delta t}{\tau_{flu}} \right) \right] \tag{4.44}$$

Therefore, a shorter fluorescence lifetime leads to a smaller detection efficiency.

The fluorescence lifetime of OH varies slightly in this system because of the varying water vapor content in ambient air. Therefore, a small water dependence of the entire sensitivity is expected and observed experimentally as shown in Section 4.7.8.

In summary, it can be assumed that the fluorescence detection as described by *Weber* (1998); *Holland et al.* (2003) for the HO_2 detection by LIF also applies for this system.

The sampling of additional reactive gases from the conversion reactor influences neither the chemical conversion of HO_2 as discussed above nor the OH fluorescence detection by fluorescence quenching as can be seen in Table 4.5. Gas is sampled from lower pressure ($25\,hPa$) in the new instrument whereas the gas is expanded from ambient pressure in the previous HO_x system. This may lead to a broader gas beam behind the inlet nozzle of the new instrument which has a larger orifice (by a factor of ten) which may influence factors affecting the detection sensitivity. However, the sufficiently high measured sensitivities (Section 4.7.6) indicate that these conditions are suitable for the HO_2 conversion and OH fluorescence detection.

4.7 Characterization of the instrument

The new instrument was characterized to optimize the efficiency of the conversion of RO_2 to HO_2 radicals in the reactor. Parameters which can be varied are the concentration of the added reactive gases NO and CO, the reaction time, the geometry and surface material of the reactor and the temperature and the pressure inside the reactor.

The experimental characterization of the instrument was accomplished by sampling radicals from a radical source as used for the calibration (Chapter 5). Either OH and HO_2 or RO_2 and HO_2 in amounts of about $1 \cdot 10^8\,cm^{-3}$ are provided. Concentrations are nearly constant and accurately known. This allows systematic investigations of the detection sensitivities.

4.7.1 Reaction time

The mean residence time of the gas is assumed to be the effective reaction time in the reactor. It can be calculated from the sampled gas flow, the pressure inside the chamber and the volume of the chamber. The gas flow is determined by the pressure in front of the nozzle, the opening diameter of the nozzle and a form factor which summarizes the specific characteristics of the nozzle. However, it is independent of the pressure inside the chamber. The reaction tube is built of parts which have a length between $1\,cm$ to $20\,cm$. This allows to chose the residence time of the sampled gas by varying the volume of the chamber.

The result of model calculations for the reaction kinetics of the conversion of CH_3O_2 radicals in pure synthetic air is shown in Figure 4.6(a). All resulting concentrations are normalized to the initial CH_3O_2 radical concentration. The CH_3O_2 radical concentration is reduced from 100 % to about 5 % within one second. In contrast, the HO_x radical concentration increases to a maximum value of 67 % at $0.6\,s$ and decreases slightly for a longer reaction time. The OH radical concentration is small and not shown in Figure 4.6. Yields of loss reactions (Figure 4.6(b)) are increasing with time. They limit the conversion efficiency to a maximum value of 67 %. Wall loss of HO_2 radicals is the dominant loss process as expected from the considerations in Section 4.5.2. In contrast, gas phase loss processes play a minor role.

An optimum reaction time for a maximum conversion efficiency of organic peroxy

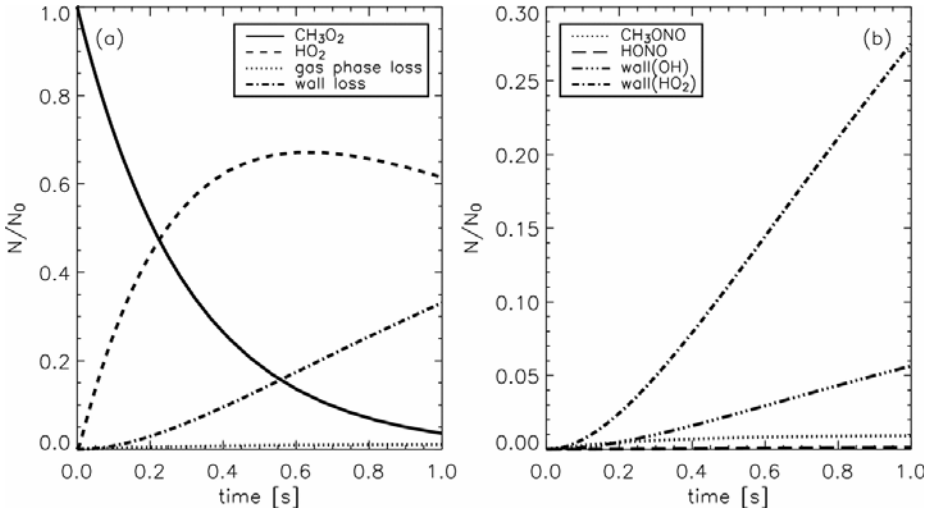

Figure 4.6: Reaction kinetics of the conversion of CH_3O_2 radicals at standard conditions (Table 4.3). Concentrations are normalized to the initial CH_3O_2 radical concentration N_0.

radicals of $0.6\,s$ can be concluded from this model calculation. This determines the length of the reaction tube to $83\,cm$ at a pressure of $25\,hPa$.

The HO_x yield in the reactor as a function of initially present OH and HO_2 radicals in the different measurement modes are shown in Figure 4.7. Yields are normalized to the initial HO_x concentrations. The HO_x yields for HO_2 and OH radicals differ in the HO_x mode I (dashed line) compared to the RO_x mode (solid line) because of small additional radical losses by reactions with NO. The kinetics for HO_2 and OH radicals are equal if CO is added in the RO_x mode and HO_x mode I because of the fast conversion of OH to HO_2 radicals.

The HO_x yields in HO_x mode I and II are identical for sampled HO_2 radicals because HO_2 radicals do not react with CO. In contrast, if the system is operated in HO_x mode II, a smaller HO_x yield for initially present OH radicals (dot dash) is obtained because of the high OH wall loss.

Figure 4.8 shows the comparison of the model results with the simplified analytic solution of the reaction kinetics calculated in Section 4.5.2. The simplified analytic solution predicts a mono-exponential decay of the initial concentration of organic peroxy radicals (Equation 4.29). The differences between modeled and analytic data are insignificant for CH_3O_2 radicals because the conversion reaction of organic peroxy with NO is dominant. Modeled and analytically calculated values of the HO_2 concentration (Equation 4.33) agree well in the beginning but differences are increasing for a longer reaction time because additional loss processes, mainly OH wall loss, is neglected in the analytic solution.

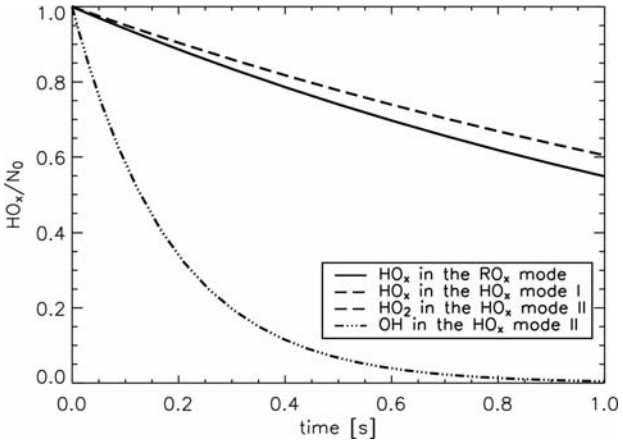

Figure 4.7: Model calculations of the HO_x yield in the reactor as a function of the reaction time for initially present HO_x or OH radicals in the RO_x and HO_x mode I/II. Values are normalized to the initial HO_x radical concentration N_0.

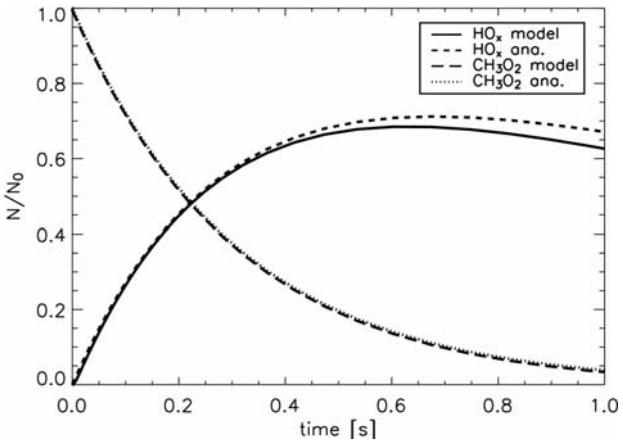

Figure 4.8: Reaction kinetics for the conversion of CH_3O_2 radicals at standard conditions (Table 4.3). Modeled data are compared to results from the simplified analytic solution of the reaction kinetics for HO_2 and CH_3O_2 concentrations. All concentration values are normalized to the initial radical concentration N_0.

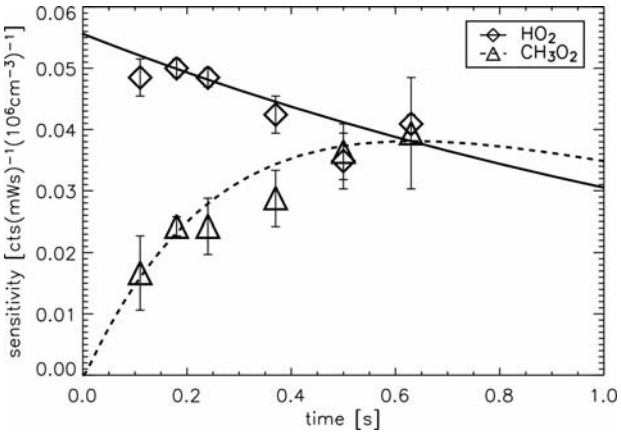

Figure 4.9: Measured sensitivities (symbols, error bars 1σ standard deviations) for CH_3O_2 and HO_2 radicals at standard conditions (Table 4.3). HO_x yields derived by numerical model calculations (solid and dashed lines) are scaled to the measured values.

The model results of the reaction kinetics are also compared to measured data in Figure 4.9. The reaction time in the reactor was varied by changing the length of the reaction tube during these measurements. Other experimental parameters were kept constant (standard conditions, Table 4.3). Sensitivities for both, HO_2 and RO_2 radicals, were determined for each length in a separate calibration measurement (see Chapter 5). The relative trend of the sensitivities can be compared to the modeled yield of HO_2 because changes in the measured sensitivities are only caused by changes in the yield of HO_2 radicals sampled into the fluorescence cell. Absolute values are not comparable because the fluorescence detection sensitivity of the instrument is not included in the chemical model. The initial concentrations of CH_3O_2 respectively of HO_2 radicals are set to the concentrations provided by the radical source for model calculations.

The relative trend of the modeled HO_x concentrations is scaled to the measured sensitivities. A good agreement is achieved within the specified measurement errors which result from the reproducibility of the measurements. Variations in the error values are caused by variations of the system's performance. The good agreement of the time dependence derived from measurements and numerical and analytic calculations (Figure 4.8 and 4.9) supports the validity of the model calculations and the analytic solution of the reaction kinetics. The chemical system is mainly determined by the lifetime of RO_2 radicals with respect to the reaction with NO leading to the conversion of RO_2 to HO_2 radicals. In addition, the conversion efficiency is mainly limited by the HO_2 wall loss.

4.7.2 Dependence on temperature and pressure

Yields of loss reactions cannot be suppressed selectively at a certain temperature in the system. The dependence of reaction rate constants of the conversion reactions and the dominant loss reactions on temperature are small within the range of ambient temperature. Therefore, the system is not heated or cooled actively.

The pressure is chosen that the reaction rate constants of termolecular loss reactions like the formation of nitrites (Reaction R4.2), nitrates (Reaction R2.10) and HONO (Reaction R2.17) are suppressed. This requires pressure reduction. However, wall loss rates increase with decreasing pressure because the diffusion length increases and therefore the probability that radicals reach the wall. The opposed character of the pressure dependence demands a compromise between minimization of wall losses and gas phase losses in the system.

The finally applied pressure of $25\,hPa$ was found in an iterative, experimental optimization of the conversion efficiency. The optimum pressure could not be determined easily by model calculations because reasonable model calculations require the knowledge of wall loss rates which were not measured for a larger number of pressure values. Furthermore, the pressure dependence of the conversion efficiency is difficult to investigate systematically by experiments because the pressure in the reactor also strongly influences the gas expansion into the fluorescence cell and thus the detection sensitivity in the second chamber.

4.7.3 Wall loss reactions

The observed wall loss rate depends on two factors. Firstly, radicals must reach the wall. This process can be described by diffusion. Secondly, radicals have to react chemically with the wall resulting in products which terminate the radical reaction chain. The observed loss rate k^{wall} can be described by the collision rate k_{coll} and the wall reaction rate k_{loss} (*Poeschl et al.*, 1998):

$$(k^{wall})^{-1} = k_{coll}^{-1} + k_{loss}^{-1} \tag{4.45}$$

Theoretical investigations of the wall loss are reported e.g. by *Brown* (1977); *Murphy and Fahey* (1987); *Bertram et al.* (2001). The two rates in Equation 4.45 can be expanded using the diffusion coefficient, the geometry of the reactor, pressure and average velocity of the gas inside the reactor. Diffusion increases with decreasing pressure because of the decreasing collision probability between molecules. Therefore, the average free path length increases and the average time of a molecule needed to reach the wall becomes shorter. In addition, the collision rate decreases with increasing diameter of the tube. k_{loss} is specific for the surface material. In this instrument, the radius of the tube is constrained by the entire design of the instrument and was not varied. A suitable value for the pressure was found experimentally at $p = 25hPa$.

Wall loss rates for OH and HO_2 radicals were measured for these conditions by varying the length of the reaction tube. This results in a variation of the residence time of the sampled gas. The fluorescence signal obtained if gas was sampled from

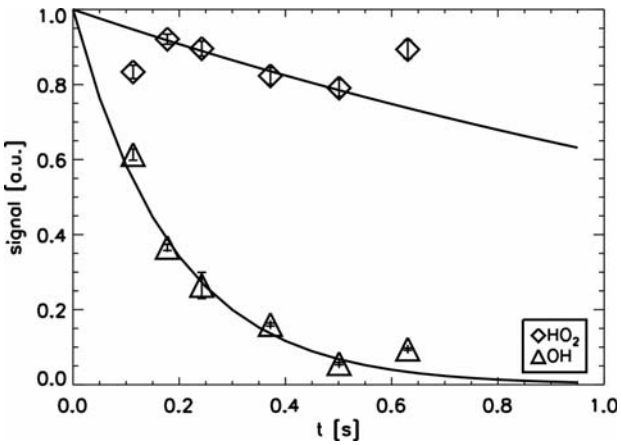

Figure 4.10: Measured fluorescence signals (symbols) depending on the reaction time without addition of reactive gases in the reactor measured for initially present radicals OH and HO_2 ($p = 25hPa$, error bars 1σ standard deviations). The wall loss rate in the reactor can be determined by fitting a mono-exponential decay (lines). Values are normalized to the signal expected from the fit function at $t = 0$.

the radical source is normalized to the radical concentration which was provided by the radical source. The system was operated without addition of reactive gases in the reactor so that initial radical concentrations are only reduced by wall loss reactions. The wall loss rate is obtained by fitting the signal to a mono-exponential decay:

$$S_i(t) = S_{0i} \exp(-k_i^{wall} t). \tag{4.46}$$

The radical source can provide either equal concentrations of OH and HO_2 radicals or only HO_2 (Chapter 5). The HO_2 wall loss rate can be determined by measurements if only HO_2 radicals are sampled. Only OH radicals are detected if NO is not added into the fluorescence cell. From this measurements the OH wall loss rate can be calculated. Figure 4.10 shows the measured fluorescence signals depending on the residence time of the sampled gas in the reactor. Values are normalized to the values expected from the fit functions at $t = 0$. The decay parameter of the fit function refers to the observed wall loss rate (Equation 4.46). A loss rate of $k_{\mathrm{OH}}^{wall} = (5.4 \pm 0.2)\, s^{-1}$ for OH and of $k_{\mathrm{HO_2}}^{wall} = (0.5 \pm 0.1)\, s^{-1}$ for HO_2 is obtained. The wall loss rate for OH radicals is larger than that for HO_2 radicals, as expected from their higher reactivity. These values are used for all model and analytic calculations presented in this work. Deviations between the fit functions and measured values cannot be explained completely by the statistical error of the measurements. This may be caused by changes in the system's performance between measurements which included to shut down the system completely and to disassemble the conversion reactor.

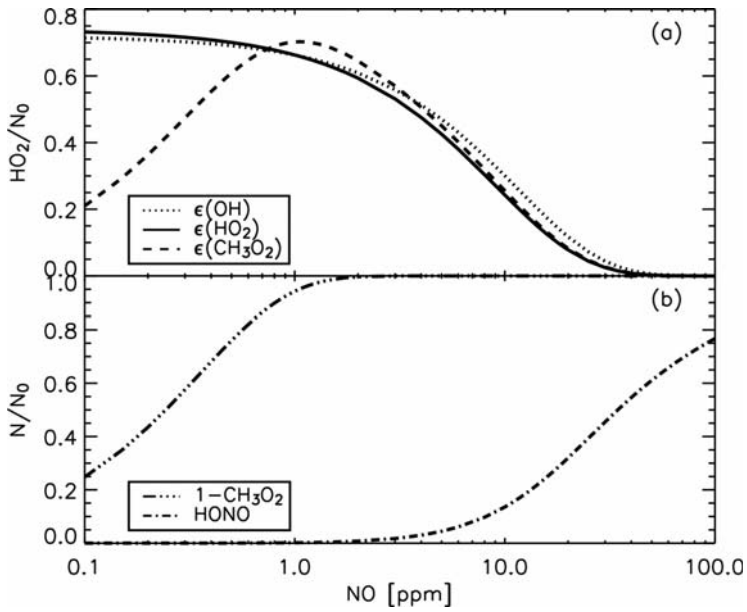

Figure 4.11: Model calculations of the conversion efficiency for CH_3O_2 radicals $\epsilon_{CH_3O_2}$ (dashed), the HO_2 yield for OH radicals ϵ_{OH} (dotted) and for HO_2 radicals ϵ_{HO_2} (solid) depending on the NO concentration (Figure (a)). Other parameter are set to standard values (Table 4.3). The yield of HONO formation (dash dot) and the part of the converted CH_3O_2 radicals (dash dot dot) in the RO_x mode are shown in Figure (b). Concentrations are normalized to the initial radical CH_3O_2 concentration.

4.7.4 Dependence of the conversion efficiency on NO

The sensitivity of the system for organic peroxy radicals depends substantially on the NO concentration in the reaction tube. On the one hand, the NO concentration determines the lifetime of peroxy radicals in the reactor by initiating the conversion process of RO_2 to HO_2 radicals. On the other hand, NO is involved in gas phase radical losses in the reactor (Figure 4.6). The optimum NO concentration value was determined firstly by model calculations (Figure 4.11). The NO concentration is varied while other parameters are kept constant (Table 4.3). Figure 4.11 (a) shows the HO_2 radical yield which is expected from the numerical model for initially present RO_2, HO_2 and OH radicals. Figure 4.11 (b) illustrates the limitations of the RO_2 conversion.

The conversion efficiency for RO_2 radicals increases with increasing NO concentration. This can be explained by the increasing fraction of radicals (Figure 4.11 (b)) which are converted to HO_2 in the reaction with NO (Reaction R2.10). The conversion efficiency reaches a maximum of nearly 70 % at a NO mixing ratio of about 1 *ppmv* and decreases with further increasing of the NO concentration for two reasons. Firstly,

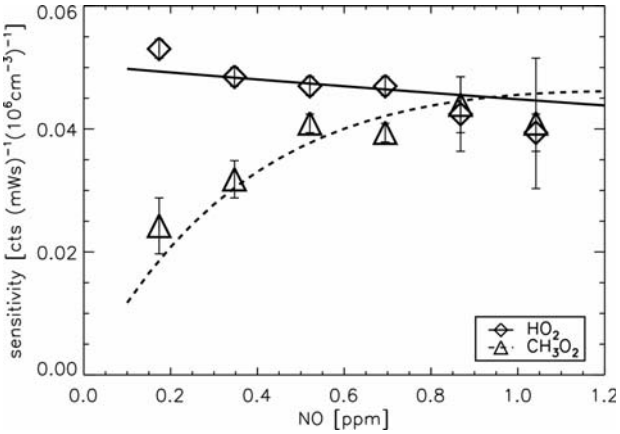

Figure 4.12: Measured sensitivities (symbols) for HO_2 and CH_3O_2 radicals depending on the NO concentration in the reactor (error bars 1σ standard deviations). Other parameter are set to standard values (Table 4.3). Results of model calculations (solid lines) are scaled to the measured trend.

the HO_x radical formation becomes faster leading to a higher yield of radical losses because HO_x radicals are more reactive than RO_2. Secondly, HONO formation (chain terminating Reaction R2.17) becomes dominant over the OH reaction with CO (chain continuing Reaction R2.1). An analogue consideration applies for the competing reaction of alkoxy radicals with oxygen (Reaction R2.11) and NO (Reaction R4.2).

In the case of HO_2, there is no production process which is driven by the NO concentration. The yield of HO_2 radicals is only limited by wall and gas phase loss reactions in the HO_x reaction cycle and decreases with increasing NO concentration (Figure 4.11) because of increasing losses by gas phase reactions. Similar results as for HO_2 apply to OH radicals because OH radicals are almost instantaneously ($\approx 6ms$) converted to HO_2 radicals in the reaction with CO. Small differences occur for small NO concentrations because the conversion of HO_2 to OH in the reaction with NO becomes slow and OH loss processes become unimportant for initially present HO_2 radicals but apply for initially present OH.

Model results are compared to measurements in Figure 4.12. The dependence of measured sensitivities for CH_3O_2 and HO_2 radicals on the added NO concentration is shown. Other parameters are kept constant at their optimum values (Table 4.3). Absolute values of modeled and measured data cannot be compared due to the additional influence of the sensitivity of the fluorescence detection which is not included in the model. However, relative trends are comparable. A good agreement between the trend of the measurements and the calculations is achieved within the specified errors which result from the reproducibility of the measurement.

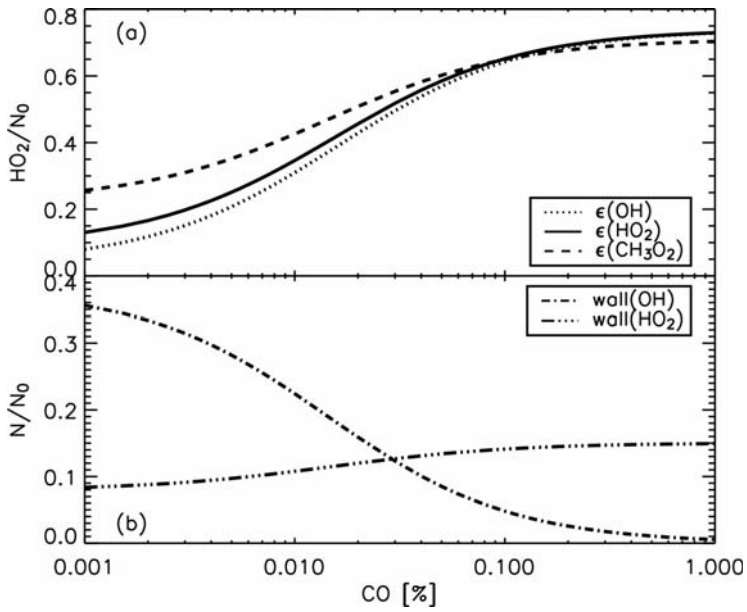

Figure 4.13: Model calculations of the conversion efficiency for CH_3O_2 radicals (dashed) and the HO_2 yields for HO_2 (dashed) and for OH radicals (dotted) depending on the CO concentration in the reactor (a). Other parameters are kept constant (Table 4.3). Yields of wall loss reactions of either OH (dash dot) and HO_2 (dash dot dot) are shown in (b) for the conversion of CH_3O_2. Concentrations are normalized to the initial CH_3O_2 radical concentration N_0.

4.7.5 Dependence of the conversion efficiency on CO

In contrast to NO, it is not necessary to add CO for the RO_2 conversion process. CO is rather added to reduce yields of loss processes. A reaction cycle between HO_2 and OH radicals is initiated in which the equilibrium is shifted to HO_2 because yields of both wall loss and gas phase loss reactions are smaller for HO_2 radicals than for OH radicals. Model calculations were done with either initially present concentrations of CH_3O_2, HO_2 and OH radicals in order to estimate the necessary CO concentration. Figure 4.13 shows the conversion efficiency of RO_2 radicals and the HO_2 yields for HO_2 and OH radicals in the reactor depending on the CO level. All other parameters are set to their optimum values (Table 4.3).

The CO concentration mainly determines the ratio of the HO_2 to the OH concentration. There are no other relevant reactions known involving CO beside the conversion reaction of OH to HO_2 in the HO_x cycle. The conversion efficiency for RO_2 radicals as well as the yields for HO_2 and OH radicals increase with increasing CO concentration because of the increasing ratio of HO_2 to OH radical concentrations. This mainly leads

to a decrease of the overall wall loss yield. The increasing HO_2 radical wall loss is overcompensated by the decreasing OH wall loss (dash dot and dash dot dot line in Figure 4.13). Efficiencies saturate with further increase of the CO concentration because the OH radical concentration becomes negligible. The resulting HO_2 yields remain below the maximum value of 1.0 because HO_2 wall loss reactions cannot be avoided.

The dependencies on the CO concentration are similar for RO_2, HO_2 and OH radicals. Differences occur for smaller CO concentrations when OH is essentially present because a certain time is needed to convert peroxy radicals to OH which is even longer for RO_2 than for HO_2. The longer it takes to convert peroxy radicals to OH, the smaller are yields of OH loss processes. They are highest for OH radicals which are directly sampled because competition between loss reactions and the reaction with CO starts immediately. Therefore, the HO_2 yield for sampled OH radicals is smaller than for HO_2 and CH_3O_2 radicals and the yield for HO_2 is smaller compared to that for CH_3O_2 for low CO concentrations.

Verification of the model calculations with experiments is technically difficult because of the way how RO_2 radicals are produced in the radical source. RO_2 radicals are formed in the reaction of OH, produced by water photolysis, with hydrocarbons added to the calibration gas in the radical source (see Chapter 5). This requires a high concentration of hydrocarbons which then is also present in the conversion reactor of the detection system. In this case, the reaction of OH radicals with hydrocarbons becomes significant at low CO concentrations. Therefore, it is not reasonable to perform calibration measurements at low CO concentrations in the conversion reactor. Accordingly, experimental verification of the dependence of the conversion efficiency on the CO concentration was not attempted.

4.7.6 Absolute detection sensitivities for CH_3O_2 and HO_2 radicals

Measured sensitivities (Table 4.6) can be compared to results of the modeled kinetics by regarding the HO_x yields at $t = 0.6\,s$ (Figure 4.6, 4.7). Only relative values are comparable because the model considers the conversion efficiency in the reactor and does not include the detection in the fluorescence cell.

The RO_2 sensitivity predicted by the model is slightly smaller than the sensitivities for HO_2 and OH radicals. In contrast, the measured RO_2 sensitivity is larger than the HO_2 and OH sensitivities. Equal sensitivities for OH and HO_2 in the RO_x and HO_x mode I are expected from the numerical model. In addition, the predicted sensitivities in the RO_x mode are slightly smaller than in the HO_x mode. Whereas this behavior can be observed for the measured OH sensitivities, the HO_2 sensitivity is considerably larger in the HO_x mode I than in the RO_x mode. In addition, measured HO_2 sensitivities in RO_x and the HO_x mode I are larger than the measured OH sensitivities.

In contrast, measured sensitivities in the HO_x mode II show the expected behavior. Whereas the HO_2 sensitivity is not influenced by the addition of CO, the OH sensitivity becomes small in the absence of CO.

Table 4.6: Sensitivities [a] of the "SaphirLIF" system measured on the 2006-06-14 compared to relative sensitivities predicted by the numerical model.

		RO_x MODE (NO,CO)	HO_x MODE I (CO)	HO_x MODE II (N_2)
meas.	CH_3O_2	0.142 ± 0.007	-	-
	HO_2	0.119 ± 0.003	0.191 ± 0.002	0.210 ± 0.004
	OH	0.086 ± 0.005	0.112 ± 0.005	0.02 ± 0.005
model	CH_3O_2	0.67	-	-
	HO_2	0.70	0.74	0.74
	OH	0.70	0.74	0.04

[a] $[cts(mWs)^{-1}\,(10^6\,cm^{-3})^{-1}]$

Discrepancies between model results and measured sensitivities must be caused by additional processes which are not included in the model. Radical losses at the inlet of the conversion reactor may lead to different sampling efficiencies for the radical species. Especially the transmission through the sampling nozzle of highly reactive OH radicals may be considerably smaller than that of HO_2 and RO_2. In addition, radical losses on surfaces between the sampling nozzle and the mixing of the reactive gases and on surfaces provided by the inlet of reactive gases may affect the radical yields. Radical losses would explain the reduced OH sensitivities and the smaller sensitivity of HO_2 compared to CH_3O_2 in the RO_x mode.

However, the difference between the HO_2 sensitivities in the RO_x and HO_x mode cannot be explained easily. The addition of NO in the RO_x mode must affect the HO_2 yield. This may be related to the area where reactive gases are mixed to the sampled gas flow. The inlet of reactive gases acts as a point source. This may lead to locally high NO mixing ratios which may cause HO_2 losses in unknown reactions.

4.7.7 Sensitivity to different RO_2 radicals

The sensitivity may not be identical for different organic RO_2 radicals because reaction constants of RO_2 and RO radicals may differ (Table 4.7). The sensitivity to different RO_2 radicals concerns only in the conversion efficiency ϵ_{RO_2} in Equation 4.9 whereas the HO_2 conversion efficiency and the OH fluorescence detection sensitivity in the fluorescence cell are independent of the radical's origin.

Firstly, the reaction of RO_2 with NO (Reaction R2.10) which is the limiting step in the reaction chain determining the time needed for the conversion to HO_2 has to be taken into account. Differences in the reaction constants of RO radicals with oxygen (Reaction R2.11) are less important because this reaction is fast. In addition, yields of loss processes may be different (formation of nitrates (Reaction R2.10) and nitrites (Reaction R4.2), decomposition and isomerization (Reaction R4.9 and R4.8) and wall loss reactions).

Reaction constants of the RO_2 reaction with NO do not differ much for most of

Table 4.7: Comparison of expected and measured relative conversion efficiencies ϵ_{RO_2} for different organic peroxy radicals.

HYDROCARBON	RO_2 RADICAL	$k_{NO}[10^{-12}\,s^{-1}]$ [a]	$\epsilon_{RO_2}/\epsilon_{CH_3O_2}$ model. [b]	meas.
methane	CH_3O_2	7.7 ± 1.1 [c]	1.00 ± 0.04	1.00 ± 0.05
ethane	$C_2H_5O_2$	8.7 ± 1.7 [c]	1.03 ± 0.04	0.91 ± 0.03
propane	$C_3H_7O_2$	9.0 ± 0.9 [d]	1.04 ± 0.02	0.96 ± 0.04
iso-butane	$C_4H_8O_2$	7.9 ± 1.3 [e]	1.01 ± 0.04	0.59 ± 0.04
ethene	$C_2H_4O_2$	8.4 [f]	1.02	0.98 ± 0.05
isoprene	$C_5H_8(OH)O_2$	9.0 ± 3.0 [g]	1.04 ± 0.07	1.21 ± 0.06

[a] reaction rate constant of the reaction $RO_2 + NO \rightarrow RO + NO_2$
[b] calculated by Equation 4.35
[c] *NASA* (2003)
[d] *IUPAC* (2005)
[e] *Eberhard and Howart* (1997)
[f] *MCM* (2003) without error estimation
[g] *Zhang et al.* (2003)

the important organic peroxy radicals as discussed in Section 4.5.1. For this reason, conversion efficiencies are expected to be in the same range. However, this has to be investigated experimentally because of the complexity of the chemical mechanisms.

Calibration measurements were performed for different organic peroxy radicals using the radical source as described in Chapter 5. Different hydrocarbons were added to the calibration gas of the radical source leading to the formation of organic peroxy radicals in the reaction with OH which is produced by water photolysis. Concentrations of added hydrocarbons are high enough to convert nearly all OH radicals between the point of OH radical production in the radical source and the point of sampling into the reaction tube of the LIF-system. In addition, the lifetime of OH radicals with respect to the reaction with the added hydrocarbon is large compared to their lifetime with respect to the reaction with CO added in the conversion reactor. Otherwise, the conversion efficiency of organic peroxy radicals would be influenced by the reaction of hydrocarbons with OH.

Sensitivities for radicals produced in the reaction of OH with methane, ethane, propane, iso-butane, ethene and isoprene were measured. Pure methane (purity 5.5) was provided by Air Liquide, all other hydrocarbons by Linde (purity 3.5). Liquid isoprene was evaporated and mixed with pure nitrogen (mixing ratio $500\,ppmv$). Values of the measured sensitivities shown in Table 4.7 are normalized to the sensitivity measured for CH_3O_2 radicals.

The measured sensitivities of the system for methylperoxy, ethylperoxy, and propylperoxy radicals as well as for peroxy radicals formed in the reaction of ethene with OH are equal within the range of 10 % (Table 4.7). Measurements are compared to expected relative sensitivities calculated by using Equation 4.33. Both agree for most of

the tested RO_2 radicals within the 2σ errors of the measurements and of the calculated values. The error in the calculation results from the uncertainty in the reaction rate constant. Discrepancies between relative measured and calculated sensitivities can be expected due to the specific losses of organic peroxy radicals which are not included in the analytic expression. This may also explain the trend to smaller measured sensitivities for larger organic peroxy radicals (Section 4.5). Larger discrepancies of the measured sensitivities occur for peroxy radicals formed in the reaction of iso-butane which cannot be explained easily. Experimental artifacts or unnoticed systematic errors cannot be excluded.

The results indicate that the conversion efficiency of RO_2 radicals is not very sensitive to deviations in the reaction rate constant of the NO reaction with RO_2 radicals. This could be explained by the relatively broad maximum of the time dependent conversion efficiency as can be seen in Figure 4.6.

There are two studies which support the experimental results in this work. *Edwards et al.* (2003) investigated the sensitivity of the PerCIMS instrument to several organic peroxy radicals. The measured sensitivities vary only within 10 % for most of the tested radicals including radicals which were tested in this work. The chemical steps for the conversion of RO_2 to HO_2 radicals are the same as used in the current instrument (Figure 3.1). Therefore, a similar behavior is expected. It is notable that the measured sensitivity for peroxy radicals formed in the reaction of iso-butane reported by *Edwards et al.* (2003) is about 20 % smaller than the calculated value like it is found for this instrument.

Secondly, peroxy radical concentrations were determined by two different instruments (PERCA and MIESR) during the BERLIOZ field measurement campaign (*Platt et al.*, 2002). Measurements of both instruments are in agreement. The radical chain reaction in PERCA systems is similar to that of the PerCIMS and to the current instrument (Figure 3.1). In contrast, the measurement principle of the MIESR instrument is totally different (Section 3.2). Possible differences of reaction constants of reactions of NO with organic peroxy radicals do not play any role for MIESR measurements. The good agreement between the two measurements suggests that differences of the sensitivities to different RO_2 radicals of the used PERCA instrument are smaller than the error of the MIESR instrument (typical error 10 %). This applies only for the mixture of RO_2 radicals measured during this campaign but *Mihelcic et al.* (2003) showed for two days of the campaign that more than 60 % of the RO_2 radicals resulted from alkanes and isoprene.

4.7.8 Sensitivity dependence on water vapor content

It is expected that the sensitivity of the instrument depends on the water vapor content in the sampled gas because the OH fluorescence is quenched efficiently by water vapor (Table 4.5). In addition, it is known that the sensitivity of PERCA systems for peroxy radicals strongly depends on the relative water vapor content (Chapter 3). An additional radical chain terminating reaction in the HO_x cycle is suggested (*Mihele and Hastie*, 1998a,b), possibly the formation of HNO_3 in the reaction of HO_2 radicals

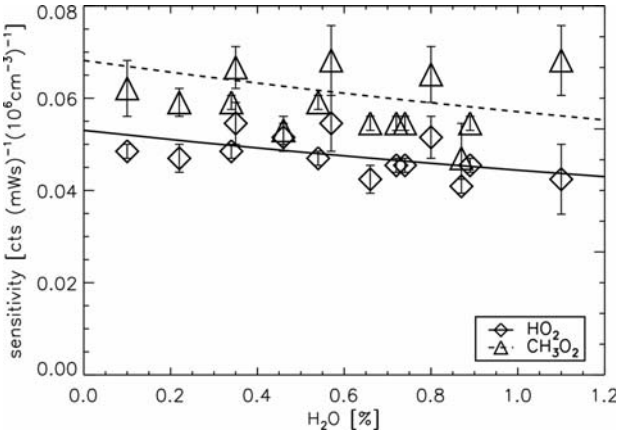

Figure 4.14: Measured sensitivities (symbols) for HO_2 and CH_3O_2 radicals depending on the H_2O mixing ratio in the reactor (error bars 1σ standard deviations). The relative trend of model calculations (solid lines) is scaled to the measured data.

with NO (*Butkovskaya et al.*, 2005). The reaction constant of this reaction depends on the water vapor content in the sampled air. This could be explained by the formation of radical water complexes (*Aloisio and Francisco*, 1998; *Aloisio et al.*, 2000). Alternatively, a catalytic function of water is discussed (*Butkovskaya et al.*, 2005).

The radical chain reaction in the present system is similar to that in PERCA systems (Figure 3.1). Therefore, a water vapor dependence has to be investigated. The sensitivity of the system is determined from calibration measurements (Chapter 5) in which the water vapor content of the calibration gas is varied (Figure 4.14). The sensitivity of the system for both, CH_3O_2 and HO_2 radicals, shows a water vapor dependence in the order of 20 % for H_2O mixing ratio of 0 % to 1 %. The relative trend of measured sensitivities (symbols) is compared to the trend expected from fluorescence quenching (lines). The measured and modeled water dependence agree well. This suggests that the dependence can be explained by fluorescence quenching. An additional dependence like for PERCA systems which is in the order of a factor of 5 between 0 % to 50 % relative humidity cannot be found. This is consistent with the interpretation of the water vapor dependence in PERCA systems. An additional loss of less than 1 % during each HO_x cycling is required to explain the observed water dependence (*Reichert et al.*, 2003). A long chain length is desired to produce a high amplification factor (about 150) in PERCA systems. Yields of loss reactions grow exponentially with the chain length. If the yield of a reaction changes about 1 % the overall loss yield accumulates to about 60 % for a chain length of 150. Therefore, a considerably large effect on PERCA systems is expected. In contrast, the chain length of the present system is between 1 to 2 for RO_2 and HO_x radicals, respectively (Equation 4.40, 4.39) so that an additional small loss process does not accumulate and does not influence the resulting radical

yields.

4.7.9 Photolytic interferences

The measurement of ambient RO_x radical concentrations with LIF may be subject to photolytic interference signals. These are signals which are caused by laser generated radicals contributing to the sampled radicals. Interference signals can be seen as additional variable background signals which have to be subtracted from the measured signal. The height of the signal depends on the concentration of the sampled species causing the interference. For example, ozone is known to cause interference signals in the HO_x detection system using LIF technique (*Holland et al.*, 1995, 2003; *Weber*, 1998). The possible mechanism for the ozone depending background signal is ozone photolysis followed by the reaction of $O(^1D)$ with ambient water forming OH radicals (Reaction R2.13 and R2.15). Two photons are necessary to produce additional fluorescence photons. One is needed for the photolysis of ozone and the second one for the excitation of the produced OH radicals. The interference signal was found to correspond to about $3 \cdot 10^5\, cm^{-3}$ per $50\, ppbv$ ozone for a previous instruments and was always corrected in the data evaluation (*Holland et al.*, 2003). It is expected that an ozone interference is also present for the RO_2 detection in this work because of the similar design of the fluorescence cell. Therefore, the possible interference signal was determined by sampling pure synthetic air with various mixing ratios of ozone and a constant water vapor mixing ratio about 0.7 % supplied by the radical source (Chapter 5). The ozone mixing ratio was measured in the excess gas of the radical source using a commercial ozone analyzer (Ansyco, ozone Photometer 41M).

The measured interference signal increases with increasing laser power and ozone concentration (Figure 4.15) as expected from a photolytic source. The measured normalized count rates can be converted to equivalent RO_x concentration values to be comparable to ambient radical concentrations. Equivalent concentrations are about $5 \cdot 10^6\, cm^{-3}$ for an ozone concentration of $100\, ppbv$ and a typical laser power of $25\, mW$. This is small compared to RO_x concentrations usually found during the day (in the order of $10^8\, cm^{-3}$). The linear function, fitted to the ozone dependence of the interference signal (right panel Figure 4.15), is used for correction of ambient air measurements during which the ozone concentration is variable. The laser power dependence is not taken into account because variations are usually small (within the range 10 %).

The addition of NO into the fluorescence cell also causes artificial HO_x radicals leading to an interference signal in ambient air measurements. Again, the source has a photolytic character as can be seen from the dependence of the interference signal on the laser power (Figure 4.15). The chemical compound causing the interference is most likely HONO which is present as a contaminant in the NO gas. In order to keep the HONO contamination small, the NO gas runs through a cartridge with Ascerite which absorbs the nitrous acid before it is injected into the fluorescence cell. The photolytic interference was found to be more than a factor of ten larger without purification of the NO.

The NO related interference is regularly checked during the calibration of the in-

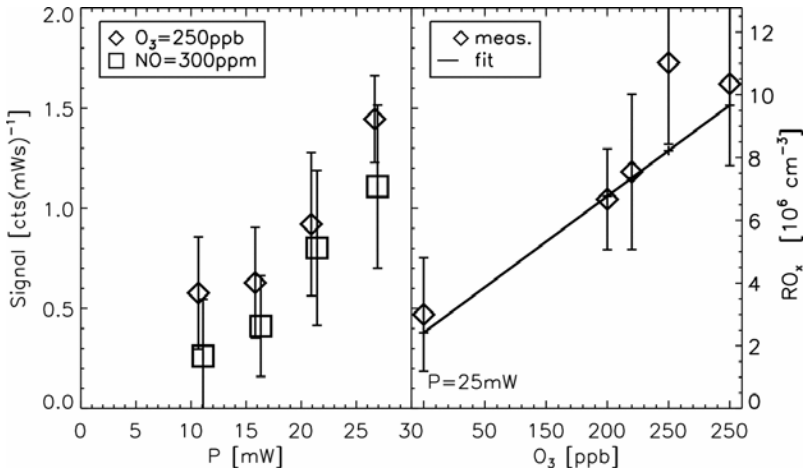

Figure 4.15: Interference signals in the fluorescence cell caused by ozone and NO depending on the laser power (left panel). The ozone interference signal at a constant laser power was fitted to a linear function (right panel). The left axes shows normalized count rates and the right axes equivalent RO_x radical concentrations.

strument. It is always subtracted from the measured signal because NO is constantly present in the fluorescence cell. However, the equivalent radical concentration of about $5 \cdot 10^6\, cm^{-3}$ is small compared to typical RO_x concentration values.

Beside the photolysis of ozone, photolysis of ambient hydrogen peroxide (H_2O_2), HCHO, HNO_3 and HONO which can be contained in the sampled air may lead to interferences. *Weber* (1998) calculated that possible interference signals caused by these photolysis reactions are small compared to that caused by the ozone/water interference for the previous HO_x-LIF instrument which contains a similar fluorescence cell. Therefore, it can be assumed that this also applies for the new instrument.

4.7.10 Possible chemical interferences

Beside background signals caused by ozone photolysis in conjunction with the reaction of $O(^1D)$ with water and by the addition of NO into the fluorescence, further possible sources of artificial production or destruction of radicals have to be considered.

Firstly, the high concentration of NO in the fluorescence which is added to convert HO_2 radicals to OH could lead principally to the conversion of RO_2 radicals in the HO_x mode of the system because the same chemical conversion reaction as in the conversion reactor would be possible in the fluorescence cell. This would lead to an additional unnoted fluorescence signal in the HO_x mode in which no detection of RO_2 radicals is assumed. However, the efficiency of a possible RO_2 conversion in the fluorescence cell is expected to be negligible because the time between the addition of NO and the

detection of OH with LIF (about $240\,\mu s$, *Weber* (1998)) is much smaller than the time needed for the conversion of RO_2 radicals (about $33\,ms$). This is mainly caused by the large reduction of the oxygen number density at the low pressure of $3.5\,hPa$ in the fluorescence cell. Oxygen is needed for the conversion reaction of RO radicals to HO_2 (Reaction R2.11). In addition, it is shown experimentally in Section 5.2 that a possible interference caused by CH_3O_2 radicals can be excluded with an accuracy of 1.5 %.

Interferences discussed so far only concern the fluorescence cell. Artificial production or destruction of radicals in the conversion reactor may also be related to changes of the reaction kinetics by trace gases contained in ambient air. This mainly concerns reactions with NO and NO_2. Ambient NO increases the NO level in the reactor. This changes possibly the reaction kinetics of the conversion process. In addition, both, ambient NO and ambient NO_2, may cause additional radical losses (HONO formation (Reaction R2.17), HNO_3 formation (Reaction R2.23)). The influence of an increased NO and additional NO_2 level on the conversion efficiencies can be determined by calculating the resulting radical concentrations using Equation 4.25.

If the NO_x concentration is increased by $50\,ppbv$ NO and $100\,ppbv$ NO_2, the conversion efficiency of radicals in the RO_x mode is almost unchanged (about 0.5 % smaller). Thus, the detection sensitivity of the RO_x is essentially independent of ambient NO_x, even in strongly polluted air. On the one hand, the conversion efficiency is not sensitive to small changes of the NO concentration in the reactor (Figure 4.12) and on the other hand, additional radical losses are negligible. The latter applies also in the HO_x mode.

However, considerable changes of the reaction kinetics can occur for high ambient NO concentrations in the HO_x mode I and II of the system. On the one hand, the ambient NO concentration may allow that RO_2 radicals are converted to HO_2 leading to an interference signal in the HO_x mode. The conversion efficiency is less than 2 % for ambient NO mixing ratios of less than $10\,ppbv$ but can reach values of 20 % for exceptionally high ambient NO mixing ratios of $100\,ppbv$ as can be seen in Figure 4.12. This indicates that sensitivities in high NO environments have to be investigated carefully with respect to the possibility of a conversion of RO_2 radicals in the HO_x mode. To avoid this, one could think of diluting the sampled air with pure nitrogen as done in the ROxMas instrument in order to change between the RO_x and HO_x mode (*Hanke et al.*, 2002). The addition of pure nitrogen would slow down both the conversion of RO_2 to RO radicals in the reaction with NO (Reaction R2.10) as well as the formation of HO_2 in the conversion of RO to HO_2 radicals (Reaction R2.11) by diluting the reaction partners NO and O_2.

On the other hand, the equilibrium between HO_2 and OH radicals can be changed by ambient NO in the HO_x mode II if CO is not added. Ambient NO would shift the equilibrium between HO_2 and OH radicals towards OH, leading to higher radical losses because of the higher OH wall loss rate compared to that of HO_2 radicals. Then, the HO_2 sensitivity would be considerably smaller for exceptionally high NO levels (about 20 % for a NO mixing ratio of about $100\,ppbv$). This can be avoided if CO is always added as done in the HO_x mode I because OH is suppressed by the fast reaction of OH with CO (see Section 4.4).

Artificial radical production from the decomposition of peroxy acetyl nitrate (PAN,

$CH_3COO_2NO_2$) and peroxynitric acid (PNA, HO_2NO_2) has been discussed for chemical amplifier systems e.g. by *Hastie et al.* (1991); *Cantrell et al.* (1993); *Reiner et al.* (1997). Both trace gases decompose easily whereby the decomposition rate depends on temperature and pressure. Possible interferences caused by the decomposition of PAN or PNA are less likely in this instrument compared to chemical amplifier systems (*Reiner et al.*, 1997) because of the reduced pressure in the conversion reactor which leads to smaller decomposition rates.

The temperature dependence does not play any role in this system because the sampled gas remains at ambient temperature. Typical PAN concentrations are within the range of 100 *pptv* to 1000 *pptv* (*Bottenheim et al.*, 2005; *Carpenter et al.*, 2000). Taking the upper limit of 1000 *pptv*, a peroxy radical production rate of about $9.5 \cdot 10^6\, cm^{-3}s^{-1}$ can be expected from PAN decomposition at a temperature of 25 °*C* (*NASA*, 2003). Thus, an interference signal which is in the range of the instrument's detection limit is possible for high PAN concentrations.

PNA can serve as a reservoir of HO_2 radicals at low temperatures and high NO_2 concentrations. *Reiner et al.* (1997) calculated typical PNA mixing ratios of about 4 *pptv* obtained by model calculations described by *Kanikidou et al.* (1991). This leads to an HO_2 production rate of about $8.8 \cdot 10^6\, cm^{-3}s^{-1}$ at a temperature of 25 °*C* (*NASA*, 2003). An interference signal in the range of the instrument's detection limit is possible for high PNA concentrations like for the decomposition of PAN.

Therefore, both PNA and PAN decomposition have to be taken into account as possible sources of interference signals if measurements are performed in environment in which very high PNA and PAN concentrations are expected.

4.8 Error discussion and detection limit

The precision describes the error with respect to the reproducibility of the measurement and the accuracy refers to systematic errors.

The value of the measurement's precision can be calculated from the statistics of a noisy signal if the same physical value is determined several times. The signal noise in the presented system is mainly determined by the statistics of photon counting (Poisson statistics).

The reproducibility of the signal derived during a calibration measurement can be taken as precision assuming that the radical concentration (about $1 \cdot 10^8\, cm^{-3}$) provided by the radical source does not change on a short time scale. This results in a 1σ precision (standard deviation of the calibration measurement) of 2 % for HO_x and RO_x radical concentration measurements (integration time: 30*s*, laser power: 25 *mW*). The precision of derived HO_2 respectively RO_2 concentration values is worse because of the necessity to calculate these values from two or three measurements (Equation 4.5 and 4.6). This requires error calculations by using gaussian error propagation. The precision of HO_2 measurements is usually determined by the HO_x measurement because the OH radical concentration is much smaller than the HO_2 concentration under atmospheric conditions. The contribution of an error of the OH radical mea-

surement becomes negligible. Therefore, the precision of HO_2 radical measurements can be estimated to about 2 % from the precision of the HO_x measurement specified above.

In contrast, the precision of RO_2 radical concentration measurements is worse. HO_2 and OH concentration values have to be subtracted from the measured RO_x concentration. Errors in the OH radical measurement again hardly contribute to the precision. However, HO_2 radical concentrations are within the range of RO_2 concentrations leading to higher errors if the RO_2 radical concentration is calculated. This is enhanced by the fact that two HO_x radical measurements are interpolated to derive the HO_2 concentration at the same time that RO_x is measured. The precision of both measurements and the interpolation error contribute to the error of the RO_x measurement. The precision of RO_2 radical measurements can be estimated to about 4 % to 5 % from the precision of the HO_x and RO_x measurement specified above, assuming equal concentrations of HO_2 and RO_2 radicals

The accuracy of absolute concentration values is determined by the error of sensitivities calculated from calibration measurements. The accuracy of sensitivities is limited by the knowledge about the exact value of the radical concentration provided by the radical source. In contrast to the statistical error in the photon counting, the error in the sensitivities leads to a systematic error because this error applies to all concentration values in the same way. The 1σ accuracy of sensitivities which is derived from measurements using the radical source described in Chapter 5 is 10 % (Table 5.1, *Holland et al.* (2003)).

The detection limit is defined as the count rate at which the signal exceeds the 1σ·noise of the background by a factor SNR where SNR is the signal-to-noise-ratio.

The error of the measurement consists of several contributions. Firstly, the statistical error σ_{stat} of the measured signal adds to the noise, described by Poisson statistics of the photon counting. Secondly, the error of the background signal σ_{bg} which occurs if NO is introduced in the fluorescence cell contributes. In addition, one has to keep in mind that the sum of radicals, either RO_x or HO_x, is measured but only the RO_2 respectively the HO_2 radical concentration is desired. The part of the fluorescence signal caused by either HO_x respectively OH radicals can be seen as an additional background signal which has to be subtracted in the same way as the NO background signal. Therefore, the error in the HO_x (σ_{HO_x}) respectively the error in the OH (σ_{OH}) concentration also contributes to the detection limit. This results in a LOD (limit of detection) calculated by using error propagation if a certain signal to noise ratio SNR is demanded as:

$$LOD_{HO_2} = \frac{SNR}{C_{HO_2} P_{ex}} \sqrt{\sigma_{stat}^2 + \sigma_{bg}^2 + \sigma_{OH}^2} \tag{4.47}$$

$$LOD_{RO_2} = \frac{SNR}{C_{RO_2} P_{ex}} \sqrt{\sigma_{stat}^2 + \sigma_{bg}^2 + \sigma_{HO_x}^2} \tag{4.48}$$

Absolute count numbers are required for calculating the detection limit. The LOD is converted to a concentration value by applying the calibration factor $C_k \cdot P_{ex}$ (C_k: normalized sensitivity, P_{ex}: laser power).

Table 4.8: Detection limits for HO_2 and RO_2 radical concentrations for the "MobiLIF" instrument used in this work [a].

$\sigma_{bg}\,[cts/s]$	1.5
$\sigma_{\mathrm{OH}}\,[cts/s]$ [b]	0.5
$\sigma_{\mathrm{HO_x}}\,[cts/s]$ [c]	4
$S_{laser}\,[cts/s]$	20
$S_{dark}\,[cts/s]$	<1
$\sigma_{stat}\,[cts/s]$	0.6
$LOD_{\mathrm{HO_2}}\,[10^6 cm^{-3}]$ [d f]	2
$LOD_{\mathrm{RO_2}}\,[10^6 cm^{-3}]$ [e f]	7

[a] $t = 5\,s$, $n = 6$, $m = 4$ (Equation 4.49), laser power $25\,mW$
[b] estimated from the OH detection limit *Holland et al.* (2003)
[c] estimated from the HO_2 detection limit
[d] HO_2 sensitivity: $0.085\,cts(mWs)^{-}1$
[e] RO_2 sensitivity: $0.060\,cts(mWs)^{-}1$
[f] SNR=2

The precision of the background signal σ_{bg} has to be determined from NO interference measurements. The value of typical $\sigma_{bg} = 1.5\,cts/s$ (laser power: $25\,mW$, integration time: $30\,s$) is identical for both HO_2 and RO_2 radical measurements because the NO concentration in the fluorescence cell is equal in both measurement modes.

In principle, error propagation is needed to determine σ_{stat} because the fluorescence signal is calculated by subtracting dark signals from the measured count rate (Section 4.3). However, only the noise of the background signals during the fluorescence counting contributes significantly to σ_{stat} because the signal caused by fluorescence is assumed to be small compared to the laser generated background and dark signal if the detection limit is calculated for small radical concentration values. In addition, the error in the detector's dark signal which is subtracted from every single measurement is small due to the long integration time for the measurement.

The overall count rate of photons which are not produced by fluorescence consists of contributions of laser generated background photons S'_{laser} and of the dark current signal of the detector S'_{dark} (see Section 4.3). The standard deviation in Poisson statistics is expressed by the square root of the count number:

$$\sigma_{stat} = \sqrt{\left(\frac{1}{m} + \frac{1}{n}\right)\frac{1}{t}(S'_{laser} + S'_{dark})}. \tag{4.49}$$

t is the integration time for each of the n on-resonance and of the m off-resonance measurements. The largest error contribution results from the laser generated background signal which is about ten times larger than the dark signal of the detector ($S'_{dark} < 1\,cts/s$). However, the contribution of the photon counting noise σ_{stat} to the entire detection limit (Equation 4.47, 4.48) is usually small compared to the con-

tribution of the precision of the background signal σ_{bg} generated by the addition of NO.

Typical values of an integration time of $5\,s$, a number of 6 on-resonance and 4 off-resonance measurements and a laser power of $25\,mW$ lead to detection limits of the "MobiLIF" system shown in Table 4.8, demanding a signal to noise ratio of $SNR = 2$. The values are calculated for conditions in which small radical concentrations of all radical species are assumed because it is expected that they are small at the same time in the atmosphere. Therefore, the detection limits of the OH and HO_2 measurements are taken as noise of the OH and HO_x background in the HO_x respectively RO_x measurement. The precision of the NO background measurement dominates the detection limit for HO_2 whereas the noise of the HO_x detection limits the RO_2 detection. Expected fluorescence signals are well above the detection limits for typical radical concentrations during the day but may reach the detection limits for nighttime conditions.

4.9 Comparison with other measurement systems

Chemical amplifier instruments are the most common devices for measurements of peroxy radicals. Although this technique has been improved in the last 10 years their detection limit is considerably higher than that of LIF instruments (Table 3.1). In addition, the strong water vapor dependence of the sensitivity limits the accuracy of PERCA instruments. This does not apply for chemical amplifier systems which make use of mass spectrometry as detection system (PerCIMS, ROxMas). Their specifications are comparable to the new instrument in this work (Table 3.1). The reaction system in amplifier system is the same (PERCA) respectively it is similar (PerCIMS, ROxMas) to the reaction system used in this instrument. However, the aim of the conversion process is different. Whereas in amplifying systems the yield of a product species formed during the HO_x cycling is maximized, the aim of the LIF-detection system is to maximize the conversion efficiency for organic peroxy radicals. Therefore, conditions in both systems are different concerning pressure and concentration of added reactive gases. In contrast to chemical amplifiers, the pressure is reduced in this system. This has the advantage of reduced chemical losses. Concentrations of reactive gases are lower in this instrument compared to amplifier systems because in amplifier systems a high conversion rate in the HO_x cycle is desired whereas in this system concentrations of reactive gases are limited by gas phase loss reactions. The PerCIMS and the ROxMas instrument can be operated in two measurement modes to distinguish between RO_2 and HO_2 radical concentration. This procedure is similar to the RO_x and HO_x mode of this instrument. In contrast, PERCA instruments measure only the RO_x radical concentration.

Only HO_x radicals are detected in previous instruments using LIF technique. It is notable that specifications for the HO_2 detection of the new instrument are as good as for previous HO_x-LIF instruments (Table 3.1) although the conversion reactor causes additional radical losses, not present in the previous design. The new instrument mainly

differs from the HO_x-version of the LIF instrument in the additional conversion reactor leading to the detection of organic peroxy radicals. They are not detected in previous instruments because the time needed for the conversion of organic peroxy radicals to OH is much longer than the residence time of the sampled gas between the point of the NO added for the HO_2 conversion and the detection with LIF in the fluorescence cell. The time limiting step in the reaction chain is the reaction of alkoxy radicals with oxygen (Reaction R2.11) because of the reduction of the reactant at the low pressure in the fluorescence cell. In contrast, the pressure in the conversion reactor of the instrument in this work is higher leading to a fast reaction between alkoxy radicals with oxygen and the reaction time is sufficiently long. However, the NO concentration is much smaller than in the fluorescence cell to avoid gas phase losses. Therefore, the RO_2 conversion is rate limited by the reaction RO_2 with NO (Reaction R2.10).

All instruments beside the MIESR instrument require a calibration which is accomplished by using radical sources of different designs. Uncertainties of radical concentrations, provided by the radical sources, limit the accuracy of all instruments between 20 % to 56 % (2σ confidence level, Table 3.1). Therefore, the accuracy of the MIESR instrument is significantly higher than for all other instruments. However, its sensitivity is lower and the temporal resolution of data is limited because of the long sampling time.

5 Calibration of the instrument

5.1 The radical source

The calibration of instruments measuring OH and HO_2 radicals is widely accomplished by producing radicals in the photolysis of water vapor using the radiation of a low pressure discharge mercury lamp (*Aschmutat et al.*, 1994; *Schultz et al.*, 1995; *Heard and Pilling*, 2003). This well established technique has been applied to a large number of measurement techniques like LIF (*Creasey et al.*, 1997; *Kanaya et al.*, 2001; *Hard et al.*, 2002; *Holland et al.*, 2003; *Faloona et al.*, 2004), PERCA and PerCIMS (*Reiner et al.*, 1999; *Mihele and Hastie*, 2000; *Sadanaga et al.*, 2004b).

A calibration is generally necessary if parameters which are essential for the determination of the sensitivity are difficult to access with high accuracy by experiments or by theory. Examples are the photon detection efficiency or the radical loss factor in Equation 4.42 in the LIF detection of OH. Therefore, the sensitivity of the instrument is calculated from signals which are obtained if air that contains an accurately known radical concentration is sampled. It is necessary to produce radicals immediately before they are sampled because highly reactive radicals cannot be stored like calibration standards used for other instruments.

The radical source used in this work (Figure 5.1) consists of a flow tube (length $600\,mm$, inner diameter $17\,mm$) in conjunction with an irradiation module. The long flow tube should ensure laminar flow conditions. This results in the formation of a nearly parabolic velocity profile of the calibration gas.

Humidified synthetic air ($20\,l/min$, Linde AG, purity 5.0) passes a photolysis region. Radiation is provided by a low pressure discharge mercury lamp which intensity is monitored by a Cs-I phototube. The spectral characteristics of the phototube and an additional interference filter ($185\,nm$, FWHM=$27.5\,nm$) in front of the phototube ensures that only radiation which is relevant for the photolysis is detected by the phototube. The intensity of the radiation can be reduced by absorbing part of the radiation in a cuvette filled with N_2O (Linde AG, purity 2.5) which is placed between the lamp and the photolysis region. The reduction of the radiation allows to produce small radical concentrations (about [OH]= $10^8\,cm^{-3}$) at a humidity within the range usually found in the troposphere (mixing ratio of H_2O about 1 %). This should avoid errors in the calibration caused by performing measurements under artificial conditions.

The water vapor content of the synthetic air can be varied by mixing dry and humidified synthetic air controlled by mass flow controllers (Brooks, 5850 TR). Humidification of synthetic air is accomplished by using a fritted wash bottle which is filled with Milli-Q-water (Millipore Corp., Milli-Q Gradient A10). Gases like CO or hydrocarbons can

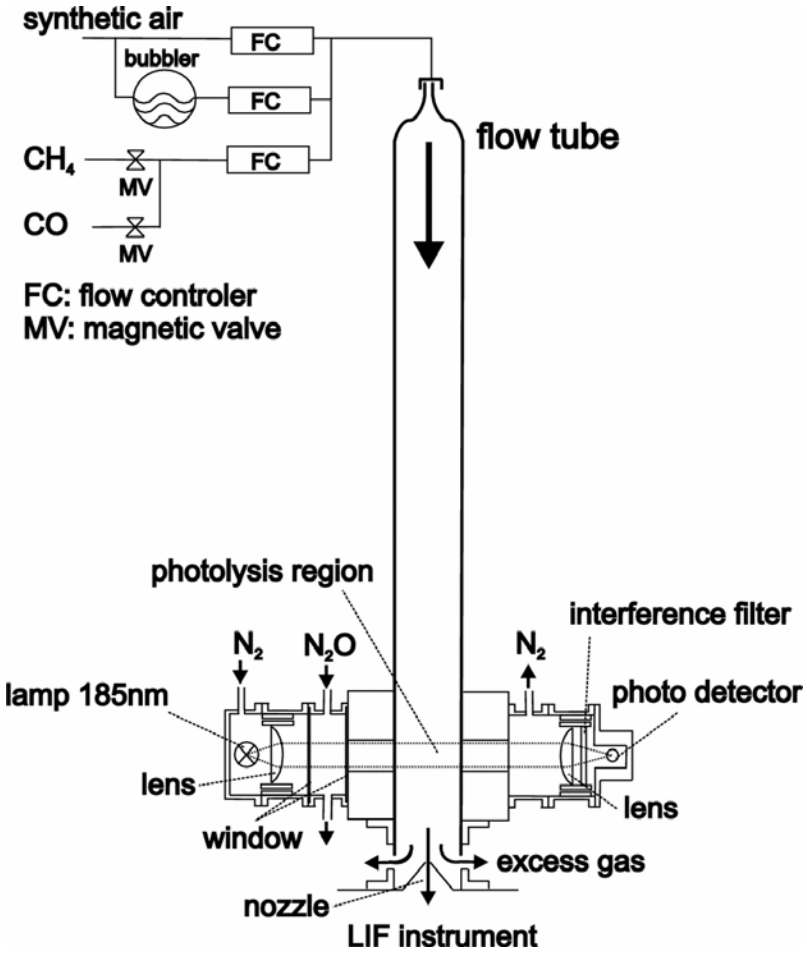

Figure 5.1: Schematic drawing of the radical source as used for calibration measurements of the instrument. The radical source consists of one part in which the carrier gas is humidified and reactive gases are added and one part in which radicals are produced by water photolysis.

be added to the synthetic air to convert radicals. The water vapor content of the calibration gas is measured both by a capacitive device (Vaisala, HMP25) and by a dew point hygrometer (General Eastern, M4/1311).

OH and HO_2 radicals are produced by water vapor photolysis:

$$H_2O + h\nu \rightarrow OH + H \qquad (\lambda = 184.9\,nm). \tag{R5.1}$$

Hydrogen atoms react rapidly with oxygen forming HO_2 radicals in synthetic air (see Section 5.2):

$$H + O_2 + M \rightarrow HO_2 + M \tag{R2.2}$$

The rate of OH production is given by

$$\frac{d}{dt}[OH] = [H_2O]\sigma_{H_2O}\Phi_{OH}F. \tag{5.1}$$

- σ_{H_2O}: water vapor absorption cross section at $184.9\,nm$
- Φ_{OH}: quantum yield of OH
- F: photon flux of the mercury lamp at $184.9\,nm$

The resulting OH radical concentration is calculated by integration of Equation 5.1 over the time t_{rad} during which the calibrations gas is exposed to the photolysis radiation:

$$[OH] = [H_2O]\sigma_{H_2O}\Phi_{OH}Ft_{rad}. \tag{5.2}$$

In principle, it would have been necessary to integrate this expression over wavelength. However, the absorption cross section of water at $184.9\,nm$ shows no distinctive structure. Therefore, it is possible to use mean values. The value of the mean absorption cross section is $\sigma_{H_2O} = (7.2 \pm 0.2) \cdot 10^{-20}\,cm^2$ (*Hofzumahaus et al.*, 1997; *Cantrell et al.*, 1997; *Creasey et al.*, 2003). The value of the dissociation quantum yield $\Phi_{OH} = 1$ is assured by theoretical considerations and experimental investigations (*Engel et al.*, 1992).

The photon flux and the exposure time depends strongly on the design of the calibration source. Therefore, the product $F \cdot t_{rad}$ is not measured directly but it is determined by ozone actinometry. The photolysis of oxygen which takes place simultaneously to the water photolysis leads to ozone production:

$$O_2 + h\nu \rightarrow O + O \qquad (\lambda = 184.9\,nm) \tag{R5.2}$$

$$2(O + O_2 + M \rightarrow O_3 + M). \tag{R5.3}$$

The resulting ozone concentration is calculated as:

$$[O_3] = [O_2]\sigma_{O_2}^{eff}\Phi_{O_3}Ft_{rad}. \tag{5.3}$$

- $\sigma_{O_2}^{eff}$: effective oxygen absorption cross section

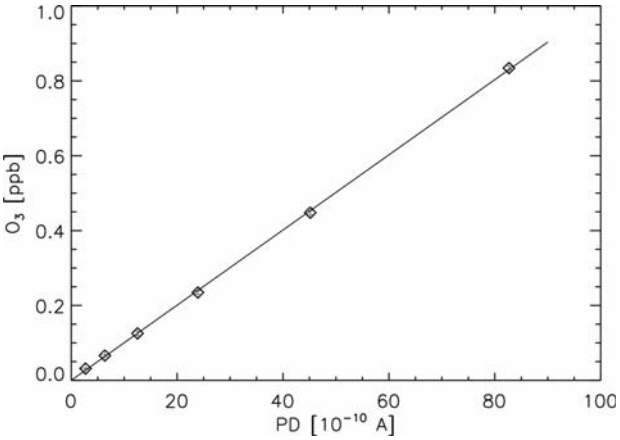

Figure 5.2: Relationship between the photolytically produced ozone in the radical source and the phototube signal (symbols). The air flow was kept constant at $20\,l/min$. Error bars are smaller than the symbol size. The line refers to the linear fit function through zero.

- Φ_{O_3}: quantum yield of ozone at $184.9\,nm$

The absorption spectrum of oxygen is highly structured in the Schumann-Runge bands around $185\,nm$. Instead of using mean values, an effective absorption cross section which is defined by

$$\sigma_{O_2}^{eff} = \frac{\int d\lambda \sigma_{O_2}(\lambda) F(\lambda)}{\int d\lambda F(\lambda)} \tag{5.4}$$

is applied which has to be determined separately. The value is specific for every mercury lamp and depends on the special design of the radical source (*Hofzumahaus et al.*, 1996, 1997; *Cantrell et al.*, 1997). The properties of the currently used lamp have not changed over years. This is assured by regular measurements of $\sigma_{O_2}^{eff}$ (*Hofzumahaus et al.*, 1996; *Creasey et al.*, 2000).

The quantum yield for the ozone production $\Phi_{O_3} = 2$ is derived from stoichiometric considerations (Reaction R5.2 and R5.3).

The OH radical concentration provided by the radical source can be calculated by summarizing Equation 5.1 and 5.3:

$$[OH] = [O_3] \frac{[H_2O]\sigma_{H_2O}}{2[O_2]\sigma_{O_2}}. \tag{5.5}$$

The typical concentration of the produced ozone (about $0.05\,ppbv$) is below the detection limit of standard ozone analyzers if the radiation of the mercury lamp is attenuated by the absorption of N_2O. Therefore, the ozone concentration is determined indirectly

Table 5.1: Relative errors of quantities which contribute to the accuracy of the calibration.

	VALUE	ERROR (1σ) [%]
σ_{H_2O}	$7.1 \cdot 10^{-20} cm^{-3}$	3
Φ_{OH}	1.0	<0.5
mixing ratio O_2	0.205	2.5
$\sigma_{O_2}^{eff}$	$1.28 \cdot 10^{-20}\, cm^{-2}$	4
Φ_{O_3}	2.0	<0.5
a	$5.75 \cdot 10^{20}\, l/minA^{-1}cm^{-3}$	4
mixing ratio H_2O	0.01	2
Q_v	$20 l/min$	3
I_P [a]	$3.5 \cdot 10^{-11}\, A$	6
sum [b]		9.8

[a] typical value if the radiation is attenuated
[b] Gaussian error propagation

from the intensity of the photolysis radiation which is monitored by the phototube. A linear relationship of the ozone production and the phototube signal is demonstrated by measurement of the produced ozone as a function of the phototube signal (Figure 5.2) The slope of the linear function is derived from a separate measurement during which the radiation of the the low pressure discharge mercury lamp is not or only partly attenuated. In this experiment the produced ozone which is sampled into the fluorescence cell is measured by using an ozone analyzer which makes use of the luminescence produced in the reaction of ozone with NO (Eco Physics, CLD 770AL) (*Ridley et al.*, 1992). A linear relationship between the phototube signal and the radiation is expected and was tested experimentally by *Sedlacek* (2001).

Using the phototube signal for determination of the ozone concentration in Equation 5.5, the OH and HO_2 radical concentrations produced by the radical source can be calculated:

$$[OH]_0 = [HO_2]_0 = \frac{aI_P}{Q_v} \cdot \frac{[H_2O]\sigma_{H_2O}}{2[O_2]\sigma_{O_2}}. \tag{5.6}$$

- a: calibration factor of the phototube's signal with regard to the produced ozone divided by the gas flow
- I_P: phototube signal
- Q_v: volume flow of the calibration gas

The ozone concentration is proportional to the irradiation time which depends on the gas velocity. Therefore, the volume flow is regarded separately. Calculation of the resulting OH radical concentration is possible because all parameters in Equation 5.6 are accessible. The concentration of oxygen in synthetic air is known and the

water vapor content, the gas flow and the phototube signal are measured during the calibration measurement. Other parameters are determined in separate experiments or are taken from literature.

The error of the calculated OH radical concentration, provided by the radical source, contributes to the accuracy of the radical measurements. The error in the sensitivity which is measured during the calibration leads to a systematic error in the calculated radical concentration values (Section 4.8). Table 5.1 summarizes the relative errors of quantities in Equation 5.6, given either by instrumental specification, by measurement errors or by literature values. The total relative error of the calculated OH concentration is 10 %, determined by Gaussian error propagation of the single errors.

5.2 OH-HO_2 radical concentration ratio

In the following section the yields of radical formation in the radical source are discussed in more detail.

The photolysis of water at $185\,nm$ is experimentally and theoretically well investigated (*Engel et al.*, 1992). Two different product channels are energetically possible:

$$H_2O(^1A_1) + h\nu \rightarrow H_2(^1\Sigma_g^+) + O(^3P) \quad \text{(R5.4)}$$

$$H_2O(^1A_1) + h\nu \rightarrow H^*(^2S) + OH(^2\Pi) \quad \text{(R5.5)}$$

Reaction R5.4 is spin-forbidden. Therefore, the OH yield of the water photolysis at $185\,nm$ (Reaction R5.5) is greater than 99 %.

Most of the excess energy ($1.57\,eV$) is transferred to translational energy of the hydrogen atom because of its smaller mass compared to oxygen. The high energetic H-atoms can undergo several chemical reactions or lose their energy by collisions with other molecules:

$$H^* + H_2O \rightarrow OH + H_2 \quad \text{(R5.6)}$$

$$H^* + O_2 \rightarrow OH + O \quad \text{(R5.7)}$$

$$H^* + M \rightarrow H + M \quad \text{(R5.8)}$$

$$H + O_2 + M \rightarrow HO_2 + M \quad \text{(R5.9)}$$

It is generally assumed that the quantum yield of Reaction R5.9 is equal one in radical sources using water photolysis.

However, Reactions R5.6 and R5.7 are known to play a role if the hydrogen atoms have enough translational energy ($>0.7\,eV$, *Bajeh et al.* (2001)). If the product yields of Reaction R5.6 and R5.7 which lead to the formation of OH radicals were unequal zero the yield of HO_2 radicals formed in Reaction R5.9 would be reduced. The assumption of equal HO_2 and OH radical production in the radical source would not be fulfilled.

About 11 collisions are possible before hydrogen atoms have lost part of their excess energy that Reaction R5.6 and R5.7 are not possible (calculated by simple collision

theory assuming atoms as spherical bodies). Reaction constants for reaction R5.6 and R5.7 are experimentally and theoretically investigated by *Bajeh et al.* (2001); *Zhang et al.* (2000). Product yields can be estimated to be less than 3 % but the error in this estimation is large because the cross sections of these reactions are not known accurately. *Zhang et al.* (2000) reports large unexpected differences of a factor of 10 between theoretical expectations and experimental investigations of the cross section of Reaction R5.6.

Therefore, small but significant product yields of reactions of hot hydrogen atoms which do not lead to HO_2 radical formation may be possible. It is notable that the entire HO_x concentration provided by the radical source is not changed. The OH radical concentration would increase by the same amount α as the HO_2 radical concentration would decrease:

$$[\mathrm{HO_x}] = (1+\alpha)[\mathrm{OH}]_0 + (1-\alpha)[\mathrm{HO_2}]_0. \tag{5.7}$$

$[HO_2]_0 = [OH]_0$ is the radical concentration calculated by Equation 5.6 assuming equal production of OH and HO_2 in the radical source.

The assumption of equal production of OH and HO_2 radicals would lead to an additional systematic error in the calculated OH and HO_2 radical concentrations provided by the radical source if α were unequal zero. In contrast to most other possible systematic errors (see Table 5.1), this would concern the OH and HO_2 radical concentrations differently and introduce an error in the ratio of measured OH and HO_2 concentrations.

The ratio of OH and HO_2 production in the radical source was investigated experimentally. This requires to determine the HO_2 radical concentration resulting from the water photolysis independently of the OH radical concentration. However, the LIF instrument only allows to measure either the OH or HO_x radical concentrations contained in the sampled air (Section 4.4).

A measurement of the HO_2 radical concentration produced by the photolysis is possible if the OH radicals are scavenged. This requires that reaction products do not lead to any OH radicals. Methane could serve as reaction partner because methylperoxy radicals are formed in the reaction of OH with methane (Reaction R2.4). However, CH_3O_2 may further react in a reaction chain with NO leading to OH radicals (Reaction R2.6, R2.7 and R2.3). Although it is proven that CH_3O_2 is not converted quantitatively, a conversion up to 5 % cannot be excluded (*Weber*, 1998). Therefore, methane of which all hydrogen atoms are replaced by deuterium scavenges OH radicals in another experiment, leading to the formation of CD_3O_2 radicals. A possible reaction chain with NO leads only to deuterated hydroxyl radicals OD. Excitation of OD radicals at the wavelength at which OH radical are excited is not possible because the absorption spectrum of OD radicals is different from that of OH (*Clyne et al.*, 1973; *Dieke and Crosswhite*, 1962). Therefore, no interfering fluorescence signal can occur from OD.

The experimental setup is identical with the usual setup during calibration measurements (Figure 5.1). In addition, it is possible to switch between normal and deuterated methane, provided by Linde AG. Three calibration measurements are performed. Firstly, CO is added to the calibration gas, secondly, normal methane and finally deuterated methane. Concentrations of the added gases are high enough to convert

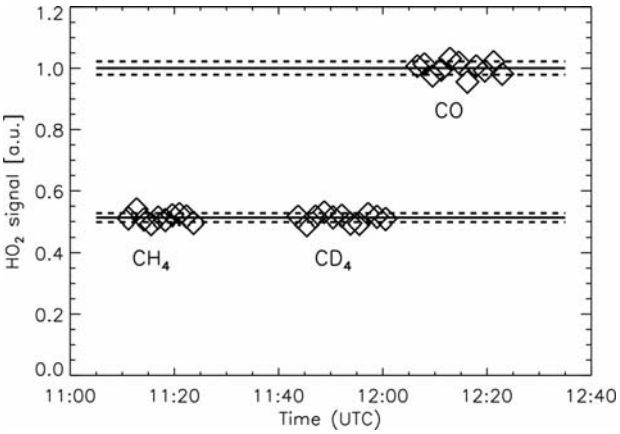

Figure 5.3: Relative fluorescence signals which are obtained in calibration measurements in the HO_x mode of the instrument if either CO, CH_4 or CD_4 is added to the calibration gas in the radical source. Solid lines refer to mean values, dashed lines to their 1σ standard deviations.

all radicals to the desired products (see Section 5.3). The LIF instrument is operated in the HO_x mode but without the additional reactor for the RO_2 radical conversion because only properties of the radical source and the fluorescence cell are investigated.

The results of the three measurements are shown in Figure 5.3. The signals are equal within the specified error if either methane or deuterated methane is added to the calibration gas. If CO is added, the signal is doubled in comparison to the signal in the two other modes. The experiment was repeated for four times on two different days. The results are summarized in Table 5.2. Fluorescence signals have been normalized to the entire HO_x concentration produced by water photolysis in the radical source (Equation 5.6) before the ratios are calculated. The mean value of the doubled ratio of the signals which are obtained if either CO or deuterated methane is added is 1.00 ± 0.035. This proves equal production of OH and HO_2 radical concentrations by water photolysis in the radical source. If CD_4 is added to the carrier gas, OH radicals which are either produced by water photolysis (Reaction R5.5) or in subsequent reactions of products (Reaction R5.6 and R5.7) are scavenged immediately in the reaction with CD_4. Therefore, only HO_2 radicals which are produced in Reaction R5.9 are detected by the HO_x radical measurement of the LIF instrument. In contrast, the entire HO_x concentration is measured if CO is added to the carrier gas (Equation 5.7). All OH radicals either produced by water photolysis or in subsequent Reaction R5.6 and R5.7 are converted to HO_2 and are detected by the LIF instrument. α in Equation 5.7 can be calculated from these measurements because all radicals are

Table 5.2: Ratios between fluorescence signals obtained in calibration measurements if either CH_4 and CD_4 respectively CD_4 and CO is added to the calibration gas in the radical source. Error values are 1σ standard deviations.

EXP. NO. [a]	$S(CH_4)/S(CD_4)$ [b]	$2 \cdot S(CD_4)/S(CO)$ [b]
1	0.99 ± 0.02	1.05 ± 0.06
2	1.01 ± 0.02	0.99 ± 0.02
3 [c]	1.02 ± 0.03	1.00 ± 0.01
4	1.02 ± 0.02	0.97 ± 0.01
mean	1.01 ± 0.015	1.00 ± 0.035

[a] 4 measurements on 2 days

[b] signals are normalized to the entire HO_x conc.

[c] measurement shown in Figure 5.3

detected with the same sensitivity:

$$2\frac{S_{CD_4}}{S_{CO}} = 2\frac{C_{HO_2}[HO_2]}{C_{HO_2}[HO_x]} = 2\frac{(1-\alpha)[HO_2]_0}{((1-\alpha)[HO_2]_0 + (1+\alpha)[OH]_0)} \overset{[HO_2]_0=[OH]_0}{=} 1-\alpha \tag{5.8}$$

The measured ratio of 1.00 ± 0.035 means $\alpha = (0.0 \pm 3.5)\,\%$. The HO_2 quantum yield for the reaction of hydrogen atoms with oxygen is equal one for the water photolysis in the radical source. Branching ratios of other possible reaction paths (R5.6 and R5.7) can be excluded with a precision of 3.5 %.

The measured OH/HO_2 radical ratio refers directly to the photolysis process. It is independent of subsequent processes between the points of production and the sampling of the radicals for the detection with the LIF instrument taking place downstream of the photolysis region because only HO_2 radicals are detected in all measurements.

The comparison of the fluorescence signals obtained if either deuterated methane or normal methane is added to the calibration gas allows to determine a possible interference caused by the conversion of CH_3O_2 radicals in the HO_x mode of the instrument in the fluorescence cell because deuterated methylperoxy radicals cannot cause any interfering signals as discussed above.

Assuming that β is the efficiency for the possible conversion of CH_3O_2 to HO_2 radicals in the fluorescence cell, the measured fluorescence signal S_{HO_x} is

$$S_{HO_x} = C_{OH}[OH] + C_{HO_2}([HO_2] + \beta[CH_3O_2]). \tag{5.9}$$

The ratio of fluorescence signals which are obtained if either CH_4 or CD_4 is added to the carrier gas of the radical source is 1.01 ± 0.015 (Table 5.2). The addition of normal methane leads to the formation of CH_3O_2 radicals whereas the same concentration of CD_3O_2 radicals is formed if deuterated methane is added. The concentration of organic peroxy radicals is equal to that of HO_2 radicals because all OH radicals produced in

the water photolysis react with methane ($[HO_2]_0 = [CH_3O_2]_0 = [CD_3O_2]_0$). Therefore β in Equation 5.9 can be estimated from this measurements:

$$\frac{S_{CH_4}}{S_{CD_4}} = \frac{C_{HO_2}([HO_2]_0 + \beta[CH_3O_2]_0)}{C_{HO_2}[HO_2]_0} \overset{[HO_2]_0=[CH_3O_2]_0}{=} 1 + \beta \tag{5.10}$$

No significant interference signal in the fluorescence cell caused by CH_3O_2 radicals in the HO_x detection of the LIF instrument can be found ($\beta = (1.0 \pm 1.5)\,\%$). It is not proven if this applies to other organic peroxy radicals but it is likely because the differences in the lifetime of peroxy radicals toward the reaction with NO (see Section 4.7) are small.

5.3 The calibration procedure

The calibration source provides equal concentrations of OH and HO_2 radicals for the well established calibration of the OH and HO_2 sensitivity of the LIF system. Since the transport of the radicals from the irradiation zone in the radical source to the sampling nozzle of the detection system is fast compared to chemical loss reactions and to radial diffusion, it is assumed that the sampled radical concentrations $[OH]_0 = [HO_2]_0$ are identical with the concentration values calculated by Equation 5.6.

Sensitivities for OH, HO_2 and RO_2 radicals in the two operation modes of the LIF system (HO_x and RO_x mode) are different and have to be determined separately (see Section 4.4). The sum of OH, HO_2 and RO_2 radicals is measured if reactive gases are added into the conversion reactor (RO_x mode) and the sum of OH and HO_2 if only CO is added (HO_x mode). Three different sensitivities have to be determined in the RO_x measurement mode and two in the HO_x mode:

- C_{OH}^{CO}: sensitivity for OH radicals (HO_x mode)
- $C_{HO_2}^{CO}$: sensitivity for HO_2 radicals (HO_x mode)
- C_{OH}^{NO+CO}: sensitivity for OH radicals (RO_x mode)
- $C_{HO_2}^{NO+CO}$: sensitivity for HO_2 radicals (RO_x mode)
- C_{RO_2}: sensitivity for RO_2 radicals (RO_x mode)

This requires to develop a certain calibration procedure during which both the detection modes of the LIF system and the production of radicals in the radical source are varied.

Both OH and HO_2 radicals produced by water photolysis in the radical source are detected in the HO_x and RO_x mode of the instrument. The measured signal is caused by OH and HO_2 radicals:

$$S_{HO_x}^k = C_{OH}^k[OH]_0 + C_{HO_2}^k[HO_2]_0 \tag{5.11}$$

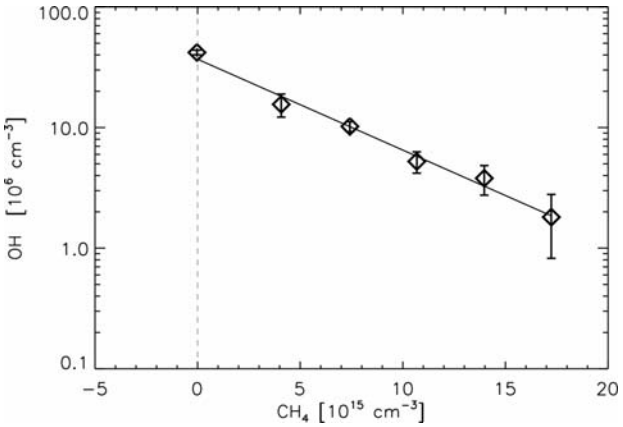

Figure 5.4: Measured OH radical concentrations (symbols) if various methane concentrations are added to the calibration gas in the radical source. The decay resulting from the fit function (line) is in good agreement with recommended values of the reaction rate constant of the OH-methane reaction.

where k denotes the kind of reactive gases added into the conversion reactor (CO or CO+NO). This measurement does not allow to determine a single sensitivity because the sensitivities in Equation 5.11 differ ($C^k_{\mathrm{OH}} \neq C^k_{\mathrm{HO_2}}$). A second measurement is required. CO is added to the calibration gas of the radical source leading to the conversion of OH to HO_2 radicals:

$$\mathrm{OH + CO} \rightarrow \mathrm{H + CO_2} \quad \text{(R2.1)}$$
$$\mathrm{H + O_2 + M} \rightarrow \mathrm{HO_2 + M} \quad \text{(R2.2)}$$

The conversion is rate limited by the first reaction. The lifetime of $2.8\,ms$ of OH radicals with respect to its reaction with a mixing ratio of CO of $60\,ppmv$ at ambient temperature and pressure (*NASA*, 2003) is small compared to the estimated transport time of about $20\,ms$ (*Sedlacek*, 2001) between the water photolysis and the sampling into the LIF instrument. This ensures that essentially all OH radicals are converted to HO_2 and the measured signal consists only of contributions of HO_2 radicals:

$$S^k_{\mathrm{HO_2}} = 2C^k_{\mathrm{HO_2}}[\mathrm{HO_2}]_0. \quad (5.12)$$

The factor 2 occurs because the primary HO_2 concentration is doubled by the converted OH radicals. The calculated HO_2 sensitivity can be used to determine the OH sensitivity of the system from the HO_x measurement (Equation 5.11).

The strategy how the HO_2 radical sensitivity is determined can be extended to calibrate the RO_2 radical sensitivity. Although only OH and HO_2 radicals are produced by the water photolysis in the radical source, it is possible to produce organic peroxy

Table 5.3: Calibration procedure of the system. Sensitivities to different radicals in the HO_x and RO_x mode of the LIF system can be calculated from these calibration measurements by operating the radical source and the LIF instrument in different modes.

LIF MODE	CALIBRATION MODE	SIGNAL
OH	HO_x	$C_{OH}^{(OH)}[OH]_0$
HO_x	HO_x	$C_{OH}^{CO}[OH]_0 + C_{HO_2}^{CO}[HO_2]_0$
HO_x	HO_2	$2\,C_{HO_2}^{CO}[HO_2]_0$
RO_x	HO_x	$C_{OH}^{NO+CO}[OH]_0 + C_{HO_2}^{NO+CO}[HO_2]_0$
RO_x	HO_2	$2\,C_{HO_2}^{NO+CO}[HO_2]_0$
RO_x	RO_2	$C_{RO_2}[RO_2]_0 + C_{HO_2}^{NO+CO}[HO_2]_0$

radicals by adding hydrocarbons to the calibration gas. This leads to the formation of organic peroxy radicals in the reaction of the hydrocarbon with OH. Methane is added to produce CH_3O_2:

$$OH + CH_4 \rightarrow CH_3 + H_2O \quad \text{(R2.4)}$$
$$CH_3 + O_2 + M \rightarrow CH_3O_2 + M. \quad \text{(R2.5)}$$

The mixing ratio of the added methane of 0.1 % is chosen such that the OH lifetime ($6.4\,ms$) with respect to the reaction with methane at ambient temperature and pressure (*NASA*, 2003) is small compared to the estimated reaction time ($t = 20\,ms$, *Sedlacek* (2001)). The idea to calibrate instruments which can perform measurements of organic peroxy radicals in this way was presented firstly by *Schultz et al.* (1995). *Hanke et al.* (2002) reported a calibration procedure for the ROxMas instrument which makes use of this principle. In order to prove that CH_3O_2 radicals are formed if methane is added, OH radical concentrations are measured by the calibrated LIF instrument while the concentration of the added methane is varied. All volume flows are determined by calibrated mass flow controllers. This allows to calculate the concentration of the added methane by fitting a linear function to the semi-logarithmic plot of the OH concentration versus the added methane concentration (Figure 5.4). The slope results in a reaction constant of $k_{fit} = (8.6 \pm 2.5) \cdot 10^{15}\,s^{-1}cm^3$ assuming a reaction time of $20\,ms$ (*Sedlacek*, 2001). The value agrees well with the value for the reaction of methane with OH recommended by *NASA* (2003) ($k = 6.3 \cdot 10^{15}\,s^{-1}cm^3$).

The addition of hydrocarbons to the calibration gas leads to equal production of organic peroxy and HO_2 radicals. The sum of both is detected in the RO_x mode of the LIF system leading to a measured fluorescence signal $S_{RO_x}^{NO+CO}$:

$$S_{RO_x}^{NO+CO} = C_{RO_2}[RO_2]_0 + C_{HO_2}^{NO+CO}[HO_2]_0. \quad (5.13)$$

C_{RO_2} can be calculated from the RO_x calibration (Equation 5.13) if the HO_2 sensitivity is known from the HO_2 calibration measurement (Equation 5.12).

The OH radical sensitivity of the OH channel of the LIF instrument that is used for a simultaneous measurement of the ambient OH radical concentration is also calibrated using the radical source. The sensitivity is obtained from the measured fluorescence signal $S_{\mathrm{OH}}^{(\mathrm{OH})}$ directly if the radical source is operated in the mode in which OH and HO_2 radicals are provided:

$$S_{\mathrm{OH}}^{(\mathrm{OH})} = C_{\mathrm{OH}}^{(\mathrm{OH})}[\mathrm{OH}]_0. \tag{5.14}$$

HO_2 radicals which are also produced by the water photolysis are not detected due to the lack of NO required for the conversion of HO_2 to OH radicals in the fluorescence cell of the OH channel.

The calibration procedure is summarized in Table 5.3. Sensitivities to different radicals in the HO_x and RO_x mode of the LIF system can be calculated from these calibration measurements.

6 Measurements at the simulation chamber SAPHIR

The instrument has been characterized by theoretical descriptions and experiments in the last chapters. In this and the next chapter of this work the applications of the new instrument in either experiments at the simulation chamber SAPHIR or in ambient air measurements during the HOxCOMP campaign in July 2005 are shown and discussed.

6.1 The atmosphere simulation chamber SAPHIR

6.1.1 Characteristics of the chamber

SAPHIR (Simulation of Atmospheric PHotochemistry In a large Reaction chamber) is designed to investigate photochemical processes under ambient conditions with small concentrations of traces gases as found in the atmosphere. Natural sunlight is used to initiate photolysis processes. In contrast to field measurements the chemical conditions are well characterized. Chemical processes are not affected by transport processes which often complicate the interpretation of data measured in field campaigns. In addition, there are no unaccounted sinks or sources of chemicals.

The reaction chamber consists of a double-walled FEP (DuPont, per-fluoro-ethylene-propylen foil) foil of 125 μm to 250 μm thickness of cylindrical shape (inner diameter 5 m, length 18 m, volume 270 m^3). The foil is chemically inert and it has an acceptable light transmission over the whole wavelength range of sunlight which penetrates the atmosphere. Both the chamber and the space between both foils are flushed permanently with pure synthetic air of highest available purity (Linde AG, purity 6.0) to keep the chamber pressured. A replenishment is necessary because of small leakages and because of the air consumption by the measurement devices. The chamber is flushed (by a maximum flow of 500 m^3/h) before experiments take place until concentrations of trace gases are below the detection limit of the measuring instruments. During experiments the air flow is usually kept as small as possible to minimize dilution of trace gases (concentration [M]). This is described by an exponential decay:

$$[\mathrm{M}](t) = [\mathrm{M}]_0 \left(\frac{1}{V_{cham}} \int_0^t Q_{exp} dt' \right) \tag{6.1}$$

([M]$_0$: start concentration of the trace gas M, V_{cham}: chamber volume (270 m^3), Q_{exp}: gas flow). Trace gas concentrations are typically reduced by 2 % to 3 % per hour during experiments. A fan ensures homogenous mixing of the gases (mixing time about 1 min)

Figure 6.1: Atmosphere simulation chamber SAPHIR with opened shutter system. The "MobiLIF" system can be seen on the scaffold (HOxComp campaign in July 2005).

which are introduced into the chamber. This is accomplished by flushing reagents in the chamber together with the experimental flow of synthetic air through one inlet line with several outlets near the chamber's floor.

The chamber can be exposed to sun light within $60\,s$ by opening a shutter system. The actinic flux in the wavelength range of $290\,nm$ to $420\,nm$ is reduced by 20 % to 30 % because of shadowing effects of the structural elements of the chamber and the characteristics of the foil (*Bohn and Zilken*, 2005).

Photolytic sources of two chemicals have been observed in the chamber, one for nitrous acid (HONO) and one for formaldehyde (HCHO). It was found in previous work that both components are formed photolytically on the surface of the teflon foil but the exact mechanism is unclear (*Rohrer et al.*, 2005; *Karl et al.*, 2004).

The HONO-source $S(\mathrm{HONO})$ depends on the photolysis rate represented by $j(\mathrm{NO_2})$, the relative humidity RH and the temperature T inside the chamber (*Rohrer et al.*, 2005):

$$S(\mathrm{HONO}) = a \cdot j(\mathrm{NO_2}) \left(1 + \left(\frac{RH}{RH_0}\right)^2\right) \exp\left(-\frac{T_{01}}{T}\right). \tag{6.2}$$

T_{01}, RH_0 are reference values ($T_{01} = 3950\,K$ and $RH_0 = 11.6\,\%$) and a is a fit parameter. a is called the HONO-source strength in the following and is adapted for the single experiments (typical values of $4.7{\cdot}10^{13}\,cm^{-3}$ to $8.5{\cdot}10^{13}\,cm^{-3}$). A HONO production within the range of $0.3\,ppbv/h$ to $0.7\,ppbv/h$ is obtained for typical conditions in the illuminated chamber ($RH > 30\,\%$, T about 12 °C to 35 °C) (*Rohrer et al.*, 2005).

In contrast to the HONO-source, the source for formaldehyde $S(\mathrm{HCHO})$ is independent of the water vapor content in the chamber but also depends on the temperature

and the radiation represented by the photolysis rate $j(NO_2)$ (*Karl et al.*, 2004):

$$S(\mathrm{HCHO}) = b \cdot j(\mathrm{NO_2}) \exp\left(-\frac{T_{02}}{T}\right). \tag{6.3}$$

T_{02} is again a reference value ($T_{02} = 6142\,K$) and $b = 3.29 \cdot 10^{17}\,cm^{-3}$ is a fit parameter calculated from zero air experiments by *Karl et al.* (2004). About $70\,pptv/h$ to $500\,pptv/h$ HCHO is produced in the illuminated chamber for typical ambient conditions (*Karl et al.*, 2004).

6.1.2 Instrumentation

The atmosphere simulation chamber SAPHIR is equipped with instruments measuring a wide range of trace gas concentrations and meteorological parameters. Only instruments which were used for experiments described in this chapter are shown in Table 6.1.

Standard instruments are used for measurements of meteorological parameters. Concentrations of inorganic, long-lived trace gases are also monitored by commercial instruments. NO_2, NO and ozone concentrations are measured by chemiluminescence detectors (Eco Physics, CLD 780TR). NO detection is achieved by observing the chemiluminescence after the reaction of NO with an excess of ozone (*Rohrer and Brüning*, 1992). The sum of NO and NO_2 is detected after NO_2 has been photolyzed. The acquisition time of the chemiluminescence detector is $1.5\,min$, the detection limit about $10\,pptv$. The ozone concentration is monitored by a standard UV absorption device (Ansyco, ozone analyzer 41M, acquisition time $1\,min$, detection limit $2\,ppbv$).

The water vapor content is measured by a dew point hygrometer (General Eastern, 1311DR). The dew point hygrometer samples air into a chamber in which the surface of a mirror is cooled down by a cascade of peltier elements until water is condensed. This is monitored by an optical system. The partial pressure of water can be calculated from the temperature of the mirror at this point. The sampling time is $3\,min$ and the detection limit is about $50\,ppmv$.

A gas chromatograph (Chrompack, Chrompack VOCAir) measures the concentration of organic compounds (non methane hydrocarbons NMHC). The system is described in detail by *Rodriguez Bares* (2003). Gas is sampled from the SAPHIR chamber through a heated inlet line. After several stages of adsorbing and heating of the sampled gas in order to separate NMHC from interfering trace gases like water or CO_2, the gas chromatogram is measured. The gas chromatograph is equipped with a flame ionization detector (FID) and a cryo focus module. The system is calibrated by a commercially available, certificated standard mixture of 30 compounds (NPL). Sampling lasts $30\,min$ and the online analyzing takes additional $20\,min$. The detection limit of the system is about $10\,pptv$ for most of the compounds.

The detection of short-lived radicals is possible with LIF and MIESR which are described in detail in Chapter 3.

A dual-channel spectroradiometer (Bentham 300) is used for the determination of photolysis frequencies in the chamber. Spectra are taken in the range between $280\,nm$

Table 6.1: Standard instruments at the atmosphere simulation chamber SAPHIR for measurements of trace gas concentrations and meteorological parameters.

Method/Instrument	Parameter, Trace Gas	LOD	Prec. (1σ)	Acc. (1σ)
Chemiluminescence (CLD)	NO_2	(1-2) $pptv$		5 %
	NO	(2-4) $pptv$		5 %
UV Photometer	O_3	2 $ppbv$	1 $ppbv$	5 %
MIESR	HO_2 , RO_2	$5 \cdot 10^7\ cm^{-3}$	10 %	2.5 %
LIF	OH [a]	$6 \cdot 10^5\ cm^{-3}$	15 %	10 %
	HO_2	$2 \cdot 10^6\ cm^{-3}$	2 %	10 %
	RO_2	$7 \cdot 10^6\ cm^{-3}$	(4-5) %	10 %
Gas chromatography (GC)	VOCs	10 $pptv$	$\leq$ 2 %	8 %
dew point hygrometer (DPH)	water vapor	50 $ppmv$		4 %
pressure transmitter	pressure			
spectroradiometer	actinic flux			
	photolysis frequencies			
ultrasonic anemometer	temp., wind speed			

[a] the performance is currently limited by a less sensitive detector (only OH detection)

to 420 nm with a spectral resolution of 1 nm. This takes about 2 min (*Bohn and Zilken*, 2005). Photolysis frequencies are calculated from the measured actinic flux using literature data on absorption cross sections and quantum yields. The instrument is not placed inside the chamber but the actinic flux F_λ of the sun is measured on top of the roof of a building next to the chamber. Photolysis frequencies from outside measurements are transferred by a model to determine values inside the chamber (*Bohn and Zilken*, 2005). Point measurements inside the chamber are not sufficient because they are influenced by shadowing effects of construction elements and reflections as well as scattering at the chamber's walls. However, the analysis of chemical processes requires photolysis frequencies averaged over the chamber volume which can be determined by transferring outside measurements.

6.2 Description of model calculations

Model calculations are performed using a near-explicit mechanism provided by the Master Chemical Mechanism MCM version 3.1 (*Saunders et al.*, 2003; *Jenkin et al.*, 2003). Expected trace gas concentrations can be calculated for conditions during the experiments. The MCM describes the degradation of 135 volatile organic compounds in the troposphere. The mechanism includes reactions with inorganic and organic compounds as well as photolytic reactions. It is divided into small packages which can be extracted to investigate a specific system. Information about the reaction kinetics is taken from actual literature recommendation or by analogy and structure-reactivity

correlations (*Jenkin et al.*, 1997).

Modules of the MCM (*MCM*, 2003) can be extracted from the whole mechanism in a format which is compatible with the differential equation solver `Facsimile` (*Malleson et al.*, 1990). An IDL (Interactive Data Language, Creaso) based program called EASY (Easy AtmoSpheric chemistrY, *Brauers and Rohrer* (1999)) was used in this work to handle the input and output of the `Facsimile` program in which time series of trace gas concentrations are calculated by solving the differential equation system resulting from their production and destruction reactions.

Modifications of the MCM for calculations of radical concentrations for the experiments discussed in this chapter are described in detail in Table 6.3 and 6.5 in conjunction with the description of the experiments.

In general, SAPHIR chamber specific properties are included additionally to the chemical mechanism described by the MCM. This concerns the dilution of trace gases (Equation 6.1) and the photolytic HONO and HCHO sources of the chamber (Equation 6.2, 6.3).

The strength of the HONO-source (Equation 6.2) is calculated for every experiment by varying its value iteratively until the measured and the modeled NO_x concentrations are in good agreement. This is possible because the NO_x concentration is mainly determined by the photolysis of HONO in the experiments described in this chapter (*Rohrer et al.*, 2005).

After the determination of the HONO source strength, the time series of short-lived species (OH, HO_2, RO_2 and NO) are calculated. NO_2, ozone, water vapor and NMHC VOCs as well as meteorological parameters temperature, pressure and dilution of trace gases and photolysis constrain the model. Measurements are taken on the shortest available time basis and interpolated to a $30\,s$ time grid. Concentration time series are calculated by solving the differential equation system for every $30\,s$ time interval. Initial values for every time interval are given by either the measured value or by the last values which have been calculated during the previous time step. This procedure results in a time series of calculated trace gas concentrations on a $30\,s$ time grid.

6.3 Reaction of OH with methane

6.3.1 Description of the experiment

Methane is the second most important, anthropogenic greenhouse gas. The reaction of CH_4 with OH radicals is the predominant sink of CH_4 leading to the formation of CH_3O_2 radicals (*Finlayson-Pitts and Pitts, Jr.*, 2000). The photochemical degradation of methane was investigated at the simulation chamber SAPHIR. The nearly simultaneous measurement of both CH_3O_2 and HO_2 radical concentrations allows to analyze the reaction kinetics. In addition, radicals were also detected by the MIESR instrument to compare data to the measurements of the new instrument. Beside the relevance of the methane-OH reaction in the atmospheric chemistry, this experiment was chosen because the instrument was best characterized for CH_3O_2 radicals.

Table 6.2: Initial concentrations and concentration ranges of trace gases during the OH-methane experiment at SAPHIR on the 2006-04-28.

	Initial Conc.	Conc. Range	Measurement
N_2, O_2	syn. air	syn. air	
CH_4	0.5 % [a]	(0.5 - 0.4) % [b]	
H_2O	0.7 %	(0.7 - 0.6) %	DPH
NO_2	< LOD	(0 - 2.7) *ppbv*	CLD
NO	< LOD	(0 - 0.33) *ppbv*	CLD
O_3	< LOD	(0 - 63) *ppbv*	UV Photometer
OH	< LOD	< LOD	LIF
HO_2	< LOD	(0 - 9)·10^8 cm^{-3}	LIF, MIESR
RO_2	< LOD	(0 - 10)·10^8 cm^{-3}	LIF, MIESR
HONO	-	(0 - 280) *pptv* [b]	
HCHO	-	(0 - 28) *ppbv* [b]	
H_2O_2	-	(0 - 1.9) *ppbv* [b]	

[a] calculated from the added volume of the trace gas

[b] calculated by the model

Here, OH radicals are produced by the photolysis of HONO which is formed in the chamber by the HONO-source described above. Temperature, pressure and experimental flow in the chamber were monitored during the experiment. Furthermore, NO_x and ozone concentrations as well as radiation were measured (Section 6.1.2).

The chamber was flushed overnight (2006-04-28) with synthetic air to reduce concentrations of all observed trace gases below the instrument's detection limit. At 6:00Z[1] water vapor was introduced into the chamber. High purity water was provided by a Milli-Q-water device (Millipore Corp., Milli-Q Gradient A10). The water was vaporized and flushed into the chamber together with a high flow of pure synthetic air. The water vapor concentration was chosen within the range of atmospheric mixing ratios to about 0.7 % (relative humidity: 50 %). Water vapor is required for the production of HONO in the chamber (Equation 6.2).

The synthetic air flow in the chamber was reduced to a small experimental flow after the addition of water vapor. Methane (Air Liquide, purity 5.5) was added using a mass flow controller (MKS, max. flow 20 l/min). The concentration of methane was not measured but the initial concentration of $[CH_4]_0 = (0.5 \pm 0.05)$ % can be calculated from the methane gas volume (1.4 m^3) added into the chamber. After addition of the trace gases water and methane the shutter system of the chamber was opened at 8:00Z to start the OH radical production. The fan was operated throughout the entire experimental time to ensure fast mixing of the air in the chamber.

The LIF instrument was running continuously during the whole day. Three samples

[1] *yyyy-mm-dd hh:mm:ss*Z international date and time notation (ISO 8601), Z means UTC (universal time)

Table 6.3: Modules of the MCM vers. 3.1 used for numerical calculations of radical concentrations in the OH-methane experiment at SAPHIR and modifications of the mechanism.

modules (*MCM*, 2003)	inorganic chemistry photolytic reactions methane
added reactions	dilution [a] HONO-source [b] ($a = (6.1 \pm 1.4) \cdot 10^{13}\, cm^{-3}$) HCHO-source [c]
input/constraints (measurements) [d]	temperature, pressure experimental flow of synth. air $[NO_2]$, $[O_3]$ $[H_2O]$ $j(O^1D)$, $j(NO_2)$, $j(HONO)$, $j(HCHO)$, $j(H_2O_2)$ sun zenith angle
initial values	CH_4=0.5 % [e]

[a] Equation 6.1
[b] Equation 6.2
[c] Equation 6.3
[d] using instruments as shown in Table 6.1
[e] calculated from the added volume of the trace gas

of the chamber's air were collected cryogenically by the MIESR instrument. Samples were taken for 30 *min* with another 30 *min* delay between two samples.

The chamber's shutter system was closed after 5.5 *h* of light conditions at 13:30Z. Measurements were stopped about 60 *min* later so that the relaxation of the chemical system could be observed.

Ranges and initial values of trace gas concentrations during this experiment are summarized in Table 6.2.

6.3.2 Model calculations

Radical concentrations were calculated by using the Master Chemical Mechanism described in Section 6.2. The adaption of the HONO-source strength resulted in a value of $a = (6.1 \pm 1.4) \cdot 10^{13}\, cm^{-3}$ (Equation 6.2) which is suitable to describe the NO_x concentration during the experiment. Measured ozone, NO_2 and water concentrations as well as photolysis rates and meteorological data were taken as constraints for the model (Table 6.3). The initial methane concentration was calculated from the gas volume added to the gas in the chamber. This is sufficient for the analysis of the experiment because the reaction of OH with methane was limited by the production of OH. The time series of short-lived species (OH, HO_2, CH_3O_2 and NO) were calculated.

6.3.3 Experimental results

Peroxy radical measurements of the LIF system and of the MIESR instrument are shown in Figure 6.2. In addition, the measured photolysis frequency of HONO j(HONO) which controls the radical production and the NO mixing ratio which controls the interconversion of radicals are plotted. The measured mixing ratios of ozone and NO_2 and calculated mixing ratios of HCHO and HONO which are produced in the radical cycle are shown in the lowest panel. The dashed vertical lines denote the opening and closing of the chamber's shutter system. Blue curves refer to results of model calculations which are discussed in the next section.

Both the HO_2 and CH_3O_2 radical concentrations increase quickly during the first minutes after the HONO photolysis has been started. Further variations over the day are mainly correlated with diurnal variations of the photolysis frequency j(HONO) which is affected by few scattered clouds and the increase of the ozone and formaldehyde concentrations (Figure 6.2). The OH radical concentration (not shown here) remains below the detection limit of the instrument as expected from the fast reaction of OH with methane.

The entire NO_x concentration increases over the day. A good correlation between the NO mixing ratio and the radiation can be observed which is expected because of the photochemical production of NO by the photolysis of NO_2.

The ozone concentration increases over the whole period of illumination as expected from the production of ozone in the photochemical degradation of methane.

The chamber was closed at 13:30Z. Photolytic sources of radicals and NO are stopped immediately. A fast decay of radical concentrations as well as of the NO mixing ratio can be observed.

The mixing ratios of initially present methane and water decrease continuously during the experiment (Table 6.2) because of the dilution of trace gases by the replenishment of synthetic air in the chamber.

A very good agreement between the measurements of the LIF system and the MIESR instrument can be seen in Figure 6.2. This indicates that the new instrument has the ability to measure absolute peroxy radical concentrations because the MIESR instrument is accepted as reference instrument for peroxy radical measurements. Details of the comparison are discussed in Section 6.5.

6.3.4 Comparison with model results

Figure 6.3 shows the reaction system including all relevant reactions of the methane-OH experiment. Conversions of reactions at 12:00Z are denoted. The radical and the NO production are initiated by the photolysis of HONO after the shutter system of the chamber has been opened. The HONO production is a property of the chamber (Section 6.1). OH radicals initiate a radical chain in the reaction with methane leading to the formation of CH_3O_2 radicals. CH_3O_2 radicals further react with NO to methoxy radicals which form rapidly HO_2 radicals in the reaction with oxygen. The chain is closed by the reaction of HO_2 radicals with NO and O_3 resulting in the formation of OH.

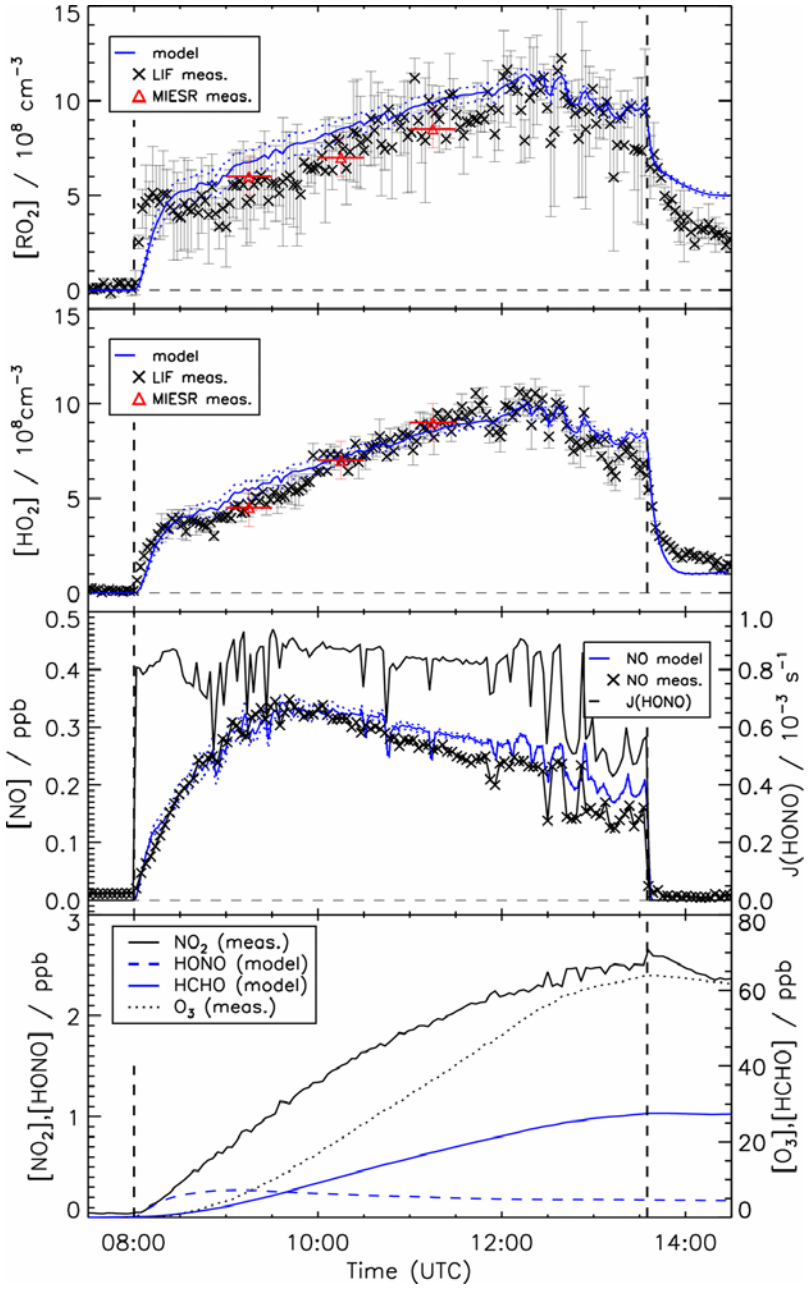

Figure 6.2: Comparison of data measured by the LIF and MIESR instrument and data from model calculations for the RO_2, HO_2 and NO concentrations. The dotted lines show the variability of the model calculations because of the uncertainty in the HONO-source strength of the chamber. Dashed vertical line refer to the opening and closing of the chamber's shutter system.

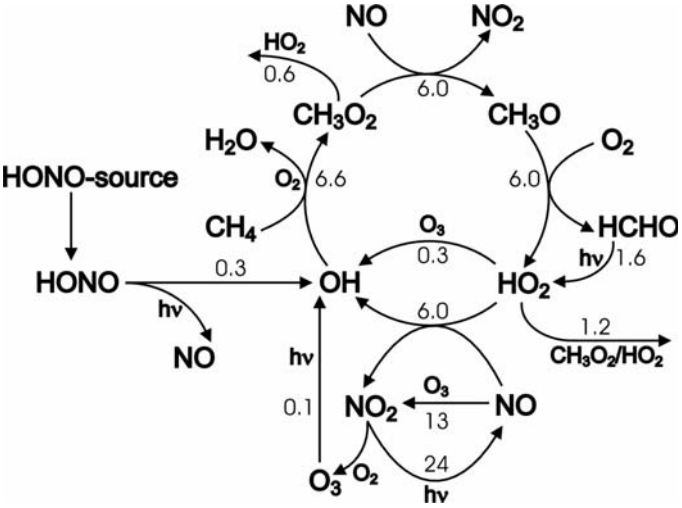

Figure 6.3: Scheme of the reaction system during light conditions in the methane-OH experiment at SAPHIR on the 2006-04-28. Numbers refer to the modeled conversions of the reactions measured in $10^7\,s^{-1}cm^{-3}$ at 12:00Z.

OH is usually reconverted to HO_2 by the reaction with CO in the atmosphere but no CO was present during this experiment. OH radicals react immediately with methane because of the high concentration of methane added into the chamber so that OH can not accumulate. HO_2 and CH_3O_2 radical concentrations increase during the experiment because the entire RO_x radical production by photolytic reactions increases. These are the photolysis of HONO and ozone leading to the production of OH and the photolysis of HCHO leading to the production of HO_2. The contribution of the ozone photolysis to the RO_x budget is small compared to the contribution of the photolysis of HONO but increases during the day with increasing ozone concentration. This applies also for HCHO but its contribution on the entire radical production is much larger. Radicals are lost in the reaction cycle by radical recombination reactions between CH_3O_2 and HO_2 and between two HO_2 radicals.

The NO and NO_2 concentrations are balanced by the photolysis of NO_2 and the reaction of NO with either ozone or peroxy radicals.

Because of the uncertainty of the HONO source strength, modeled concentration values are calculated by using the best fit value (solid line) and the two limiting values (dotted lines) which result in acceptable NO_x concentrations (see Section 6.2). The model results are within the range of the errors of the measured radical concentrations. The influence of the variability of the HONO source strength decreases over the day because the contribution of the photolytic source to the entire conversions of radicals decreases. Therefore, the solid and dashed lines (variability of the modeled radical concentrations) converge in Figure 6.2.

The agreement between modeled and measured CH_3O_2 and HO_2 data is very good except for the first $30\,min$ after the shutter system has been opened and after the shutter system has been closed again (Figure 6.2).

The entire production and destruction of CH_3O_2 and HO_2 radicals is dominated by the interconversion of RO_x radicals. Therefore, a high correlation between CH_3O_2 and HO_2 is expected and can be observed in the measurements. This is independent of the NO mixing ratio because the rate limiting reactions for both radical species are the destruction in their reactions with NO. Furthermore, the reaction rate constants of the reactions of HO_2 and CH_3O_2 with NO are similar (Table 4.4). Thus, similar concentrations of HO_2 and CH_3O_2 are expected and can be found in the measurements.

During the initial phase after opening the chamber's shutter system, the CH_3O_2 radical concentration increases faster than the model predicts whereas the HO_2 and the NO concentrations are well described. The reason for this behavior is unclear. The initial phase of radical concentrations is mainly determined by the development of the HONO source. Similar behavior of trace gas concentrations which cannot be explained by model calculations has been observed in other SAPHIR experiments before (*Richter*, 2006).

After closing the chamber's shutter system the time constant of the CH_3O_2 decay is underestimated while the time constant of the HO_2 decay is overestimated by the model. This period is characterized by the absence of NO and radiation. It is expected from model calculations that CH_3O_2 is mainly lost by radical recombination reactions whereas HO_2 mainly react with ozone leading to the interconversion to OH and further to CH_3O_2. Therefore a slower decay of HO_2 as described by the model would explain the faster decay of CH_3O_2. However, it is unclear if this behavior is caused by a lack of the understanding of the radical chemistry or if this is caused by chamber properties which are not described in the model.

The very good agreement between modeled data and the results of two independent measurements for conditions with radiation indicates that the photochemical degradation of methane by its reaction with OH can be well described by existing models like the MCM. This applies for conditions in which the interconversion of radicals dominates the overall production and destruction of radicals. Although the methane concentration during this experiment was about a factor of 2800 higher than the typical concentration found in the atmosphere, conditions are comparable to conditions for moderately polluted air because the NO_x and ozone concentrations were within the range of atmospheric conditions. The high methane concentration did not play any role because methane does not react with other chemicals beside OH for the chosen conditions. In this experiment the high methane concentration only suppressed other reactions of OH with e. g. HCHO which would have led to a more complex reaction mechanism. However, the velocity of the degradation of methane was limited by the availability of OH in this experiment like it is usually the case in the atmosphere.

The unexpected behavior of radical concentrations for dark conditions in the absence of NO and radiation could be the starting point of further investigations of the radical chemistry under these conditions.

6.4 Ozonolysis of 1-butene

6.4.1 Description of the experiment

Ozonolysis reactions of alkenes are important nighttime sources of peroxy radicals and contribute considerably to the entire degradation of alkenes in the dark (*Bey et al.*, 2001; *Geyer et al.*, 2003).

The ozonolysis of an alkene allows to drive the peroxy radical concentration in the SAPHIR chamber actively and independently of variable radiation. Nearly constant radical concentrations can be achieved. Their levels can be controlled by varying the O_3 concentration. This allows a more accurate comparison of measurements of the MIESR measurements which represent mean values integrated over 30 *min* to measurements of the LIF instrument. The ozonolysis of 1-butene was chosen because of the experiences in former experiments (*Rodriguez Bares*, 2003).

The chamber was flushed overnight until trace gas concentrations were below the detection limit of the instruments. In contrast to the methane-OH experiment, the shutter system of the chamber was kept closed during this experiment. Ozone was generated by a silent discharge ozonizer (O3Onia) and flushed into the chamber together with the experimental flow of synthetic air. An accurate addition of ozone was accomplished by a magnetic valve in the inlet line which was opened and closed by a timer. The ozone concentration was increased in four steps (Table 6.4).

1-butene was injected initially into the chamber for three times. The content of a glass bottle filled with pure 1-butene (Linde AG, purity 3.5) was flushed into the chamber leading to an increase of 12 *ppbv* each time. This resulted in an initial concentration of 36 *ppbv*. The loss of 1-butene during the experiment was balanced by further additions of 1-butene corresponding to a mixing ratio of 12 *ppbv* which was added at the same time when the ozone concentration was increased.

500 *ppmv* CO was introduced into the chamber. CO served as a scavenger for OH radicals. The CO concentration was such high that OH radicals were instantaneously converted to HO_2. This simplifies the reaction system because reactions of the alkene with OH are suppressed which would lead to the production of further organic peroxy radicals that are different to those that are formed during the ozonolysis.

Ozone concentration measurements were performed by the UV-absorption instrument during this experiment. The concentration of 1-butene was measured by the GC instrument. In addition, relative 1-butene values with a higher time resolution than those of the GC measurement could be determined from a special measurement mode of the chemiluminescence detector used for the NO_x measurements. This mode is designed to correct the NO_x measurement for an interference signal which occurs from products of the reaction of sampled alkenes with ozone which is added to the sampled gas in the CLD instrument (*Rohrer*, 2006). In this experiment 1-butene was the only alkene which caused the interference signal. Therefore, the interference signal could be ascribed to the 1-butene concentration. GC measurements of 1-butene were disturbed by the high ozone concentration present during this experiment (*Wegener*, 2006). Therefore, results from the chemiluminescence detector were taken for model

Table 6.4: Mean concentrations of trace gases during the four stages of constant conditions during the 1-butene ozonolysis experiments at SAPHIR on the 2006-05-17 and the 2006-05-24.

	1st Stage	2nd Stage	3rd Stage	4th Stage	Measurement
N_2, O_2	syn. air	syn. air	syn. air	syn. air	
C_4H_8	36 *ppbv*	42 *ppbv*	45 *ppbv*	45 *ppbv*	CLD
C_2H_6	0.1 *ppbv*	0.6 *ppbv*	1.7 *ppbv*	3.3 *ppbv*	GC
O_3	50 *ppbv*	150 *ppbv*	290 *ppbv*	460 *ppbv*	UV Photometer
CO	480 *ppmv* [a]	470 *ppmv* [b]	460 *ppmv* [b]	450 *ppmv* [b]	
H_2O	0.04 %	0.04 %	0.04 %	0.04 %	DPH
NO_2	< LOD	< LOD	< LOD	< LOD	CLD
NO	< LOD	< LOD	< LOD	< LOD	CLD
OH	< LOD	< LOD	< LOD	< LOD	LIF
RO_2	$0.35{\cdot}10^9$ *cm*$^{-3}$	$0.65{\cdot}10^9$ *cm*$^{-3}$	$0.9{\cdot}10^9$ *cm*$^{-3}$	$1.1{\cdot}10^9$ *cm*$^{-3}$	LIF, MIESR
HO_2	$0.6{\cdot}10^9$ *cm*$^{-3}$	$1.2{\cdot}10^9$ *cm*$^{-3}$	$1.8{\cdot}10^9$ *cm*$^{-3}$	$2.2{\cdot}10^9$ *cm*$^{-3}$	LIF, MIESR

[a] calculated from the added volume of the trace gas
[b] calculated by the model

calculations. They were scaled by the accurately known initial concentrations at the points in time when 1-butene was added.

The experiment was performed for two times on the 2006-05-17 and on the 2006-05-24. Four samples were collected cryogenically for the analysis with the MIESR instrument on the 2006-05-17. Ozone and 1-butene were added during the duty time of the MIESR in order to avoid uncertainties of the data (averaged values for 30 *min*) caused by fast changes of the 1-butene and ozone concentrations.

Data of the LIF-instrument derived on the 2006-05-17 could not be evaluated because the pressure regulator which controls the pressure in the reaction chamber failed. Fluctuations of the pressure leads to unknown changes of the detection sensitivities. Therefore, the experiment was reproduced on the 2006-05-24. However, the MIESR instrument was not available in the second experiment.

6.4.2 Model calculations

Model calculations of the ozonolysis experiment were done using the 1-butene module of the Master Chemical Mechanism (MCM) as described in Section 6.2. In contrast to experiments with opened shutter system, photolysis reactions are excluded because they do not play any role for experiments in the dark. In addition, there are no photolytic chamber sources of HONO and HCHO. Some of the reaction rate coefficients are replaced as discussed in detail in Section 6.4.4 (Table 6.5).

Constraints of the model are given by meteorological data (temperature, pressure), the dilution and the measured concentrations of the trace gases ozone and 1-butene.

Table 6.5: Modules of the MCM vers. 3.1 used for numerical calculations of radical concentrations in the 1-butene ozonolysis experiments at SAPHIR and modifications of the mechanism.

modules (*MCM*, 2003)	inorganic chemistry 1-butene		
added reactions	dilution [a]		
modifications	reaction	MCM [bc]	mod. MCM
	$C_4H_8+O_3 \rightarrow CH_2OO^*+C_2H_5CHO$	$k_0 \cdot 0.5$	$k_0 \cdot 0.35$ [d]
	$C_4H_8+O_3 \rightarrow C_2H_5CHOO^*+HCHO$	$k_0 \cdot 0.5$	$k_0 \cdot 0.65$ [d]
	$CH_2OO^* \rightarrow CO+H_2O$	KDEC·0.40	KDEC·0.31 [ef]
	$CH_2OO^* \rightarrow CH_2OO$	KDEC·0.24	KDEC·0.24 [ef]
	$CH_2OO^* \rightarrow CO+OH+HO_2$	KDEC·0.36	KDEC·0.45 [e]
	$C_2H_5CHOO^* \rightarrow C_2H_5CHOO$	KDEC·0.24	KDEC·0.46 [e]
	$C_2H_5CHOO^* \rightarrow C_2H_6$	KDEC·0.20	KDEC·0.24 [e]
	$C_2H_5CHOO^* \rightarrow C_2H_5O_2+CO+OH$	KDEC·0.36	KDEC·0.30 [eg]
	$C_2H_5CHOO^* \rightarrow C_2H_5O_2+HO_2$	KDEC·0.20	KDEC·0.0 [eg]
input/constraints (measurements) [h]	temperature, pressure experimental flow of synth. air $[O_3]$ $[C_4H_8]$		
initial values	CO=500 *ppmv* [i]		

[a] Equation 6.1
[b] $k_0 = 3.36 \cdot 10^{-15} \cdot \exp(-1744/T)\, s^{-1} cm^3$, from in the MCM
[c] KDEC denotes a nearly instantaneous reaction from the MCM
[d] *Grosjean and Grosjean* (1997)
[e] this work
[f] two equivalent paths in this experiment because products were not measured
[g] two equivalent paths regarding the HO_x yield
[h] using instruments as described in Table 6.1
[i] calculated from the added volume of the trace gas

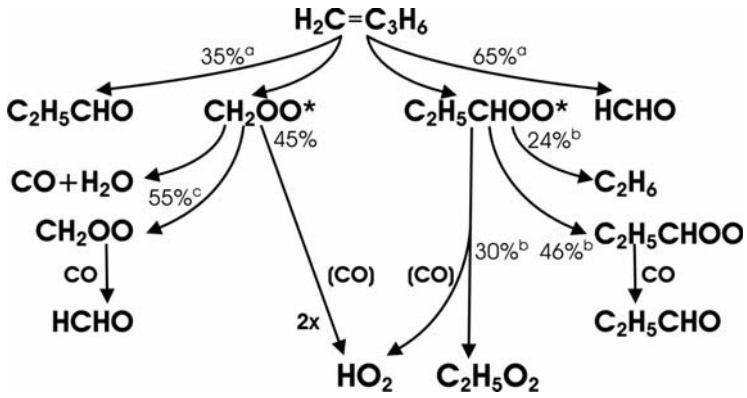

Figure 6.4: Scheme of the simplified reaction system of the ozonolysis of 1-butene for conditions of the SAPHIR experiment. Only reaction paths relevant with respect to the formation of radicals are shown. (CO) is denoted for reaction paths including either direct HO_2 production or production via the reaction of OH+CO. Branching ratios are suggested by the MCM beside [a] *Grosjean and Grosjean* (1997), [b] this work. [c] Only the sum of both branching ratios could be determined from this experiment

The ozone concentration is taken from measurements of the UV photometer and 1-butene data are taken from the interference signal of the chemiluminescence detector which is scaled with the accurately known, initial concentration of 1-butene.

A simplified reaction mechanism of the ozonolysis of 1-butene for conditions of this experiment is shown in Figure 6.4. The principles of the mechanism were proposed firstly by *Criegee and Wenner* (1949). The ozone molecule is added to the double bond of the alkene, forming the primary ozonide which decomposes in a carbonyl compound and a carbonyl oxide. The carbonyl oxide is a biradical in the gas phase (*Wadt and Goddard*, 1975), called the Criegee intermediate. Because of the exothermic ozonide decomposition, the Criegee intermediate is vibrationally excited. For asymmetric alkenes like 1-butene the primary ozonide can decompose at two different positions, leading to different carbonyls and Criegee intermediates. Either formaldehyde (HCHO) is formed together with the excited Criegee intermediate $C_2H_5CHCOO^*$ or propanal (C_2H_5CHO) is formed together with the excited Criegee radical CH_2OO^* by the ozonolysis of 1-butene.

Aldehydes are stable products in this experiment because neither OH as reaction partner nor radiation for photolytic reactions are available.

Collision stabilization competes with further reactions for the excited Criegee intermediate. The MCM suggests that stabilized Criegee radicals react with CO to form an aldehyde in the presence of high CO concentrations and in the absence of water, nitrogen oxides and sulfur oxides like in this experiment.

Further reactions of the excited Criegee intermediate are complex reaction sequences

including uni- and bimolecular reactions. A detailed description is beyond the scope of this work. Refer e.g. to *Grosjean et al.* (1996); *Grosjean and Grosjean* (1997); *Olzman et al.* (1997); *Hasson et al.* (2001) for a more detailed discussion. Here, reactions paths are only differentiated with respect to the yield of RO_x radical species.

Firstly, stable products like alkanes, CO, CO_2 and H_2O can be formed from excited Criegee intermediates. Secondly, reactions can lead to the production of two radicals. Regarding the aim of this experiment, one can distinguish between the formation of either two HO_x radicals or of one HO_x and one RO_2 radical. OH and HO_2 radical production cannot be distinguished because of the fast interconversion of OH to HO_2 in the reaction with CO. In addition to the formation of radicals, other stable trace gases are produced which do not lead to the production of further radicals.

Production of organic peroxy radicals is not possible from the excited carbonyl oxide CH_2OO^*. Decomposition processes are taking place after the isomerization of the Criegee intermediate (*Grosjean and Grosjean*, 1997) leading to the formation of two HO_x radicals or non-radical products. Equivalent reaction paths are suggested for the excited ethyl substituted carbonyloxide ($C_2H_5CHOO^*$). In contrast to CH_2OO^*, one ethylperoxy radical in conjunction with one HO_x radical is produced by the decomposition to radicals.

6.4.3 Experimental results

The experiment was performed two times for almost identical conditions as mentioned in Section 6.4.1. The amount of O_3 and 1-butene and the time sequence of the incremental additions of the two compounds were essentially the same as shown in Figure 6.5 (lowest panel). Therefore, it is expected that the time series of the peroxy radicals were very similar on both days. This is demonstrated by the model simulation in Figure 6.5.

Unfortunately, valid LIF measurements of HO_2 and RO_2 are only available for the second experiment while MIESR was only available for the first experiment. Therefore, a direct comparison of both methods is not possible. However, based on the assumption that the radical concentrations were almost the same during both experiments (Figure 6.5), the MIESR data from the first experiment (2006-05-17) are used for the comparison with the LIF data from the 2006-05-24 (Figure 6.6). The data calculated for the first experiment are split into four periods during which radical concentrations exhibit constant levels. The periods are shifted in order to match the data points of the ozone addition on the second day (differences are in the range of a few minutes).

In order to account for the slightly different experimental conditions, the MIESR data are corrected by the relative difference of peroxy radical concentrations predicted by the two model calculations shown in Figure 6.5. The corrections are small (maximum 5 %) and in the order of the 1σ standard deviations of the MIESR measurements (Table 6.6 and 6.7).

RO_2 and HO_2 radical measurements of both, the LIF and the MIESR instrument, agree well for all of the four stages of the experiment (Figure 6.6). Both data sets are compared in more detail in Section 6.5.

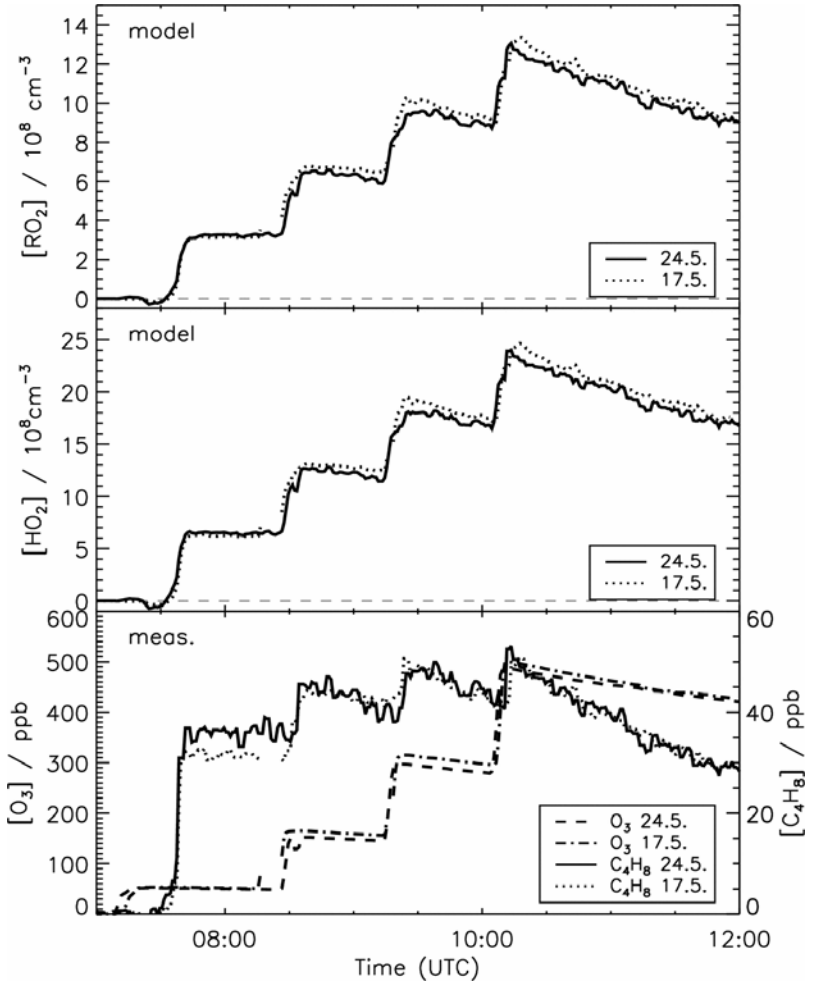

Figure 6.5: Comparison of modeled radical concentrations and measured 1-butene and ozone mixing ratios (3 *min* averaged data) on the 2006-05-17 and on the 2006-05-24.

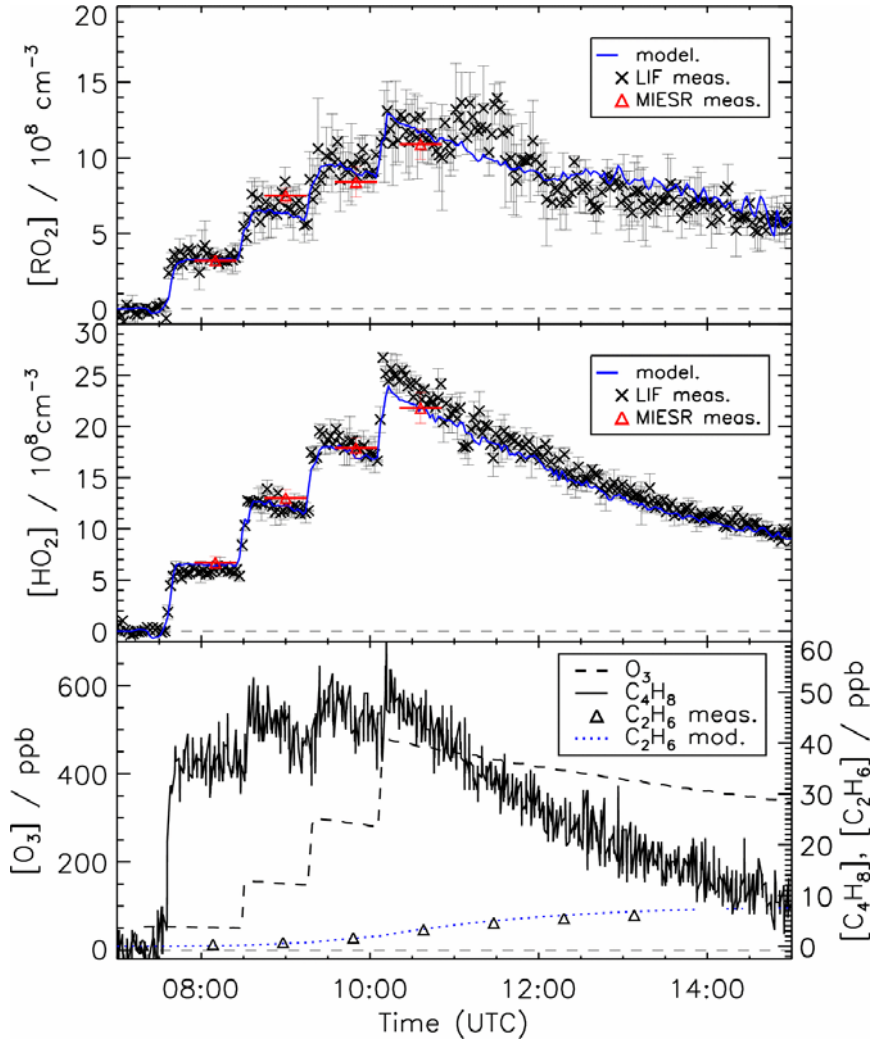

Figure 6.6: Measured radical concentrations (LIF and MIESR) and ozone, 1-butene and ethane mixing ratios during the ozonolysis experiment at SAPHIR on the 2006-05-24. Model results of the modified MCM are shown for radical concentrations (blue lines) and ethane (blue dotted line). Measurements of the MIESR instrument are taken from the experiment on the 2006-05-17 and corrected for the conditions during the experiment on the 2006-05-24.

Ethylperoxy radical concentrations measured by the new instrument are highly reliable. The sensitivity of the instrument towards ethylperoxy radicals is similar to the instrument's sensitivity for methylperoxy radicals as shown in Section 4.7.7. The formation of only one species of organic peroxy radicals has the advantage that additional systematic errors do not occur which would be possible if a mixture of peroxy radicals were detected with slightly differing sensitivities.

Nearly constant levels of both RO_2 and HO_2 radicals could be achieved as expected. The increase between two levels corresponds to the addition of ozone and 1-butene. The HO_2 radical concentration is higher than the concentration of RO_2 radicals. This can be expected because ethylperoxy radicals are formed in only one of the reaction paths (Section 6.4.2). Both ozone and 1-butene are consumed in the ozonolysis and are diluted by the replenishment of the chamber's air so that mixing ratios decrease after the addition.

The ethane concentration measured by the GC increase continuously during the experiment as can be expected because ethane ist a stable product of the ozonolysis for conditions during this experiment.

6.4.4 Comparison with model results

The results of model calculations using the MCM without modifications of branching ratios do not agree well with the measured organic radical concentrations and the ethane mixing ratio. In Figure 6.7 results of calculations with the original MCM are compared to the results obtained if the modifications are applied as noted in Table 6.5. Organic peroxy radical concentrations are overestimated by about 25 % to 30 % by the original MCM. The discrepancy between modeled ethane concentrations accumulates to about 100 % at the end of the experiment. In contrast, HO_2 concentrations do not differ significantly with respect to the agreement with measured concentrations (Figure 6.6). This indicates that the overall HO_x yield can be described by the original MCM.

The discrepancy between measurements and results of the original MCM are used to adjust branching ratios (Figure 6.4) so that the time series of measured concentrations are in agreement with model predictions.

The branching ratios of the decomposition of the primary ozonide are not accurately known for 1-butene. Product studies which investigate the yield of the primary carbonyls HCHO and C_2H_5CHO propose that the formation of HCHO is preferred (*Grosjean et al.*, 1996; *Grosjean and Grosjean*, 1997). The yield of formaldehyde measured by *Grosjean and Grosjean* (1997) is (65±3) % and the yield of propanal (35±2) % whereas *Rodriguez Bares* (2003) determined a higher yield of formaldehyde of (80±6) %. An equal probability of both reaction paths is assumed in the MCM because of the lack of a larger number of studies. Therefore, estimated MCM values are replaced by measured values derived by *Grosjean and Grosjean* (1997). However, one has to keep in mind that all branching ratios of the subsequent reactions depend on the product yields of the primary ozonide's decomposition.

The measured ethane concentration constrains the yield of non-radical products of the decomposition of the excited ethyl substituted carbonyloxide ($C_2H_5CHOO^*$) to

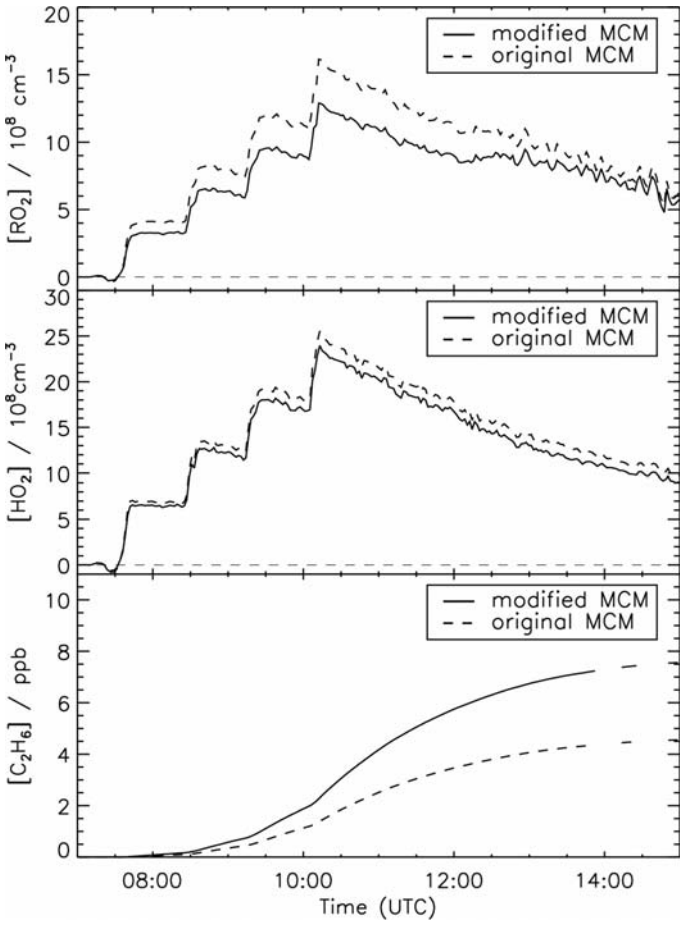

Figure 6.7: Comparison of model results calculated by the original MCM and by the MCM which has been modified by replacing branching ratios as denoted in Table 6.5.

0.24.

Two decomposition paths are suggested by the MCM leading to radical production. However, both are equivalent for conditions in this experiment because one ehtylperoxy radical ($C_2H_5O_2$) together with one HO_x radical is produced by each of them. The sum of branching ratios of these two paths can be determined by comparing measured and modeled RO_2 concentrations because these are the only ones in the chemical system in which RO_2 radicals are produced. This leads to a branching ratio of 30 %.

In the reaction system suggested by the MCM collision stabilization of the excited Criegee intermediate ($C_2H_5CHOO^*$) is the only reaction path left for the remaining 41 % of the entire Criegee intermediates.

The HO_x concentration measurement further constrains the branching ratio of the radical reaction path of the second Criegee intermediate (CH_2OO^*) formed in the ozonolysis mechanism of 1-butene. HO_x which is not produced in conjunction with RO_2 by the decomposition of $C_2H_5CHOO^*$ is assigned to this reaction path leading to a branching ratio of 45 %.

Collision stabilization and decomposition into non-radical products of CH_2OO^* cannot be distinguished in this experiment. Therefore, only the sum of branching ratios can be determined to 55 %.

The RO_2 radical concentrations measured by the LIF and by the MIESR instrument agree excellent with the concentrations of ethylperoxy radicals ($C_2H_5O_2$) predicted by the modified model (Figure 6.6). In addition, a good agreement between measured and calculated HO_x and ethane concentrations is achieved.

Although the reaction paths are simplified and may not reflect the details of the mechanism, the determined branching ratios can be used to calculate radical yields of the mechanism. The entire HO_x productions yield in the ozonolysis of 1-butene can be estimated to 0.51. The unmodified MCM suggests an HO_x yield of 0.64. As mentioned above, the HO_2 concentration calculated by the original MCM agrees reasonably with the measured values. Therefore, the difference in the HO_x yields calculated by both models is taken as error estimation, leading to a HO_x yield of (0.51 ± 0.13).

There is only one study in which the entire HO_x yield was also investigated. *Rodriguez Bares* (2003) reports an HO_x yield of 1.6 ± 0.8 for dry conditions but without using CO as scavenger for OH. The HO_x yield was acquired from the concentration-time profile of the measured alkene concentration. The value agrees with the yield calculated in this work within the relatively large error. *Rodriguez Bares* (2003) determined also the HO_2 yield separately to $1.15^{+0.8}_{-0.35}$ from direct observations of HO_2 radical concentrations measured by LIF. This is a lower limit of the entire HO_x yield and only agrees with the measurement in this work within the 2σ error.

In contrast to other previous studies in which only the OH radical yield of the ozonolysis of 1-butene was investigated (*Atkinson and Aschmann*, 1993; *Paulson et al.*, 1999; *Fenske et al.*, 2000) the entire yield of ethylperoxy radicals can be determined to 20 % from this experiment. This allows to differentiate between reaction paths of the ozonolysis mechanism in more detail. The lack of experimental investigations in the past may explain that the yield of RO_2 predicted by the MCM is significantly larger (28 %) than calculated from this measurement.

Measurement of stable products like aldehydes as well as of short-lived radicals are desirable for a detailed analysis of the complete ozonolysis reaction mechanism. Measurements of the new instrument could be helpful for this investigations. Although some products were not measured in this experiment, the potential of using peroxy radical measurements for the analysis of the ozonolysis mechanism could be shown.

6.5 Comparison between MIESR, LIF and modeled data

One aim of the two experiments at the SAPHIR chamber was the validation of the data measured by the new instrument with an independent reference instrument, the MIESR technique (Section 3.2). In contrast to the LIF technique, no calibration of the MIESR instrument is required. Therefore, concentrations measured by MIESR are more accurate than those measured by the LIF instrument (see Table 3.1).

The LIF data are averaged for the sampling time of the MIESR to compare both data sets (Table 6.6, 6.7). MIESR data of the ozonolysis experiment are taken from the experiment on the 2006-05-17 and corrected for the comparison as described in Section 6.4. Errors of the LIF represents the 1σ standard deviation of the mean radical concentration value during the sampling time of the MIESR instrument.

$30min$ averaged values measured by the LIF and by the MIESR instrument agree very well within their statistical errors. In addition, corrections of MIESR data due to the transfer between the two ozonolysis experiments are within the range of the standard deviations of the MIESR data.

The good agreement between measurements of both instruments can also be seen in the correlation plot (Figure 6.8) of the two data sets. The discrepancy between measurements of both instruments are not significant indicated by the errors in the fitted slopes and offsets in the correlation plots (Figure 6.8). A possible systematic error of the calibration of the LIF instrument cannot be found.

This results validate the data of the new instrument for methylperoxy and ethylperoxy radicals with an independent established reference instrument. As a result, it is possible to derive reliable organic peroxy as well as HO_2 radical concentration values with the new instrument. The SAPHIR experiments confirm the results of the laboratory calibration for the two different organic peroxy radicals and the reliability of the measurement procedure.

Modeled data which are averaged for the sampling time of the MIESR are shown in Table 6.6 and 6.7 in addition to the comparison of the two measured data sets. Modeled data were calculated using the MCM ver. 3.1 with modification and constraining measurements as noted in Table 6.3 and 6.5. Modifications include SAPHIR specific properties (dilution of trace gases and sources of HONO and HCHO) as well as replacement of branching ratios in the ozonolysis mechanism of 1-butene. Modeled and measured values agree well for both instruments (LIF and MIESR) if these modifications are applied. This can be also seen in the fitted slopes which are around unity and

Table 6.6: Comparison of $30min$ averaged HO_2 concentrations. Errors are 1σ standard deviations of the mean values (LIF, model) respectively of the measurements (MIESR).

	LIF $[10^8\,cm^{-3}]$	MIESR $[10^8\,cm^{-3}]$		MODEL $[10^8\,cm^{-3}]$
		WITHOUT CORR.	WITH CORR.	
1^a	5.9 ± 0.3	7.0 ± 0.6	6.7 ± 0.6	6.5 ± 0.1
2^a	12.2 ± 0.7	12.0 ± 0.8	13.0 ± 0.8	12.1 ± 0.3
3^a	18.2 ± 0.7	16.8 ± 1.0	17.9 ± 1.0	17.3 ± 0.5
4^a	23.4 ± 1.0	21.6 ± 1.5	21.8 ± 1.5	21.7 ± 0.7
5^b	4.6 ± 0.4	4.5 ± 1.0		5.5 ± 0.3
6^b	7.1 ± 0.4	7.0 ± 1.0		7.2 ± 0.2
7^b	8.9 ± 0.4	9.0 ± 1.0		8.6 ± 0.2

[a] data from the ozonolysis experiment

[b] data from the methane-OH experiment

Table 6.7: Comparison of $30min$ averaged RO_2 concentrations. Errors are 1σ standard deviations of the mean values (LIF, model) respectively of the measurements (MIESR).

	LIF $[10^8\,cm^{-3}]$	MIESR $[10^8\,cm^{-3}]$		MODEL $[10^8\,cm^{-3}]$
		WITHOUT CORR.	WITH CORR.	
1^a	3.4 ± 0.4	3.4 ± 0.3	3.2 ± 0.3	3.3 ± 0.1
2^a	6.8 ± 0.7	6.0 ± 0.5	6.5 ± 0.5	6.3 ± 0.2
3^a	9.5 ± 0.7	8.0 ± 1.0	8.6 ± 1.0	9.1 ± 0.3
4^a	11.6 ± 0.8	9.9 ± 1.0	10.9 ± 1.0	11.7 ± 0.4
5^b	5.2 ± 0.8	6.0 ± 1.0		6.7 ± 0.2
6^b	7.3 ± 0.7	7.0 ± 1.0		8.5 ± 0.3
7^b	9.3 ± 1.0	8.5 ± 1.0		9.9 ± 0.2

[a] data from the ozonolysis experiment

[b] data from the methane-OH experiment

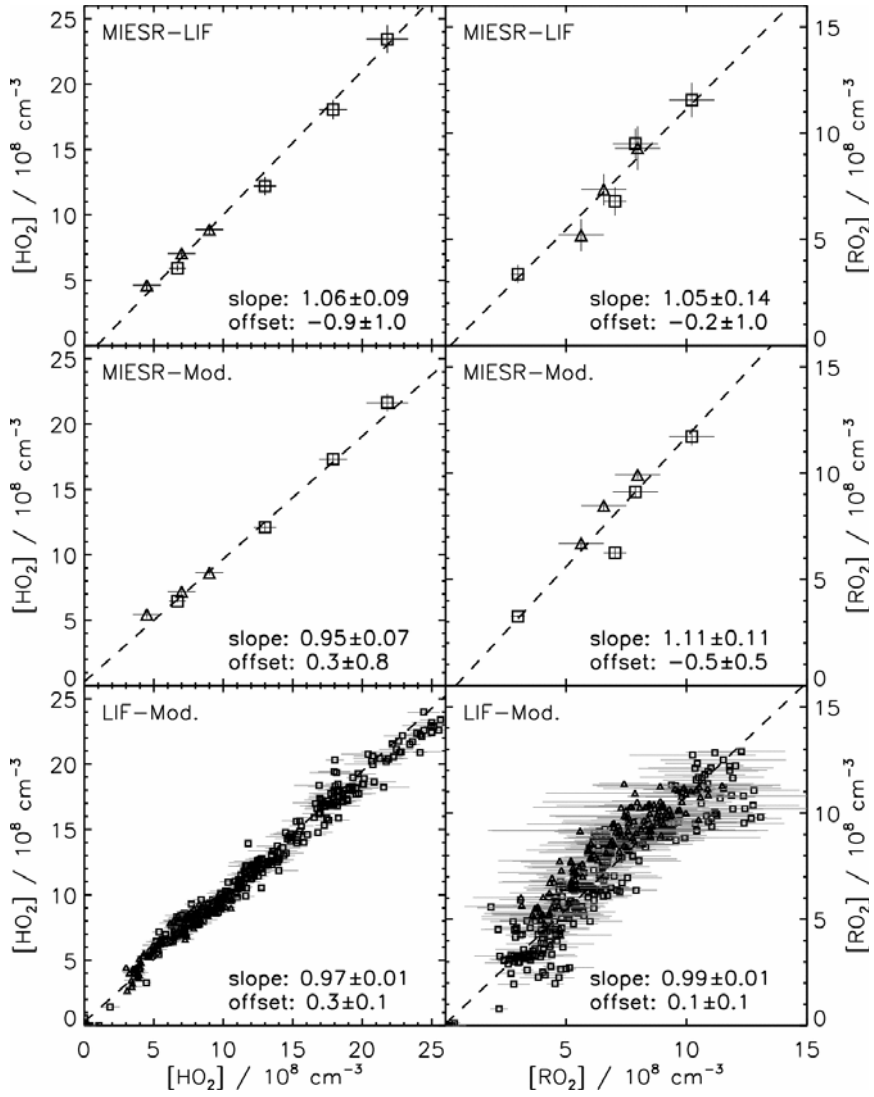

Figure 6.8: Correlation plots between LIF, MIESR and modeled data. Squares refer to the data derived from the ozonolysis experiment and triangles refer to the data derived from the OH-methane experiment. Error bars are 1σ standard deviations of the mean values (LIF, model) respectively of the measurements (MIESR).

insignificant offsets in the correlation plots (Figure 6.8).

Both experiments are of relevance for the atmospheric chemistry. Methane is one important anthropogenic green house gas. It is mainly removed by the reaction with OH. The results of the experiment in this work show that the methylperoxy and hydroperoxy radical concentrations can be derived from model calculations. This indicates the validity of the photochemical reaction mechanism of methane as implemented in models like the MCM.

Ozonolysis reactions of alkenes are one major reaction path leading to the degradation of alkenes during nighttime. Therefore, they contribute to the self-cleaning ability of the atmosphere. The ozonolysis experiment shows the potential to use measurements of the new instrument for kinetic studies. The results of the experiment indicate that the reaction mechanism of the ozonolysis of 1-butene as implemented by the MCM is not fully understood. The yields of RO_2 radicals and ethane calculated from the experiment differ from yields predicted by the original MCM.

Beside their relevance for the understanding of the atmospheric chemistry these experiments have the potential to serve as reference experiments at the SAPHIR chamber for quality assurance of the instrument's performance in the future. The reaction mechanisms are relatively simple that a high reproducibility can be expected as shown for the ozonolysis experiment in this chapter. Therefore, the long-term reproducibility of radical measurements could be observed by comparing measurements to model results regularly.

7 Ambient Air Measurements

7.1 The HOxComp campaign

The first application of the new LIF instrument for detection of ambient OH, HO_2 and RO_2 radicals took place during the international HOxComp campaign from the 2005-07-03 to the 2005-07-23 at the research center Jülich (longitude: 6°24'E, latitude: 50°54'N). The research center is surrounded by a forest and is situated in an area dominated by agriculture and strip mining. The aim of this campaign was an intercomparison of instruments measuring atmospheric OH and HO_2 radicals. The campaign was divided into two parts. Firstly, the instruments were compared with respect to ambient air measurements. They were placed close together between the SAPHIR chamber and the institute's building. A formal blind intercomparison took place for three days (2005-07-09 to 2005-07-11) whereas informal comparison measurements were done before. During the second part of the campaign measurements were performed by sampling air from the atmosphere simulation chamber SAPHIR (2005-07-17 to 2005-07-23). This allowed a systematic investigation of differences between measurements regarding the chemical regime in which the instruments are operated.

The "MobiLIF" platform took part during ambient air measurements of the campaign. It was running in the previous "HO_x configuration" (as described by *Holland et al.* (2003)) on the 2005-07-09 and the 2005-07-10 and in the configuration developed in this work on the other days. The "SaphirLIF" instrument performed measurements during the chamber experiments but was not modified for the detection of RO_2 radicals. Beside the instruments of the research center Jülich, LIF instruments of several other institutes performed OH and HO_2 radical measurements (Table 7.1). In addition to radical concentrations, the lifetime of OH (τ(OH)) was measured by instruments of the Tokyo Metropolitan University (TMU) (*Sadanaga et al.*, 2004a) and of the research center (FZJ).

A wider range of concentrations of inorganic and organic species were measured to support the interpretation of radical measurements. Most of the instruments were operated by the research center and were identical during the measurements outside and at the SAPHIR chamber as described in Section 6.1.2. An overview about all instruments which took part during outside measurements of the HOxComp campaign is shown in Table 7.1.

Since RO_x radicals were only detected by the new instrument during outside measurements, ambient air measurements are discussed in this work. A detailed comparison between results of the different instruments is beyond the scope of this work but will be the subject of several publications which are in preparation. Concerning the aim of this

Table 7.1: Instruments which took part of the HOxComp campaign during the outside measurements.

METHOD	PARAMETER, TRACE GAS	OPERATOR
MIESR	NO_2 , NO_3, HO_2 , RO_2	FZJ
LIF	OH, HO_2	MPI Mainz
	OH, HO_2	FRCGC Tokyo
	OH, HO_2	University Leeds
	OH, HO_2, RO_2	"MobiLIF" FZJ
CIMS	OH	Deutscher Wetterdienst
LIF	τ(OH)	TMU Tokyo
	τ(OH)	FZJ
spectroradiometer	actinic flux	FZJ
gas chromatography	VOC	FZJ
chemiluminescence	NO_2,	FZJ, University Wuppertal
	NO	FZJ, University Wuppertal
UV Photometer	ozone	FZJ
spectrofluorometry	HCHO	FZJ
LOPAP	HONO	FZJ, University Wuppertal
dew point hygrometer	water vapor	FZJ
pressure transmitter	pressure	FZJ
ultrasonic anemometer	temperature, wind speed	FZJ

work the measurements during the HOxComp campaign allow to show the instrument's performance during ambient air measurements.

7.2 Measurement results

Ambient air measurements were performed by the "MobiLIF" instrument between the 2005-07-07 and the 2005-07-11 and on the 2005-07-14. This also includes the nights from the 2005-07-07 to the 2005-07-08 and the two nights between the 2005-07-09 and the 2005-07-11. The "MobiLIF" instrument was running in the former "HO_x configuration" on the 2005-07-09 and the 2005-07-10. Only OH radicals were detected between noon and the evening of the 2005-07-10 because of technical problems with the addition of the reagent NO into the fluorescence cell of the HO_x channel of the instrument. RO_x radical concentrations were measured by the new instrument on the other days.

OH radical concentrations exhibited a distinctive diurnal profile as can be seen in Figure 7.1 to 7.6. Maximum concentrations reached from $3 \cdot 10^6\, cm^{-3}$ on cloudy days to $7 \cdot 10^6\, cm^{-3}$ on days with clear sky. After sunset the OH concentrations felt quickly to values within the range of the instrument's detection limit. No OH radicals could be detected during the nights.

A generally good correlation of the measured OH concentrations and $j(O^1D)$ can be

observed for daylight conditions (Figure 7.1 to 7.6) with deviations in the early morning hours when $j(O^1D)$ was very small. This behavior is expected because photolysis of ozone is supposed to be the major daytime source of OH (*Ehhalt and Rohrer*, 2000). HONO accumulated during the nights to a mixing ratio of about 400 *pptv* to 500 *pptv* as can be seen from the measurements (Figure 7.1 to 7.6) but the mixing ratio was smaller during the day with about 100 *pptv* to 200 *pptv*. Therefore, in the early morning hours HONO photolysis may have been an important source of OH because HONO photolysis starts earlier than the ozone photolysis. A similar behavior of OH has been observed before by e.g. *Holland et al.* (2003).

In contrast to OH, the maximum of diurnal profiles of peroxy radicals were shifted towards the end of the day. High midday concentrations of $0.2{\cdot}10^8\,cm^{-3}$ to $4{\cdot}10^8\,cm^{-3}$ persisted into the afternoon. This form of asymmetric profiles has been noted before for low NO_x environments (e.g. *Monks et al.* (1996); *Carpenter et al.* (1997)) as well as for high NO_x environments (e.g. *Holland et al.* (2003); *Mihelcic et al.* (2003); *Fleming et al.* (2006)).

Here, chemical conditions reached from moderately polluted (indicated by NO_x mixing ratios of less than 10 *ppbv*) to polluted (indicated by NO_x mixing ratios of more than 25 *ppbv*). NO_x levels were typically higher during the morning which may have been caused partly by emissions of cars during the rush hour traffic. High concentrations of NO react with HO_2 and RO_2 radicals to shift the equilibrium between OH and peroxy radicals towards OH. Thus, the HO_2 and RO_2 may have been suppressed in the morning by high NO.

Peroxy radical concentrations decreased during the evening but remained significantly higher than the instrument's detection limit throughout the nights. It is known that nighttime sources of peroxy radicals like ozonolysis of alkenes or reactions of VOCs with NO_3 radicals exist (*Geyer et al.*, 2003; *Fleming et al.*, 2006). This may also explain the nighttime peroxy radical concentrations observed in this campaign.

Features of diurnal profiles of radicals which are not described by their general behavior are discussed briefly for single days in the following.

Both the 2005-07-07 and the 2005-07-08 were characterized by cloudy conditions. Radical concentrations were small (OH concentration maximum about $3{\cdot}10^6\,cm^{-3}$, RO_2 and HO_2 concentration about $2 \cdot 10^7\,cm^{-3}$). This corresponded to a small photolysis rate of $j(O^1D)$ of maximum $1 \cdot 10^{-5}\,s^{-1}$. An unexplained peak in the HO_2 radical concentration (about $1.7 \cdot 10^8\,cm^{-3}$) occurred around 13:30Z on the 2005-07-07. In addition an exceptionally high NO_x peak of a maximum mixing ratio of 1600 *ppbv* was observed around 10:15Z on the 2005-07-08.

Nearly clear sky conditions with only few scattered clouds prevailed on the other days. Fog was present in the morning of the 2005-07-09 and there was a thunder storm with heavy rain in the afternoon of the 2005-07-11. The OH concentration reached maximum values of about $7 \cdot 10^6\,cm^{-3}$ and maximum HO_2 and RO_2 concentrations were about $2 \cdot 10^8 cm^{-3}$ to $5 \cdot 10^8 cm^{-3}$. Diurnal profiles of radicals followed the general features described above.

A high peak of formaldehyde of about 7 *ppbv* was observed between 08:00Z and 09:00Z on the 2005-07-09. This was accompanied by a rise of the ozone mixing ratio

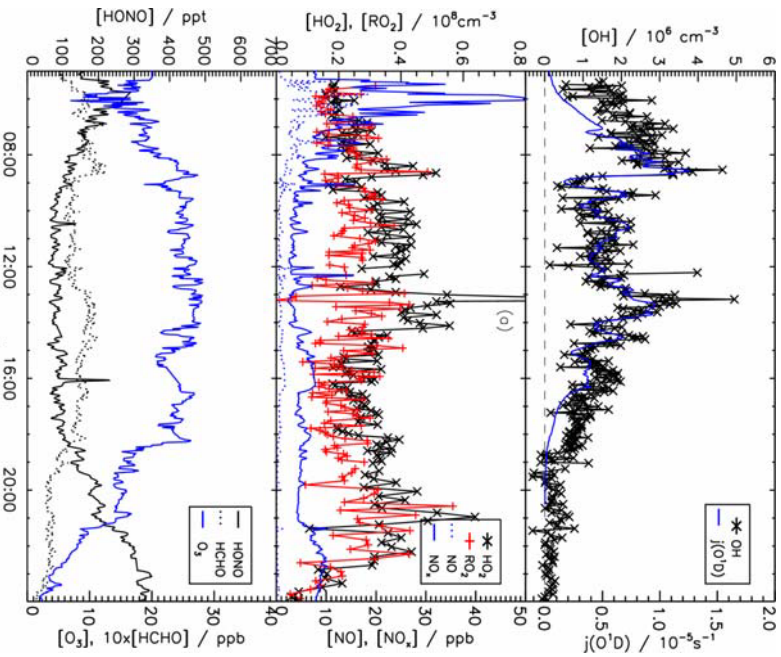

7.1 Measurements during the HOxComp campaign on the 2005-07-07. (a) HO_2 peak about $1.7 \cdot 10^8\, cm^{-3}$.

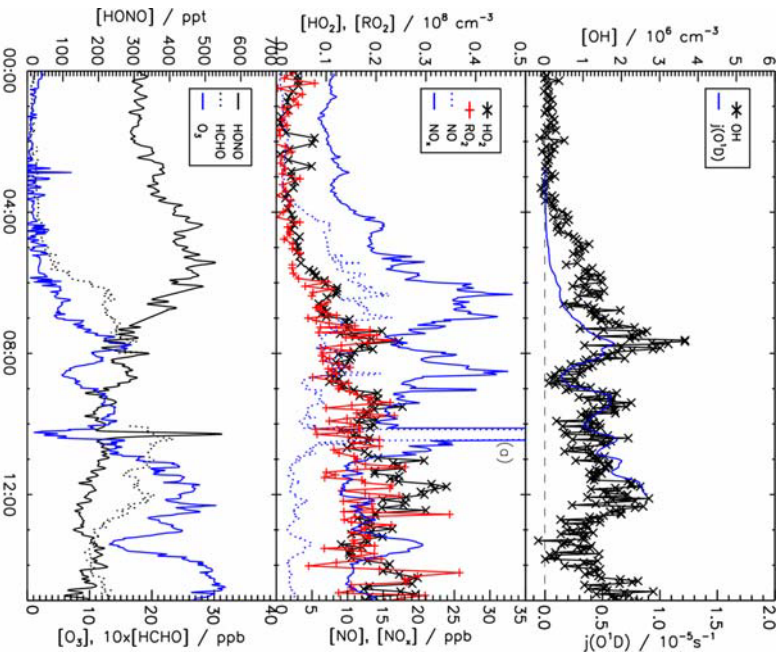

7.2 Measurements during the HOxComp campaign on the 2005-07-08. Measurements of the actinic flux are only available until noon. (a) NO_x peak about 1600 *ppbv*.

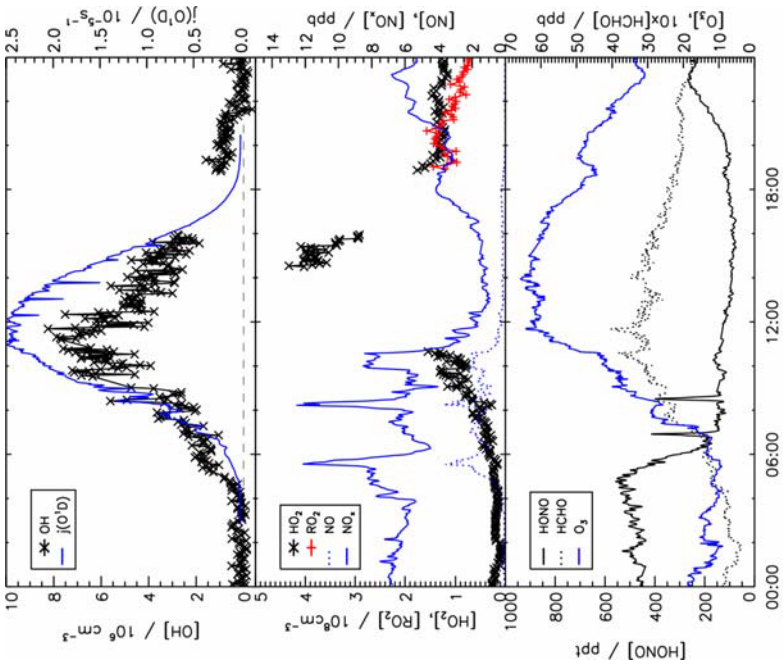

7.4 Measurements during the HOxComp campaign on the 2005-07-10. The "MobiLIF" instrument was running in the HO_x configuration until the evening. No RO_2 radical measurements are available for this period. HO_2 measurements are not present during 11:00Z and 13:00Z because of technical problems. Calibration measurements were performed during 17:00Z and 19:00Z.

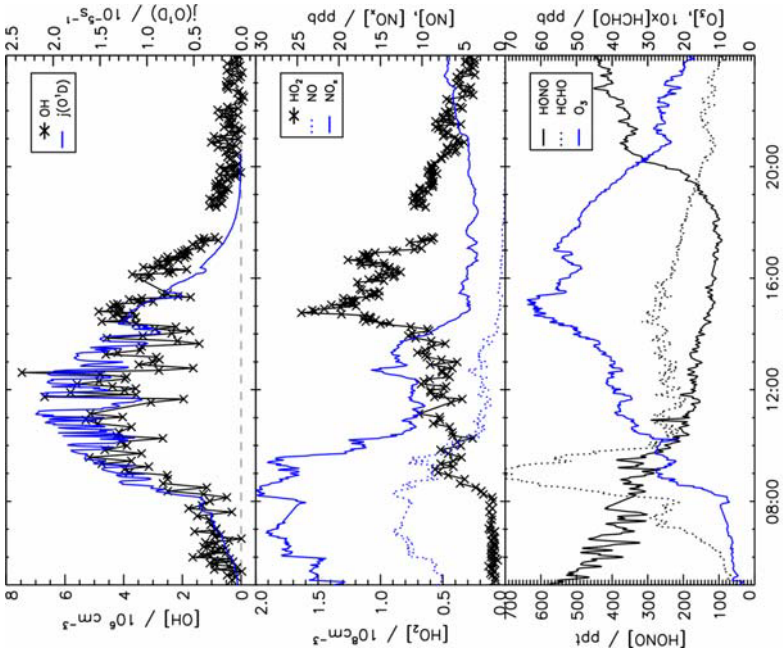

7.3 Measurements during the HOxComp campaign on the 2005-07-09. The "MobiLIF" instrument was running in the HO_x configuration. No RO_2 radical measurements are available.

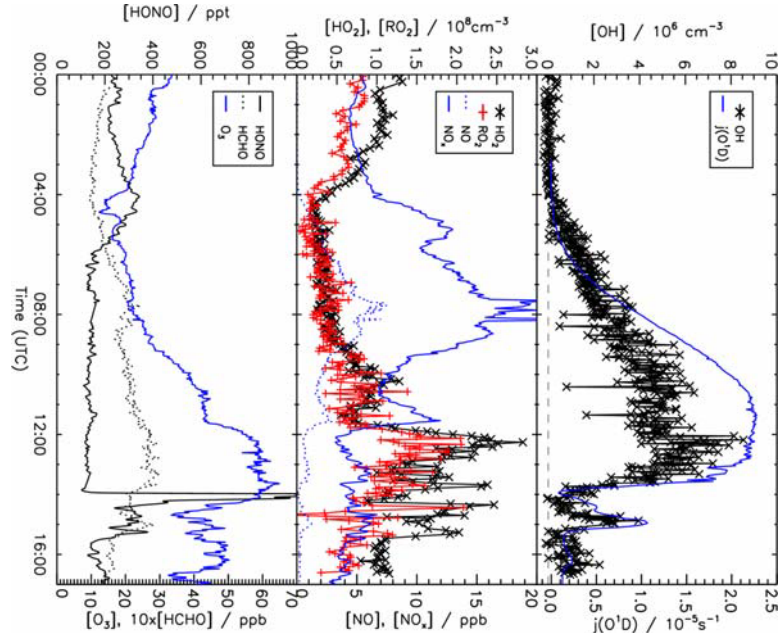

7.5 Measurements during the HOxComp campaign on the 2005-07-11.

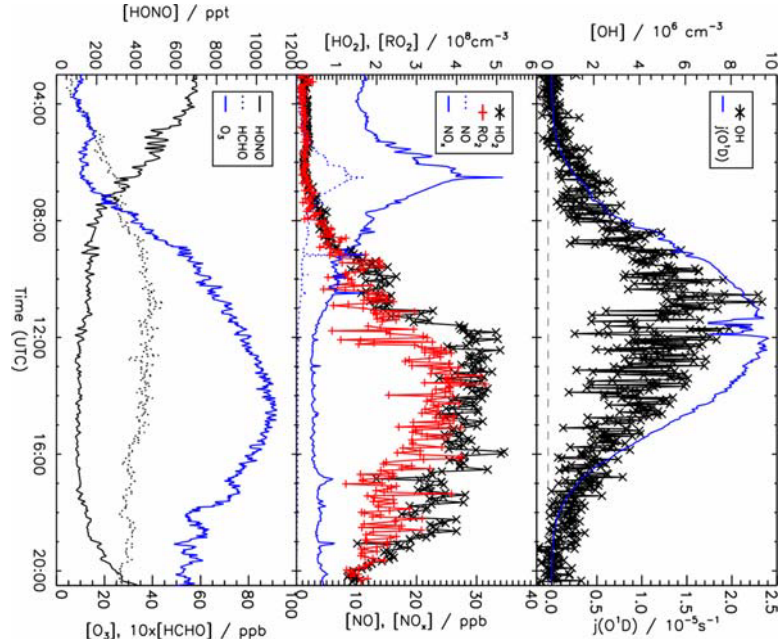

7.6 Measurements during the HOxComp campaign on the 2005-07-14.

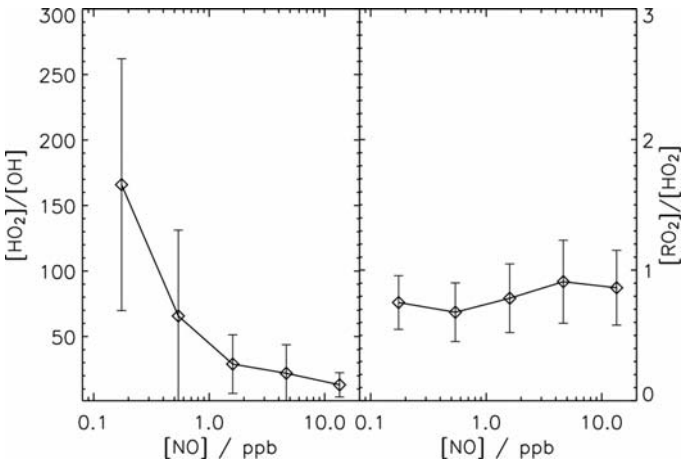

Figure 7.7: Ratios between measured radical concentrations depending on the NO concentration during the HOxComp campaign. Only data during the day are used and are binned to the same log(NO) interval.

to 65 *ppbv* and a rise of radical concentrations. The latter may be caused partly by the photolysis of HCHO which is a source of HO_2.

The ratio of HO_2 to OH radical concentrations (Figure 7.7) shows a clear dependence on the NO mixing ratio. HO_2 concentrations are expected to be larger than the OH concentration because of the generally higher reactivity of OH. HO_2 concentrations are about a factor of 100 higher than OH concentrations for small NO mixing ratios of about 0.1 *ppbv* but they are only a factor of 15 larger for high NO mixing ratios of about 10 *ppbv*. This trend can be understood qualitatively if the photochemical cycling between OH and HO_2 dominates the overall production and destruction of radicals. High NO shifts HO_2 towards OH so that HO_2 concentrations are small. In contrast, HO_2 concentrations can reach higher values for small NO mixing ratios.

This behavior have been also found in other campaigns. Observations by *Ren et al.* (2005) agree with the HO_2/OH ratio found during the HOxComp campaign. *Ren et al.* (2005) reports a decrease of the ratio from about 100 to about 20 for a similar range of NO mixing ratios between 0.1 *ppbv* and 10 *ppbv*. HO_2/OH ratios presented by *Stevens et al.* (1997) are slightly smaller for small NO mixing ratios but the data set is sparse. Measurements by *Cantrell et al.* (2003b) show a qualitatively similar behavior as observed during the HOxComp campaign but NO mixing ratios were in a different range between 1 *pptv* to 300 *pptv*. As can be expected, the HO_2/OH ratios reported by *Cantrell et al.* (2003b) are higher than found during the HOxComp campaign.

In contrast to OH and HO_2 radical concentrations, HO_2 and RO_2 are highly correlated (Figure 7.7). The ratio of measured RO_2 and HO_2 radical concentrations is about 0.8. This is nearly independent of the NO mixing ratio. The good correlation could be explained if assuming that the production and destruction of peroxy radicals

is dominated by interconversion reactions between radical species. The velocity of the interconversion is determined by the destruction of HO_2 and RO_2 because OH and RO radicals are highly reactive. They are converted to RO_2 respectively HO_2 very fast. Both, HO_2 and RO_2 radicals, are destroyed in the reaction with NO. This would explain that the measured ratio is independent of the NO mixing ratio. In addition, the reaction rate constants of the reaction of NO with HO_2 and RO_2 are similar so that similar concentrations can be expected. This is found for the measurements during the HOxComp campaign. Therefore, a dominance of interconversion reactions would explain the observed behavior of the RO_2/HO_2 ratio.

This result has been also found in the methane-OH experiment at SAPHIR (Section 6.3.4) and could be explained by the fast interconversion between HO_2 and CH_3O_2 radicals.

Similar HO_2 and RO_2 radical concentration ratios have been also found by *Mihelcic et al.* (2003) and by *Ren et al.* (2005) for measured as well as for modeled data. Both report a RO_2/HO_2 ratio around 1 which is nearly independent of the NO mixing ratio. However, contrary results for ambient air measurements are presented by *Stevens et al.* (1997); *Cantrell et al.* (2003b); *Fleming et al.* (2006) with respect to the dependence of the RO_2/HO_2 ratio on NO and the value of the ratio.

Peroxy radicals are responsible for the ozone production in the atmosphere as discussed in Chapter 2. Measured peroxy radical concentrations can be used to estimate the ozone production rate $P(O_3)$. It is generally assumed that the photochemical ozone formation rate $P(O_3)$ is approximately determined by the rate at which NO is oxidized to NO_2 by reactions with peroxy radicals (e.g. *Kleinmann et al.* (1995); *Mihelcic et al.* (2003)). In this approach losses of peroxy radicals by the formation of nitrates and the loss of NO_2 by its reaction with OH are neglected. This leads to an upper limit of $P(O_3)$ of:

$$P(O_3) = [NO](k_3[HO_2] + k_1[RO_2]) \tag{7.1}$$

The ozone production rate calculated for measured peroxy radical concentrations during the HOxComp campaign is shown in Figure 7.8. An average rate coefficient of $k_1 = 8.6 \cdot 10^{-12}\, s^{-1} cm^{-3}$ for the reaction of organic peroxy radicals with NO was assumed as done by *Mihelcic et al.* (2003) who estimated the rate coefficient from evaluations of different rate coefficients.

The observed ozone production rate shows an increase from $0.1\,ppbv/h$ to $10\,ppbv/h$ with increasing NO mixing ratio between $0.01\,ppbv$ to $10\,ppbv$. The data set is divided into two subsets. The increase of $P(O_3)$ is shifted to higher NO for one of the subsets but the slopes are similar. An increase of $P(O_3)$ within the same range of NO with increasing NO was also observed by *Mihelcic et al.* (2003); *Ren et al.* (2005). $P(O_3)$ was within the same range with a maximum of $10\,ppbv/h$ as calculated in this work. In contrast to values found by *Ren et al.* (2005) and the calculations in this work, $P(O_3)$ decreases for NO mixing ratios which are higher than $0.5\,ppbv$ in the data set discussed by *Mihelcic et al.* (2003) in which data of several campaigns were summarized. A decrease of $P(O_3)$ at higher NO mixing ratios was also calculated by *Kleinmann et al.* (2000) using a steady state photochemical model and by *Ren et al.* (2005) using the

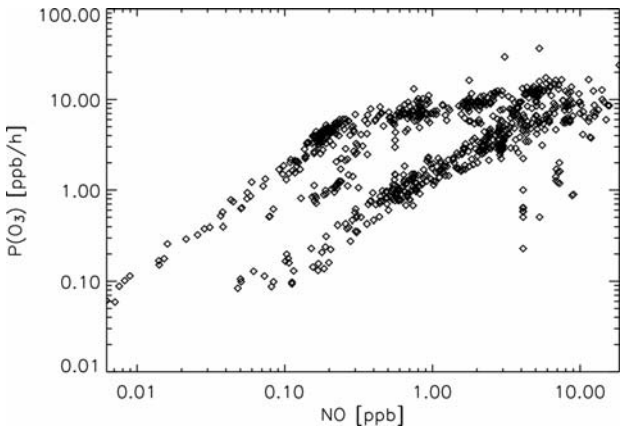

Figure 7.8: Ozone production rate calculated by Equation 7.1 depending on the NO concentration during the HOxComp campaign.

Regional Atmospheric Chemistry Mechanism (RACM, *Stockwell et al.* (1997)). *Ren et al.* (2005) concluded from the observed deviation between model calculations and measurements that current chemical mechanisms miss important processes which lead to higher O_3 production at high NO concentrations.

A detailed analysis of the ambient air measurements during the HOxComp campaign is beyond the scope of this work. Radical concentrations are determined by complex chemical and transport processes. Therefore, this analysis will be the subject of further investigations. However, the diurnal profiles of radical concentrations as well as ratios of concentrations and the ozone production show reasonable results which are similar to those found in literature. This indicates that the instrument has the ability to perform peroxy radical measurement under atmospheric conditions.

8 Conclusions

The aim of this work was to develop a highly sensitive instrument for measurements of ambient peroxy radical concentrations. LIF technique which is an established method for the detection of ambient HO_2 and OH radicals is used in conjunction with the chemical conversion of organic peroxy radicals to HO_2. This is realized by using two differentially pumped chambers. The conversion of RO_2 to HO_2 radicals is achieved in the first chamber by the addition of reactive gases NO and CO. HO_2 is transformed in the second chamber by a further addition of NO leading to the formation of OH radicals which are detected by LIF.

Chemical and physical conditions in the conversion reactor were optimized to maximize the efficiency of the RO_2 radical conversion. This was achieved in laboratory experiments by varying the parameters which determine the conversion efficiency in the reactor. The results were compared to numerical and analytic calculations of the reaction kinetics in the reactor. A good agreement can be observed between experiments and expectations from the calculations. The conversion efficiency is sufficiently high at a reduced pressure of $25\,hPa$ and is maximized for mixing ratios of reactive gases CO of $0.17\,\%$ and NO of $0.7\,ppmv$. The reduced pressure suppresses termolecular gas phase loss reactions. The optimum mixing ratio of NO needed for the conversion of peroxy radicals results from the competition of NO dependent conversion reactions with NO dependent loss reactions. A high concentration of CO is added to shift the OH concentration to HO_2 because OH radicals are easily lost on surfaces and by reactions with trace gases. The optimum reaction time of $0.6\,s$ is mainly determined by the lifetime of RO_2 radicals with respect to the conversion reaction of RO_2 radicals with NO for the chosen conditions. The resulting conversion efficiency of about $65\,\%$ is mainly limited by the loss of HO_2 radicals on the reactor's surfaces. The sensitivities for different organic peroxy radicals are similar in the system because the reaction rate constants of their reaction with NO are within the same range.

The addition of reactive gases leads to the measurement of the sum of OH, HO_2, RO and RO_2 (=RO_x) radicals. Chemical modulation allows to distinguish between the RO_2 and HO_x radical concentrations. If only CO is added to the sampled gas, RO_2 radicals are not converted to HO_2 but the HO_x radical concentration can be measured in the fluorescence cell.

The detection limit of the system is mainly determined by the precision of background signal measurements. The addition of NO in the fluorescence cell causes a background signal which is equivalent to a peroxy radical concentration of about $5 \cdot 10^6\,cm^{-3}$. This is small compared to typical radical concentrations during the day but determines the typical detection limit for HO_x radicals to about $2 \cdot 10^6\,cm^{-3}$. RO_2 radical concentrations are calculated by subtracting the measured HO_x concentration from the measured

RO_x radical concentration. Therefore, the detection limit for RO_2 radicals is mainly determined by the precision of the HO_x measurement to about $7 \cdot 10^6\, cm^{-3}$. The high sensitivity of the LIF detection allows a high temporal resolution of the measurements in the range of one minute.

The system was characterized for being operated in moderately polluted environments. Radical measurements in exceptionally high NO environments (more than $20\, ppbv$) have to be investigated in more detail with respect to a possible detection of RO_2 radicals in the HO_x mode of the system because ambient NO may be sufficiently high for the conversion of RO_2 radicals in the reactor in this case. A possible solution to avoid resulting interference signals could be dilution of the sampled gas with pure nitrogen.

Only a weak dependence of the sensitivity on the water vapor content of the sampled air could be found which can be explained by water dependent quenching of the OH fluorescence.

The sensitivity of the system towards RO_2 and HO_2 radicals is calibrated by using a radical source. Water photolysis is an established method to produce accurately known OH and HO_2 radical concentrations. This technique was extended to produce organic peroxy radicals by the reaction of OH with hydrocarbons which are added to the calibration gas in the radical source. A calibration procedure was developed to determine sensitivities of the system for the different radicals. The accuracy of radical concentration measurements is determined by the calibration to about 10 %.

The exact product yield of OH and HO_2 radicals in the water photolysis is required for an accurate calibration. It was shown experimentally that exactly the same OH and HO_2 concentrations are produced. The precision of the result (1.5 %) was higher than achieved in other experiments before.

Absolute peroxy radical measurements were validated by performing comparison measurements with a reference instrument (MIESR). The results of two experiments under controlled conditions at the atmosphere simulation chamber SAPHIR showed an excellent agreement between the measurements of both instruments. This indicates that absolute radical concentrations measured by the new instrument are reliable.

The reaction mechanisms of the experiments were analyzed by numerical model calculations. Measurements and model calculations of the experiment in which the reaction of OH with methane was studied exhibited a very good agreement. This indicates that the formation of peroxy radicals and thus the potential to form ozone photochemically can be well described by numerical models as implemented e.g. in the MCM vers. 3.1.

Model calculations of the more complex ozonolysis experiment were used to show the potential of the measurements to be used in kinetic studies. Ozonolysis is one important source of nighttime radicals and contributes considerably to the degradation of alkenes in the dark. It was possible to determine branching ratios of different radical reaction paths of the Criegee intermediate which is produced in the ozonolysis of 1-butene with respect to the yields of HO_2 and RO_2 radicals. This allowed to calculate the entire HO_x and RO_2 yields of this mechanism for the first time. The measurements indicate that the RO_2 yield is overestimated by about 30 % by the MCM whereas the HO_x yield

can be described reasonably well.

First ambient air measurements were performed during the international measurement campaign HOxComp in July 2005 showing reasonable diurnal profiles of peroxy radical concentrations. Experimental results are similar to results found in other field measurements. This indicates that the instrument can be operated in field measurements.

The new instrument outperforms most of the existing techniques for measurements of ambient peroxy radical concentrations regarding the detection limit and the time resolution of measurements. The LIF system as a whole is the only system that includes nearly simultaneous measurements of OH, HO_2 and RO_2 radical concentrations.

The sensitivity of PERCA instruments which are the most common devices for ambient RO_x measurements exhibits a strong water vapor dependence which has to be determined carefully. In addition, the detection of peroxy radicals by PERCA instruments is less sensitive, resulting in higher detection limits compared to those of this development. A separation of HO_2 and RO_2 radical concentrations is not possible which complicates the interpretation of data. The second instrument used for ambient RO_x measurements is the MIESR instrument. However, only small data sets with limited time resolution can be achieved. Only PerCIMS instruments which are another class of chemical amplifiers show a similar performance compared to this development with respect to the detection limit, the time resolution and the ability to distinguish between HO_2 and RO_2 radical concentrations.

The ability and performance of the new development to measure RO_2 and HO_2 radical concentrations accurately has been proven. The new instrument can be used for kinetics studies e. g. at the simulation chamber SAPHIR and for ambient air measurements in field campaigns. A full set of sensitive measurements of different radical species with a high temporal resolution will help to analyze measurements in future campaigns and will complete the understanding of the atmospheric chemistry.

Bibliography

Aloisio, S., and J. S. Francisco, Existence of a hydroperoxy and water HO_2-H_2O radical complex, *J. Phys. Chem. A*, *102*, 1899–1902, 1998.

Aloisio, S., J. S. Francisco, and R. R. Friedl, Complexes of hydroxyl and hydroperoxy radicals with formaldehyde, acetaldehyde and acetone, *J. Phys. Chem. A*, *104*, 3211–3224, 2000.

Andrés Hermandéz, M. D., J. Burkert, L. Reichert, D. Stöbener, J. Meyer-Arnek, and J. P. Burrows, Marine boundary layer peroxy radical chemistry during the AEROSOL99 campaign: Measurement and analysis, *J. Geophys. Res.*, *106*, 2001.

Aschmutat, U., M. Heßling, F. Holland, and A. Hofzumahaus, *Physico-Chemical Behaviour of Atmospheric Pollutants*, chap. A tunable source of hydroxyl (OH) and hydroperoxy (HO_2) radicals: In the range between 10^6 and $10^9 cm^{-3}$, pp. 811–816, European Commission, Brussels, 1994.

Atkinson, R., Atmospheric chemistry of VOCs and NO_x, *Atmos. Environ.*, *34*, 2063–2101, 2000.

Atkinson, R., Kinetics of the gas-phase reactions of OH radicals with alkanes and cycloalkanes, *Atmos. Chem. Phys. Discuss.*, *3*, 4183–4358, 2003.

Atkinson, R., and J. Arey, Gas-phase tropospheric chemistry of biogenic volatile organic compounds: A review, *Atmos. Env.*, *37*, 197–219, 2003a.

Atkinson, R., and J. Arey, Atmospheric degradation of volatile organic compounds, *Chem. Rev.*, *103*, 4605–4638, 2003b.

Atkinson, R., and S. M. Aschmann, OH radical production from the gas phase reactions of O_3 with a series of alkenes under atmospheric conditions, *Environ. Sci. Technol.*, *27*, 1357–1363, 1993.

Atkinson, R., W. P. L. Carter, and A. M. Winer, Effects of temperature and pressure on alkyl nitrate yields in the NO_x photooxidations of n-pentane and n-heptane, *J. Phys. Chem.*, *87*, 2012–2018, 1983.

Atkinson, R., S. M. Achmann, and A. M. Winer, Alkyl nitrate formation from the reaction of a series of branched RO_2 radicals with NO as a function of temperature and pressure, *J. Atmos. Chem.*, *5*, 91–102, 1987.

Bacak, A., M. W. Bardwell, M. T. Raventos, C. J. Percival, G. Sanchez-Reyna, and D. E. Shallcross, Kinetics of the reaction of CH_3O_2+NO: A temperature and pressure depence study with chemical ionization mass spectrometry, *J. Phys. Chem. A*, *108*, 10,681–10,687, 2004.

Bajeh, M. A., E. M. Goldfield, A. Hanf, C. Kappel, A. J. H. Meijer, H. Volpp, and J. Wolfrum, Dynamics of the H + O_2 → O + OH chain-branching reaction: A accurate quantum mechanical and experimental absolute reaction cross section, *J. Phys. Chem. A*, *105*, 3359–3364, 2001.

Berresheim, H., T. Elste, C. Plass-Dülmer, F. L. Eisele, and D. J. Tanner, Chemical ionization mass spectrometer for long-term measurements of atmospheric OH and H_2SO_4, *Int. J. Mass Spec.*, *202*, 91–109, 2001.

Berresheim, H., C. Plass-Dülmer, T. Elste, N. Mihalopoulos, and F. Rohrer, OH in the coastal boundary layer of Crete during MINOS: Measurements and relationship with ozone photolysis, *Atmos. Chem. Phys.*, *3*, 639–645, 2003.

Bertram, A. K., A. V. Invanov, M. Hunter, L. T. Molina, and M. J. Molina, The reaction probability of OH on organic surfaces of tropospheric interest, *J. Phys. Chem. A*, *105*, 9415–9421, 2001.

Bey, I., B. Aumont, and G. Toupance, A modeling study of the nighttime radical chemistry in the lower continental troposphere 1. development of a detailed chemical mechanism including nighttime chemistry, *J. Geophys. Res*, *106*, 9959–9990, 2001.

Bloss, W. J., T. J. Gravestock, D. E. Heard, T. Ingham, G. P. Johnson, and J. D. Lee, Application of a compact solid-state laser system to the in situ detection of atomospheric OH, HO_2, NO and IO by laser-induced fluorescence, *J. Environ. Monit.*, *5*, 21–28, 2003.

Bohn, B., and A. Zilken, Model-aided radiometric determination of photolysis frequencies in a sunlight atmosphere simulation chamber, *Atmos. Phys. Chem.*, *5*, 191–206, 2005.

Bottenheim, J. W., A. Sirois, K. A. Brice, and A. J. Gallant, Five years of continuous obervations of PAN and ozone at a rural location in eastern canada, *Atmos. Phys. Chem.*, *5*, 493–503, 2005.

Brauers, T., and F. Rohrer, *Easy AtmoSpheric chemistrY (Vers.2.)*, Forschungzentrum Jülich, FZJ-ICG3-BHB-1234, Version 2.9, 1999.

Brown, R. L., Tubular flow reactor with first-order kinetics, *J. Res. Nat. Bur. Stand.*, *83*, 1977.

Brune, W. H., P. S. Stevens, and J. H. Mather, Measuring OH and HO_2 radicals in the troposphere by laser-induced fluorescence at low pressure, *J. Atmos. Sci.*, *52*, 3328–3336, 1995.

Burkert, J., M.-D. Andrés Hermandéz, D. Stöbener, M. Weissenmayer, and A. Kraus, Peroxy radical and related trace gas measurements in the boundary layer above the atlantic ocean, *J. Geophys. Res.*, *106*, 2001.

Butkovskaya, N. I., A. Kukui, N. Pouvesle, and G. Le Bras, Fomation of nitric acid in the gas-phase HO_2+NO reation: Effects on temperature and water vapor, *J. Phys. Chem. A*, *109*, 6509–6520, 2005.

Cantrell, C. A., D. H. Stedman, and G. J. Wendel, Measurement of atmospheric peroxy radicals by chemical amplification, *Anal. Chem.*, *56*, 1496–1502, 1984.

Cantrell, C. A., R. E. Shetter, J. A. Lind, A. H. McDaniel, J. G. Calvert, D. D. Parrish, F. C. Fehsenfeld, M. P. Buhr, and M. Trainer, An improved chemical amplifier technique for peroxy radial measurements, *J. Geophys. Res.*, *98*, 1993.

Cantrell, C. A., A. Zimmer, and G. S. Tyndall, Absorption cross sections for water vapor from 183 to 193nm, *Geophys. Res. Lett.*, *24*, 2195–2198, 1997.

Cantrell, C. A., G. D. Edwards, S. Stephens, L. Mauldin, E. Kosciuch, M. Zondlo, and F. Eisele, Peroxy radical observations using chemical ionization mass spectrometry during TOPSE, *J. Geophys. Res.*, *108*, 8611, doi: 10.1029/2002JD002,715, 2003a.

Cantrell, C. A., G. D. Edwards, S. Stephens, R. L. Mauldin, M. A. Zondlo, E. Kosciuch, F. L. Eisele, and A. D. Clarke, Peroxy radical behavior during the Transport and Chemical Evolution over the Pacific (TRACE-P) campaign as measured aboard the NASA P-3B aircraft, *J. Geophys. Res.*, *108*, 8797, 2003b.

Carpenter, L. J., T. J. Green, J. P. Mills, S. B. andS. A. Penkett, P. Zanis, E. Schuepbach, N. Schmidbauer, P. S. Monks, and C. Zellweger, Oxidized nitrogen and ozone production efficiencies in the springtime free troposphere over the Alpes, *J. Geophys. Res.*, *102*, 18,917–18,933, 1997.

Carpenter, L. J., P. S. Monks, B. J. Bandy, and S. A. Penkett, A study of peroxy radicals and ozone photochemistry at coastal sites in the northern and southern hemispheres, *J. Geophys. Res.*, *105*, 14,547–14,559, 2000.

Chow, J. M., A. M. Miller, and M. J. Elrod, Kinetics of the $C_3H_7O_2$+NO reaction: Temperature dependence of the overall rate constant and the $i-C_3H_7ONO_2$ branching channel, *J. Phys. Chem. A*, *107*, 3040–3047, 2003.

Clyne, M. A. A., J. A. Coxon, and A. R. Woon Fat, The $A^2\Sigma^+$-$X^2\Pi$ electronic band system of the OD free radical, *J. Mol. Spect.*, *46*, 149–170, 1973.

Copeland, R. A., M. J. Dyer, and D. R. Crosley, Rotational-level-dependent quenching of $A^2\Sigma^+$ OH and OD, *J. Chem. Phys.*, *82*, 1985.

Creasey, D. J., P. A. Halford-Maw, D. E. Heard, M. J. Pilling, and B. J. Whitaker, Implementation and initial deployment of a field instrument for measurement of OH and HO_2 in the troposphere by laser-induced fluorescence, *J. Chem. Soc., Farad. Trans.*, *93*, 1997.

Creasey, D. J., D. E. Heard, and J. D. Lee, Absorption cross section measurements of water vapour and oxygen at 185 *nm*. Implications for the calibration of field instruments to measure OH, HO_2 and RO_2 radicals, *Geophys. Res. Lett.*, *27*, 1651–1654, 2000.

Creasey, D. J., G. E. Evans, D. E. Heard, and J. D. Lee, Measurements of OH and HO_2 concentrations in the southern ocean marine boundary layer, *J. Geophys. Res.*, *108*, 4475, 2003.

Criegee, R., and B. Wenner, Die Ozonisierung des 9-10-Oktalins, *Liegis Ann. Chem.*, *546*, 9–16, 1949.

Dieke, G. H., and H. M. Crosswhite, The ultraviolet bands of OH, *J. Quant. Spectrosc. Radiat. Transfer*, *2*, 97–199, 1962.

Eberhard, J., and C. J. Howart, Rate coefficient for the reactions of some C_3 to C_5 hydrocarbon peroxy radicals with NO, *J. Phys. Chem. A*, *101*, 3360–3366, 1997.

Edwards, G. D., C. A. Cantrell, S. Stephens, B. Hil, O. Goyea, R. E. Shetter, R. L. Mauldin, E. Kosciuch, D. J. Tanner, and F. L. Eisele, Chemical ionization mass spectrometer instrument for the measurement of tropospheric HO_2 and RO_2, *Anal. Chem.*, *75*, 5318–5327, 2003.

Ehhalt, D. H., Photooxidation of trace gases in the troposphere, *Phys. Chem. Chem. Phys.*, *1*, 5401–5408, 1999.

Ehhalt, D. H., and F. Rohrer, Dependence of the OH concentration on solar UV, *J. Geophys. Res.*, *105*, 2000.

Eisele, F. L., and D. J. Tanner, Ion-assisted tropospheric OH measurements, *J. Geophys. Res.*, *96*, 1991.

Elrod, M. J., D. L. Ranschaert, and N. J. Schneider, Direct kinetic study of the temperature dependence of the CH_2O branching channel for the CH_3O_2+HO_2 reaction, *Int. J. Chem. Kinet.*, *33*, 363–376, 2001.

Engel, V., V. Staemmler, R. L. Vander Wal, F. F. Crim, R. J. Sension, B. Hudson, P. Andresen, S. Hennig, K. Weide, and R. Schinke, Photodissociation of water in the first absorption band: A prototype for dissociation on a repulsive potential energy surface, *J. Phys. Chem.*, *96*, 3201–3213, 1992.

Faloona, I. C., D. Tan, R. L. Lehser, N. L. Hazen, C. L. Frame, J. B. Simpas, H. Harder, M. Martinez, P. Di Carlo, X. Ren, and W. H. Brune, A laser-induced fluorescence instrument for detecting tropospheric OH and HO_2: Characteristics and calibration, *J. Atmos. Chem.*, *47*, 139–167, 2004.

Fenske, J. D., A. S. Hasson, S. E. Paulson, K. T. Kuwata, A. Ho, and K. N. Houk, The pressure dependence of the OH-radical yield from ozone-alkene reactions, *J. Phys. Chem. A*, *104*, 7821–7833, 2000.

Finlayson-Pitts, B. J., and J. N. Pitts, Jr., *Chemistry of the upper and lower atmosphere*, Academic Press, 2000.

Fleming, Z. L., P. S. Monks, A. R. Rickard, D. E. Heard, W. J. Bloss, P. W. Seakins, T. J. Still, R. Sommariva, M. J. Pilling, R. Morgan, T. J. Green, N. Brough, G. P. Mills, S. A. Penkett, A. C. Lewis, J. D. Lee, A. Saiz-Lopez, and J. M. C. Plane, Peroxy radical chemistry and the control of ozone photochemistry at Mace Head, Irland during the summer of 2002, *Atmos. Chem. and Phys.*, *6*, 2193–2214, 2006.

Freeman, A. J., Configuration interaction study of the electronic structure of the OH radical by the atomic and molecular orbital model, *J. Chem. Phys.*, *28*, 230–243, 1958.

German, K. R., Direct measurement of the radiative lifetime of the $A^2\Sigma^+, \nu' = 0$ states of OH and OD, *J. Chem. Phys.*, *62*, 2584–2587, 1975.

Geyer, A., K. Bächmann, A. Hofzumahaus, F. Holland, S. Konrad, T. Klüpfel, H. W. Pätz, J. Schäfer, and U. Platt, Nighttime formation of peroxy and hydroxyl radicals during the BERLIOZ campaign: Observations and modeling studies, *J. Geophys. Res.*, *108*, 8249, 2003.

Glover, B. G., and T. A. Miller, Near-IR cavity ringdown spectroscopy and kinetics of the isomers and conformers of the butyl peroxy radical, *J. Phys. Chem. A*, *109*, 11,191–11,197, 2005.

Green, T. J., C. E. Reeves, N. Brough, G. D. Edwards, P. S. Monks, and S. A. Penkett, Airborne measurements of peroxy radicals using the PERCA technique, *J. Eviron. Mon.*, *5*, 75–83, 2003.

Green, T. J., C. E. Reeves, Z. L. Fleming, N. Brough, A. R. Rickard, B. J. Bandy, P. S. Monks, and S. A. Penkett, An improved dual channel PERCA instrument for atmospheric measurements of peroxy radicals, *J. Eviron. Mon.*, *8*, 530–536, 2006.

Grosjean, E., and D. Grosjean, Gas phase reaction of alkenes with ozone: Formation yields of primary carbonyls and biradicals, *Environ. Sci. Technol.*, *31*, 2421–2427, 1997.

Grosjean, E., J. Bittencourt de Andrade, and D. Grosjean, Carbonyl products of the gas-phase reaction of ozone with simple alkenes, *Environ. Sci. Technol.*, *30*, 975–983, 1996.

Guenther, A., C. N. Hewitt, D. Erickson, R. Fall, C. Geron, T. Graedel, P. Harley, L. Klinger, M. Lerdau, W. A. McKay, T. Pierce, B. Schooles, R. Steinbrecher, R. Tallamraju, J. Taylor, and P. Zimmermann, A global model of natural volatile organic compound emissions, *J. Geophys. Res.*, *100*, 8873–8892, 1995.

Guenther, A., C. Geron, T. Pierce, B. Lamb, P. Harlez, and R. Fall, Natural emissions of non-methane volatile organic compounds, carbon monoxide, and oxides of nitrogen from north america, *Atmos. Environ.*, *34*, 2205–2230, 2000.

Hanke, M., J. Uecker, T. Reiner, and F. Arnold, Atmospheric peroxy radicals: ROXMAS, a new mass-spectrometric methodology for the speciated measurements of HO_2 and $\sum RO_2$ and first results, *Int. J. Mass. Spectr.*, *213*, 91–99, 2002.

Hanson, D., J. Orlando, B. Noziere, and E. Kosciuch, Proton transfer mass spectrometry studies of peroxy radicals, *Int. J. Mass Spec.*, *239*, 147–159, 2004.

Hard, T. M., R. J. O'Brian, C. Y. Chan, and a. A. Mehrabzadeh, Tropospheric free radical determination by FAGE, *Environ. Sci. Technol.*, *18*, 768–777, 1984.

Hard, T. M., L. A. George, and R. J. O'Brien, An absolute calibration for gas-phase hydroxyl measurements, *Environ. Sci. Technol.*, *36*, 1783–1790, 2002.

Hasson, A. S., A. W. Ho, K. T. Kuwata, and S. E. Paulson, Production of stabilized Criegee intermediates and peroxides in the gas phase ozonolysis of alkenes: 2. asymmetric and biogenic alkenes, *J. Geophys. Res.*, *106*, 34,143–34,154, 2001.

Hastie, D. R., M. Weissemayer, J. P. Burrows, and G. W. Harris, Calibrated chemical amplifier for atmospheric RO_x measurements, *Anal. Chem.*, *63*, 2048–2057, 1991.

Heard, D. E., and M. J. Pilling, Measurement of OH and HO_2 in the troposphere, *Chem. Rev.*, *103*, 5163–5198, 2003.

Hofzumahaus, A., U. Aschmutat, M. Heßling, F. Holland, and D. H. Ehhalt, The measurement of tropospheric OH radicals by laser-induced fluorescence spectroscopy during POPCORN field campaign, *Geophys. Res. Let.*, *23*, 1996.

Hofzumahaus, A., T. Brauers, U. Aschmutat, U. Brandenburger, H.-P. Dorn, M. Hausmann, M. Heßling, F. Holland, C. Plass-Dülmer, M. Sedlacek, M. Weber, and D. H. Ehhalt, Reply, *Geophys. Res. Lett*, *24*, 3039–3040, 1997.

Holland, F., M. Hessling, and A. Hofzumahaus, In situ measurement of tropospheric OH radicals by laser-induced fluorescence - a description of the KFA instrument, *J. Atm. Sci*, *52*, 1995.

Holland, F., A. Hofzumahaus, J. Schäfer, A. Kraus, and H.-W. Pätz, Measurements of OH and HO_2 radical concentrations and photolysis frequencies during BERLIOZ, *J. Geophys. Res.*, *108*, 2003.

Hu, J., and D. H. Stedman, Free radical detector for tropopheric measurement using chemical amplification, *Anal. Chem.*, *66*, 1994.

IUPAC, Subcommitee on gas kinetic data evaluation for atmospheric chemistry, 2005, http://www.iupac-kinetic.ch.cam.ac.uk.

Jenkin, M. E., S. M. Saunders, and M. J. Pilling, The troposheric degradation of volatile organic compounds: A protocol for mechanism development, *Atmos. Chem. Phys.*, *1*, 81–104, 1997.

Jenkin, M. E., S. M. Saunders, V. Wagner, and M. J. Pilling, Protocol for the development of the Master Chemical Mechanism, MCMv3 (Part B): Tropospheric degradation of aromatic volatile organic compounds, *Atmos. Chem. Phys.*, *3*, 181–193, 2003.

Just, G. M. P., E. N. Sharp, S. J. Zalyubovsky, and T. A. Miller, Cavity ringdown spectroscopy of the $\tilde{A} - \tilde{X}$ electronic transition of the phenyl peroxy radical, *Chem. Phys. Lett.*, *417*, 378–382, 2006.

Kanaya, Y., Y. Sadanaga, J. Matsumoto, U. Sharma, J. Hirokawa, Y. Kajii, and H. Akimoto, Nighttime observation ot the HO_2 radical by a LIF instrument at Oki island, Japan and its possible origins, *J. Geophys. Lett.*, *26*, 2179–2182, 1999.

Kanaya, Y., Y. Sadanaga, K. Nakamura, and H. Akimoto, Development of a ground-based LIF instrument for measuring HO_x radicals: Instrumentation and calibration, *J. Atmos. Chem.*, *38*, 73–110, 2001.

Kanikidou, M., H. B. Singh, K. M. Valentin, and P. J. Crutzen, At two-dimensional study of ethane and propane oxidation in the troposphere, *J. Geophys. Res.*, *96*, 15,395–15,413, 1991.

Karl, M., Modellierung atmosphärisch-chemischer Reaktionen in der Tageslicht-Atmosphären-Simulationskammer SAPHIR, Ph.D. thesis, Universität Münster, 2004.

Karl, M., T. Brauers, H.-P. Dorn, F. Holland, M. Komenda, D. Poppe, F. Rohrer, L. Rupp, A. Schaub, and A. Wahner, Kinetic study of the OH-isoprene and O_3-isoprene reaction in the atmosphere simulation chamber SAPHIR, *Geophys. Res. Let.*, *31*, L05,117, 2004.

Kenner, R. D., F. P. Capetanakis, and F. Stuhl, Kinetic isotope effects in the electronic quenching of OD/OH($A^2\Sigma^+, \nu = 0$) at $296 \pm 4K$, *J. Phys. Chem.*, *94*, 2442–2446, 1990.

Killinger, D. K., Absorption and fluorescence spectrum of OH studied using tunable dye lasers, Ph.D. thesis, University of Michigan, 1978.

Kleffmann, J., R. Kurtenbach, J. Lörzer, P. Wiesen, N. Kalthoff, B. Vogel, and H. Vogel, Measured and simulated vertical profiles of nitrous acid - Part I: Field measurements, *Atmos. Environ.*, *37*, 2949–2955, 2003.

Kleffmann, J., T. Gavriloaiei, A. Hofzumahaus, F. Holland, R. Koppmann, L. Rupp, E. Schlosser, M. Siese, and A. Wahner, Daytime formation of nitrous acid: A major source of OH radicals in a forest, *Geophys. Res. Lett.*, *32*, L05,818, doi:10.1029/2005GL022,524, 2005.

Kleinmann, L., Y. Lee, S. R. Springston, J. H. Lee, L. Nunneracker, J. Weinstein-Lloyd, X. Zhou, and L. Newman, Peroxy radical concentration and ozone formation rate at a rural site in the southeastern United States, *J. Geophys. Res.*, *100*, 1995.

Kleinmann, L., P. H. Daum, D. G. Imre, J. H. Lee, Y. Lee, J. Nunnermacker, S. R. Springston, J. Weinstein-Lloyd, and L. Newman, Ozone production in the New York City urban plume, *J. Geophys. Res.*, *105*, 14,495–14,511, 2000.

Langhoff, S. R., Radiative lifetimes and dipole moments of the $A^2\Sigma^+$, $B^2\Sigma^+$ and $C^2\Sigma^+$ states of OH, *J. Chem. Phys.*, *77*, 1379–1390, 1982.

Lesar, A., M. Hodoscek, E. Drougas, and A. M. Kosmas, Quantum mechanical investigation of the atmospheric reaction CH_3O_2+NO, *J. Phys. Chem. A*, *110*, 7898–7903, 2006.

Lindinger, W., A. Hansel, and A. Jordan, Proton-transfer-reaction mass spectrometry (PTR-MS): On-line monitoring of volatile organic compounds at ppt levels, *Chem. Soc. Rev.*, *27*, 347–354, 1998.

Malleson, A. M., H. M. Kellett, R. G. Myhill, and W. P. Sweetenham, *FACSIMILE User guide*, Technical report, Oxfordshire OX11 0RA, 1990.

Matsumi, Y., F. J. Comes, G. Hancock, A. H. ans A. J. Hynes, M. Kawasaki, and A. R. Ravishankara, Quantum yields for production of $O(^1D)$ in the ultraviolet photolysis of ozone: Recommendation based on evaluation of laboratory data, *J. Geophys. Res.*, *107*, 2002.

MCM, Master Chemical Mechanism, 2003, http://mcm.leeds.ac.uk/MCM/.

Mihelcic, D., P. Müsgen, and D. H. Ehhalt, An improved method of measuring tropospheric NO_2 and RO_2 by matrix isolation and electron spin resonance, *J. Atmos. Chem.*, *3*, 341–361, 1985.

Mihelcic, D., A. Volz-Thomas, H. W. Pätz, D. Kley, and M. Mihelcic, Numerical analysis of ESR spectra from atmospheric samples, *J. Atmos. Chem.*, *11*, 271–297, 1990.

Mihelcic, D., F. Holland, A. Hofzumahaus, L. Hoppe, P. Müsgen, H. W. Pätz, and G. K. Moortgat, Peroxy radicals during BERLIOZ at Pabstthum: Measurements, radical budgets and ozone production, *J. Geophys. Res.*, *108*, 9–1, 2003.

Mihele, C. M., and D. R. Hastie, The sensitivity of the radical amplifier to ambient water vapor, *Geophys. Res. Lett.*, *25*, 1911–1913, 1998a.

Mihele, C. M., and D. R. Hastie, Correction to the sensitivity of the radical amplifier to ambient water vapor, *Geophys. Res. Lett.*, *25*, 3167, 1998b.

Mihele, C. M., and D. R. Hastie, Radical loss in a chain reaction of CO and NO in the presence of water: Implications for the radical amplifier and atmospheric chemistry, *Int. J. Chem. Kinet.*, *31*, 145–152, 1999.

Mihele, C. M., and D. R. Hastie, Optimized operation and calibration procedures for radical amplifyer-type detectors, *J. Atmos. Oc. Tech.*, *17*, 788–794, 2000.

Mohan, H., and Shardanand, *Free radical OH*, NASA Scientific and technical Information office, 1975.

Monks, P. S., L. J. Carpenter, and S. A. Penkett, Night-time peroxy radical chemistry in the remote marine boundary layer over the southern ocean, *Geophys. Res. Lett.*, *23*, 535–538, 1996.

Murphy, D. H., and D. W. Fahey, Mathematical treatment of the wall loss of a trace species in denuder and catalytic converter tubes, *Anal. Chem.*, *59*, 2753–2759, 1987.

NASA, Panel for Data Evaluation, 2003, http://jpldataeval.jpl.nasa.gov/index.html.

Olzman, M., E. Kraka, D. Cremer, R. Gutbrod, and S. Andersson, Energetics, kinetics and product distributions of the reactions of ozone with ethene and 2.3-dimethyl-2-butene, *J. Phys. Chem. A*, *101*, 9421–9429, 1997.

Orlando, J. J., G. S. Tyndall, and T. J. Wallington, The atmospheric chemistry of alkoxy radicals, *Chem. Rev.*, *103*, 4657–4689, 2003.

Paulson, S. E., M. Y. Chung, and A. S. Hasson, OH radical formation from the gas phase reaction of ozone with terminal alkenes and the relationship between structure and mechanism, *J. Phys. Chem.*, *103*, 8125–8138, 1999.

Placet, M., C. O. Mann, R. O. Gilbert, and M. J. Niefer, Emissions of ozone precursors from stationary sources: A critical review, *Atmos. Environ.*, *34*, 2183–2204, 2000.

Platt, U., B. Alicke, R. Dubois, A. Geyer, A. Hofzumahaus, F. Holland, M. Martinez, and J. Stutz, Free radicals and fast photochemistry during BERLIOZ, *J. Atm. Chem.*, *42*, 359–394, 2002.

Poeschl, U., M. Canagaratna, J. T. Jayne, L. T. Molina, D. R. Worsnop, C. E. Kolb, and M. J. Molina, Mass accomodation coefficient of H_2SO_4 vapor on aqueous sulfuric acid surfaces and gaseous diffusion coefficient of H_2SO_4 in N_2/H_2O, *J. Phys. Chem. A*, *102*, 9427–9432, 1998.

Pushkarsky, M. B., S. J. Zalyubovsky, and T. A. Miller, Detection and characterization of alkyl peroxy radicals using cavity ringdown spectroscopy, *J. Chem. Phys.*, *112*, 10,695–10,698, 2000.

Ranschaert, D. L., N. J. Schneider, and M. J. Elrod, Kinetics of the $C_2H_5O_2$+NO_x reactions: Temperature dependence of the overall rate constant and the $C_2H_5ONO_2$ branching channel of $C_2H_5O_2$+NO, *J. Phys. Chem. A*, *104*, 5758–5765, 2000.

Reichert, L., M. D. Andrés Hermandéz, D. Stöbener, J. Burkert, and J. P. Burrows, Investigation of the effect of water complexes in the determination of peroxy radical ambient concentrations: Implications for the atmosphere, *J. Geophys. Res.*, *108*, 4017, 2003.

Reiner, T., M. Hanke, and F. Arnold, Atmospheric peroxy radical measurement by ion molecule reaction-mass spectroscopy: A novel analytic method using amplifying chemical conversion to sulfuric acid, *J. Geophys. Res.*, *102*, 1997.

Reiner, T., M. Hanke, F. Arnold, H. Zierreis, H. Schlager, and W. Junkermann, Aircraft-borne measurements of peroxy radicals by chemical conversion/ion molecule reaction mass spectrometry: Calibration, diagnostics and results, *J. Geophys. Res.*, *104*, 1999.

Ren, X., , W. H. Brune, C. A. Cantrell, G. D. Edwards, T. Shirley, A. R. Metcalf, and R. L. Lesher, Hydroxyl and peroxy radical chemistry in a rural area of central Pennsylvania: Oberservations and model comparisons, *J. Atmos. Chem.*, *52*, 231–257, 2005.

Richter, C., Personal communication, 2006.

Ridley, B. A., F. E. Grahek, and J. G. Walega, A small, high-sensitivity, medium-response ozone detector suitable for measurements from light aircraft, *J. Atmos. Ocean Tech.*, *9*, 142–148, 1992.

Rodriguez Bares, S., Untersuchungen zur Ozonolyse einfacher Alkene in der Atmosphärensimulationskammer SAPHIR, Ph.D. thesis, Universität Köln, 2003.

Rohrer, F., Personal communication, 2006.

Rohrer, F., and D. Brüning, Surface NO and NO_2 mixing ratios measured between 30°N and 30°S in the atlantic region, *J. Atmos. Chem.*, *15*, 253–267, 1992.

Rohrer, F., B. Bohn, T. Brauers, D. Brüning, F. Johnen, A. Wahner, and J. Kleffmann, Characterisation of the photolytic HONO-source in the atmosphere simulation chamber SAPHIR, *Atmos. Chem. Phys.*, *5*, 2189–2201, 2005.

Sadanaga, Y., J. Matsumoto, K. Sakurai, R. Isozaki, S. Kato, T. Nomaguchi, H. Bandow, and Y. Kajii, Development of a measurement system of OH reactivity in the atmosphere by using a laser-induced pump and probe technique, *Rev. Sci. Instr.*, *75*, 2004a.

Sadanaga, Y., A. Yoshino, K. Watanaba, A. Yoshioka, Y. Wakazono, Y. Kanaya, and Y. Kajii, Development of a measurement system of peroxy radicals using a chemical amplification/laser-induced fluorescence technique, *Rev. Sci. Inst.*, *75*, 864–872, 2004b.

Saunders, S. M., M. E. Jenkin, R. G. Derwent, and M. J. Pilling, Protocol for the development of the Master Chemical Mechanism, MCMv3 (Part A): Tropospheric degradation of non-aromatic volatile organic compounds, *Atmos. Chem. Phys.*, *3*, 161–180, 2003.

Saywer, R. F., R. A. Harley, S. H. Cadle, J. M. Norbeck, R. Slott, and H. A. Bravo, Mobile sources critical review: 1998 NARSTO assessment, *Atmos. Environ.*, *34*, 2161–2181, 2000.

Scholtens, K. W., B. M. Messer, C. D. Cappa, and M. J. Elrod, Kinetics of the CH_3O_2+NO reaction: Temperature dependence of the overall rate constant and improved upper limit for the CH_3ONO_2 branching channel, *J. Geophys. Res.*, *100*, 18,811–18,816, 1995.

Schultz, M., M. Heitlinger, D. Mihelcic, and A. Volz-Thomas, Calibration source for peroxy radicals with built-in actinometry using H_2O and O_2 photolysis at $185\,nm$, *J. Geophys. Res.*, *100*, 18,811–18,816, 1995.

Sedlacek, M., Messung der Hydroxylradikal-Konzentration in der marinen Troposphäre mittels laserinduzierter Fluoreszenz, Ph.D. thesis, Universität Bonn, 2001.

Stevens, P. S., J. H. Mather, and W. H. Brune, Measurement of tropospheric OH and HO_2 by laser-induced fluorescence at low pressure, *J. Geophys. Res.*, *99*, 3543–3557, 1994.

Stevens, P. S., J. H. Mather, W. H. Brune, F. Eisele, D. Tanner, A. Jefferson, C. Cantrell, R. Shetter, S. Sewall, A. Fried, B. Henry, E. Williams, K. Baumann, P. Goldan, and W. Kruster, HO_2/OH and RO_2/HO_2 ratios during the tropospheric OH photochemistry experiment: Measurement and theory, *J. Geophys. Res.*, *102*, 6379–6391, 1997.

Stockwell, W. R., F. Kirchner, and M. Kuhn, A new mechanism for regional atmospheric chemistry modeling, *J. Geophys. Res.*, *102*, 25,847–25,879, 1997.

van Dishoeck, E. F., and A. Dalgarno, Photodissociation processes in the OH molecule, *J. Chem. Phys.*, *79*, 1983.

Wadt, W. R., and W. A. Goddard, The electronic structure of Criegee intermediate. Ramifications of the mechanism of ozonolysis, *J. Am. Chem. Soc.*, *97*, 3004–3021, 1975.

Weber, M., Entwicklung und Einsatz eines Instrumentes zur Bestimmung der Konzentration von HO_2-Radikalen in der Troposphäre, Ph.D. thesis, Universität Köln, 1998.

Wegener, R., Personal communication, 2006.

Zalyubovsky, S. J., D. Wang, and T. A. Miller, Observation of the $\tilde{A} - \tilde{X}$ electronic transition of the CF_3O_2 radical, *Chem. Phys. Lett.*, *335*, 298–304, 2001.

Zalyubovsky, S. J., B. G. Glover, and T. A. Miller, Cavity ringdown spectroscopy of the $\tilde{A} - \tilde{X}$ electronic transition of the $CH_3C(O)O_2$ radical, *J. Phys. Chem. A*, *107*, 7704–7712, 2003.

Zalyubovsky, S. J., B. G. Glover, and T. A. Miller, Observation of the $\tilde{A} - \tilde{X}$ electronic transition of the 1-$C_3H_7O_2$ and 2-$C_3H_7O_2$ radicals using cavity ringdown spectroscopy, *J. Phys. Chem. A*, *109*, 1308–1315, 2005.

Zhang, D., R. Zhang, and S. W. North, Experimental study of NO reaction with isoprene hydroxyalkyl peroxy radical, *J. Phys. Chem. A*, *107*, 26,916–16,925, 2003.

Zhang, D. H., M. A. Collins, and S. Lee, First-principle theory for the H+H_2O, D_2O reactions, *Science*, *290*, 961–963, 2000.

Zhang, J., T. Dransfield, and N. M. Donahue, On the mechanism for nitrate formation via the peroxy radical + NO reaction, *J. Phys. Chem. A*, *108*, 9082–9095, 2004.

A The absorption spectrum of OH

Detailed descriptions of the OH absorption spectrum can be found in *Freeman* (1958); *Killinger* (1978); *Dieke and Crosswhite* (1962); *van Dishoeck and Dalgarno* (1983); *Mohan and Shardanand* (1975); *Langhoff* (1982).

The absorption lines of OH radicals used for the excitation of OH in this work can be explained by transitions between the ground state $X^2\Pi$ and the first excited state $A^2\Sigma^+$ (Figure A.1). The rotational states of the ground state are divided in two electronic substates $^2\Pi_{1/2}$ and $^2\Pi_{3/2}$ because of the spin-orbit coupling (fine structure). The energy levels of the substates are labeled with F_1 and F_2. There is no spin-orbit coupling in the excited electronic state $A^2\Sigma^+$ due to the lack of any angular momentum.

Quantum numbers in Figure A.1 refer to:

- N: angular momentum (rotation+orbit) as defined by *Mohan and Shardanand* (1975)
- F: fine structure (spin-orbit coupling)
- J: total angular momentum
- P: parity

Absorption lines are labeled by $X_{F'F"}(N')$ whereby X denotes the rotational branch Q,R or P and N' the quantum number of the angular momentum in the ground state. Subscripts $_{F'F"}$ show the fine structure whereby F" refers to the ground state and F' to the excited state (*Dieke and Crosswhite*, 1962). Only transitions which refer to the excitation spectrum in Figure 4.4 are shown.

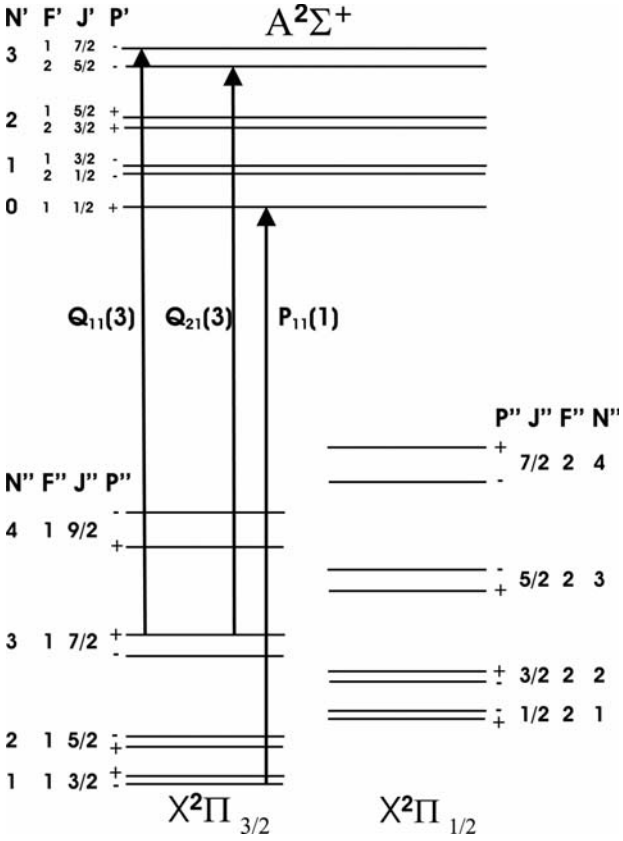

Figure A.1: Schematic of the branches in the rotational structure of OH showing the transitions used for laser excitation in this work.

B List of abbreviations

BERLIOZ	BERLIner OZon Kampagne in 1998
BBO	Beta-BariumbOrate crystal
CL	Chain Length
CLD	ChemiLuminescence Detector
DOAS	Differential Optical Absorption Spectroscopy
DPH	Dew Point Hygrometer
FAGE	Fluorescence Assay by Gas Expansion
FEP	per-Fluoro-Ethylene-Propylen
FZJ	Forschungzentrum Jülich
FWHM ...	Full Width Half Maximum
GC	Gas Chromatograph
HO_x	sum of OH and HO_2 radicals
HOxComp	HO_x measurements Comparison campaign in 2005
LIF	Laser-Induced Fluorescence
LoD	Limit of Detection
MCM	Master Chemical Mechanism
MCP	Micro Channel Plate photomultiplier
MIESR ...	Matrix Isolation and Electron Spin Resonance
MobiLIF .	name of the mobile LIF instrument
NMHC ...	Non-Methane HydroCarbon
NO_x	sum of NO and NO_2
PERCA ..	PEroxy Radical Chemical Amplifier
PerCIMS .	Peroxy radical Chemical Ionization Mass Spectrometry
PAN	Peroxy Acetyl Nitrate
PMT	PhotoMultiplier Tube
PNA	PeroxyNitric Acid
ppbv	parts per billion per volume
ppmv	parts per million per volume
pptv	parts per trillion per volume
PSS	Photo Stationary State
PTR-MS .	Proton Transfer Reaction Mass Spectrometry
RO_x	sum of RO_2, RO, HO_2 and OH radicals
ROxMas .	RO_x Chemical Conversion/CIMS

SAPHIR .	Simulation of Atmospheric PHotochemistry In a large Reaction chamber
SaphirLIF	name of the LIF instrument at the SAPHIR chamber
SHG	Second Harmonic Generation
slm	flow of one liter per minute at $1atm$, $20°C$
$sccm$	flow of one cm^3 per minute at $1atm$, $20°C$
SNR	Signal-to-Noise-Ratio
UTC	universal time
UV-VIS ..	ultraviolet and visible wavelength range
VOC	Volatile Organic Compound

Acknowledgements

I thank Prof Dr Beate Röder for accepting the scientific supervision of this thesis for the Humboldt-University Berlin. Furthermore, I thank PD Dr Andreas Hofzumahaus for the supervision of this thesis for the Forschungszentrum Jülich and for many fruitful discussions about this work. I am indebted to all other members, especially Dr Frank Holland, and former members of the LIF group at the ICG-II who were always helpful with hints and comments.

I thank Dr Eric Schlosser, Dr Frank Holland and Danielle Cohn for proofreading of this work.

In addition, I thank all people who were involved in the experiments at the SAPHIR chamber for operating the chamber and for providing supporting data, especially Dr Djuro Mihelcic and Peter Müssgen who performed the MIESR measurements.

Schriften des Forschungszentrums Jülich
Reihe Umwelt / Environment

1. **Energiemodelle in der Bundesrepublik Deutschland. Stand der Entwicklung**
   IKARUS-Workshop vom 24. bis 25. Januar 1996
   herausgegeben von S. Molt, U. Fahl (1997), 292 Seiten
   ISBN: 3-89336-205-3

2. **Ausbau erneuerbarer Energiequellen in der Stromwirtschaft**
   Ein Beitrag zum Klimaschutz
   Workshop am 19. Februar 1997, veranstaltet von der Forschungszentrum Jülich GmbH und der Deutschen Physikalischen Gesellschaft
   herausgegeben von J.-Fr. Hake, K. Schultze (1997), 138 Seiten
   ISBN: 3-89336-206-1

3. **Modellinstrumente für CO_2-Minderungsstrategien**
   IKARUS-Workshop vom 14. bis 15. April 1997
   herausgegeben von J.-Fr. Hake, P. Markewitz (1997), 284 Seiten
   ISBN: 3-89336-207-X

4. **IKARUS-Datenbank - Ein Informationssystem zur technischen, wirtschaftlichen und umweltrelevanten Bewertung von Energietechniken**
   IKARUS. Instrumente für Klimagas-Reduktionsstrategien
   Abschlußbericht Teilprojekt 2 „Datenbank“
   H.-J. Laue, K.-H. Weber, J. W. Tepel (1997), 90 Seiten
   ISBN: 3-89336-214-2

5. **Politikszenarien für den Klimaschutz**
   Untersuchungen im Auftrag des Umweltbundesamtes
   Band 1. Szenarien und Maßnahmen zur Minderung von CO_2-Emissionen in Deutschland bis zum Jahre 2005
   herausgegeben von G. Stein, B. Strobel (1997), 410 Seiten
   ISBN: 3-89336-215-0

6. **Politikszenarien für den Klimaschutz**
   Untersuchungen im Auftrag des Umweltbundesamtes
   Band 2. Emissionsminderungsmaßnahmen für Treibhausgase, ausgenommen energiebedingtes CO_2
   herausgegeben von G. Stein, B. Strobel (1997), 110 Seiten
   ISBN: 3-89336-216-9

7. **Modelle für die Analyse energiebedingter Klimagasreduktionsstrategien**
   IKARUS. Instrumente für Klimagas-Reduktionsstrategien
   Abschlußbericht Teilprojekt 1 „Modelle“
   P. Markewitz, R. Heckler, Ch. Holzapfel, W. Kuckshinrichs, D. Martinsen, M. Walbeck, J.-Fr. Hake (1998), VI, 276 Seiten
   ISBN: 3-89336-220-7

8. **Politikszenarien für den Klimaschutz**
   Untersuchungen im Auftrag des Umweltbundesamtes
   Band 3. Methodik-Leitfaden für die Wirkungsabschätzung von Maßnahmen zur Emissionsminderung
   herausgegeben von G. Stein, B. Strobel (1998), VIII, 95 Seiten
   ISBN: 3-89336-222-3

9. **Horizonte 2000**
   6. Wolfgang-Ostwald-Kolloquium der Kolloid-Gesellschaft
   3. Nachwuchstage der Kolloid- und Grenzflächenforschung
   Kurzfassungen der Vorträge und Poster
   zusammengestellt von F.-H. Haegel, H. Lewandowski, B. Krahl-Urban (1998), 150 Seiten
   ISBN: 3-89336-223-1

10. **Windenergieanlagen - Nutzung, Akzeptanz und Entsorgung**
    von M. Kleemann, F. van Erp, R. Kehrbaum (1998), 59 Seiten
    ISBN: 3-89336-224-X

11. **Policy Scenarios for Climate Protection**
    Study on Behalf of the Federal Environmental Agency
    Volume 4. Methodological Guideline for Assessing the Impact of Measures for Emission Mitigation
    edited by G. Stein, B. Strobel (1998), 103 pages
    ISBN: 3-89336-232-0

12. **Der Landschaftswasserhaushalt im Flußeinzugsgebiet der Elbe**
    Verfahren, Datengrundlagen und Bilanzgrößen
    Analyse von Wasserhaushalt, Verweilzeiten und Grundwassermilieu im Flußeinzugsgebiet der Elbe (Deutscher Teil). Abschlußbericht Teil 1.
    von R. Kunkel, F. Wendland (1998), 110 Seiten
    ISBN: 3-89336-233-9

13. **Das Nitratabbauvermögen im Grundwasser des Elbeeinzugsgebietes**
    Analyse von Wasserhaushalt, Verweilzeiten und Grundwassermilieu im Flußeinzugsgebiet der Elbe (Deutscher Teil). Abschlußbericht Teil 2.
    von F. Wendland, R. Kunkel (1999), 166 Seiten
    ISBN: 3-89336-236-3

14. **Treibhausgasminderung in Deutschland zwischen nationalen Zielen und internationalen Verpflichtungen**
    IKARUS-Workshop am 27.05.1998, Wissenschaftszentrum Bonn-Bad Godesberg. Proceedings
    herausgegeben von E. Läge, P. Schaumann, U. Fahl (1999), ii, VI, 146 Seiten
    ISBN: 3-89336-237-1

15. **Satellitenbildauswertung mit künstlichen Neuronalen Netzen zur Umweltüberwachung**
Vergleichende Bewertung konventioneller und Neuronaler Netzwerkalgorithmen und Entwicklung eines integrierten Verfahrens
von D. Klaus, M. J. Canty, A. Poth, M. Voß, I. Niemeyer und G. Stein (1999), VI, 160 Seiten
ISBN: 3-89336-242-8

16. **Volatile Organic Compounds in the Troposphere**
Proceedings of the Workshop on Volatile Organic Compounds in the Troposphere held in Jülich (Germany) from 27 – 31 October 1997
edited by R. Koppmann, D. H. Ehhalt (1999), 208 pages
ISBN: 3-89336-243-6

17. **CO_2-Reduktion und Beschäftigungseffekte im Wohnungssektor durch das CO_2-Minderungsprogramm der KfW**
Eine modellgestützte Wirkungsanalyse
von M. Kleemann, W. Kuckshinrichs, R. Heckler (1999), 29 Seiten
ISBN: 3-89336-244-4

18. **Symposium über die Nutzung der erneuerbaren Energiequellen Sonne und Wind auf Fischereischiffen und in Aquakulturbetrieben**
Symposium und Podiumsdiskussion, Izmir, Türkiye, 28.-30.05.1998. Konferenzbericht
herausgegeben von A. Özdamar, H.-G. Groehn, K. Ülgen (1999), IX, 245 Seiten
ISBN: 3-89336-247-9

19. **Das Weg-, Zeitverhalten des grundwasserbürtigen Abflusses im Elbeeinzugsgebiet**
Analyse von Wasserhaushalt, Verweilzeiten und Grundwassermilieu im Flußeinzugsgebiet der Elbe (Deutscher Teil). Abschlußbericht Teil 3.
von R. Kunkel, F. Wendland (1999), 122 Seiten
ISBN: 3-89336-249-5

20. **Politikszenarien für den Klimaschutz**
Untersuchungen im Auftrag des Umweltbundesamtes
Band 5. Szenarien und Maßnahmen zur Minderung von CO_2-Emissionen in Deutschland bis 2020
herausgegeben von G. Stein, B. Strobel (1999), XII, 201 Seiten
ISBN: 3-89336-251-7

21. **Klimaschutz durch energetische Sanierung von Gebäuden. Band 1**
von J.-F. Hake, M. Kleemann, G. Kolb (1999), 216 Seiten
ISBN: 3-89336-252-2

22. **Electroanalysis**
Abstracts of the 8th International Conference held from 11 to 15 June 2000 at the University of Bonn, Germany
edited by H. Emons, P. Ostapczuk (2000), ca. 300 pages
ISBN: 3-89336-261-4

23. **Die Entwicklung des Wärmemarktes für den Gebäudesektor bis 2050**
von M. Kleemann, R. Heckler, G. Kolb, M. Hille (2000), II, 94 Seiten
ISBN: 3-89336-262-2

24. **Grundlegende Entwicklungstendenzen im weltweiten Stoffstrom des Primäraluminiums**
von H.-G. Schwarz (2000), XIV, 127 Seiten
ISBN: 3-89336-264-9

25. **Klimawirkungsforschung auf dem Prüfstand**
Beiträge zur Formulierung eines Förderprogramms des BMBF
Tagungsband des Workshop „Klimaforschung“, Jülich, vom 02. bis 03.12.1999
von J.-Fr. Hake, W. Fischer (2000), 150 Seiten
ISBN: 3-89336-270-3

26. **Energiezukunft 2030**
Schlüsseltechnologien und Techniklinien
Beiträge zum IKARUS-Workshop 2000 am 2./3. Mai 2000
herausgegeben von U. Wagner, G. Stein (2000), 201 Seiten
ISBN: 3-89336-271-1

27. **Der globale Wasserkreislauf und seine Beeinflussung durch den Menschen**
Möglichkeiten zur Fernerkundungs-Detektion und -Verifikation
von D. Klaus und G. Stein (2000), 183 Seiten
ISBN: 3-89336-274-6

28. **Satelliten und nukleare Kontrolle**
Änderungsdetektion und objektorientierte, wissensbasierte Klassifikation von Multispektralaufnahmen zur Unterstützung der nuklearen Verifikation
von I. Niemeyer (2001), XIV, 206 Seiten
ISBN: 3-89336-281-9

29. **Das hydrologische Modellsystem J2000**
Beschreibung und Anwendung in großen Flußgebieten
von P. Krause (2001), XIV, 247 Seiten
ISBN: 3-89336-283-5

30. **Aufwands- und ergebnisrelevante Probleme der Sachbilanzierung**
von G. Fleischer, J.-Fr. Hake (2002), IV, 64 Blatt
ISBN: 3-89336-293-2

31. **Nachhaltiges Management metallischer Stoffströme**
Indikatoren und deren Anwendung
Workshop, 27.-28.06.2001 im Congresscentrum Rolduc, Kerkrade (NL)
herausgegeben von W. Kuckshinrichs, K.-L. Hüttner (2001), 216 Seiten
ISBN: 3-89336-296-7

32. **Ansätze zur Kopplung von Energie- und Wirtschaftsmodellen zur Bewertung zukünftiger Strategien**
IKARUS-Workshop am 28. Februar 2002, BMWi, Bonn. Proceedings
herausgegeben von S. Briem, U. Fahl (2003), IV, 184 Seiten
ISBN: 3-89336-321-1

33. **TRACE. Tree Rings in Archaeology, Climatology and Ecology**
Volume 1: Proceedings of the Dendrosymposium 2002,
April 11th – 13th 2002, Bonn/Jülich, Germany
edited by G. Schleser, M. Winiger, A. Bräuning et al., (2003), 135 pages, many partly coloured illustrations
ISBN: 3-89336-323-8

34. **Klimaschutz und Beschäftigung durch das KfW-Programm zur CO_2-Minderung und das KfW-CO_2-Gebäudesanierungsprogramm**
von M. Kleemann, R. Heckler, A. Kraft u. a., (2003), 53 Seiten
ISBN: 3-89336-326-2

35. **Klimaschutz und Klimapolitik: Herausforderungen und Chancen**
Beiträge aus der Forschung
herausgegeben von J.-Fr. Hake, K. L. Hüttner (2003), III, 231 Seiten
ISBN: 3-89336-327-0

36. **Umweltschutz und Arbeitsplätze, angestoßen durch die Tätigkeiten des Schornsteinfegerhandwerks**
Auswertung von Schornsteinfeger-Daten
von M. Kleemann, R. Heckler, B. Krüger (2003), VII, 66 Seiten
ISBN: 3-89336-328-9

37. **Die Grundwasserneubildung in Nordrhein-Westfalen**
von H. Bogena, R. Kunkel, T. Schöbel, H. P. Schrey, F. Wendland (2003), 148 Seiten
ISBN: 3-89336-329-7

38. **Dendro-Isotope und Jahrringbreiten als Klimaproxis der letzten 1200 Jahre im Karakorumgebirge/Pakistan**
von K. S. Treydte (2003), XII, 167 Seiten
ISBN: 3-89336-330-0

39. **Das IKARUS-Projekt: Energietechnische Perspektiven für Deutschland**
herausgegeben von P. Markewitz, G. Stein (2003), IV, 274 Seiten
ISBN: 3-89336-333-5

40. **Umweltverhalten von MTBE nach Grundwasserkontamination**
von V. Linnemann (2003), XIV, 179 Seiten
ISBN: 3-89336-339-4

41. **Climate Change Mitigation and Adaptation: Identifying Options for Developing Countries**
Proceedings of the Summer School on Climate Change, 7-17 September 2003, Bad Münstereifel, Germany
edited by K. L. Hüttner, J.-Fr. Hake, W. Fischer (2003), XVI, 341 pages
ISBN: 3-89336-341-6

42. **Mobilfunk und Gesundheit: Risikobewertung im wissenschaftlichen Dialog**
von P. M. Wiedemann, H. Schütz, A. T. Thalmann (2003), 111 Seiten
ISBN: 3-89336-343-2

43. **Chemical Ozone Loss in the Arctic Polar Stratosphere: An Analysis of Twelve Years of Satellite Observations**
by S. Tilmes (2004), V, 162 pages
ISBN: 3-89336-347-5

44. **TRACE. Tree Rings in Archaeology, Climatology and Ecology**
Volume 2: Proceedings of the Dendrosymposium 2003,
May 1st – 3rd 2003, Utrecht, The Netherlands
edited by E. Jansma, A. Bräuning, H. Gärtner, G. Schleser (2004), 174 pages
ISBN: 3-89336-349-1

45. **Vergleichende Risikobewertung: Konzepte, Probleme und Anwendungsmöglichkeiten**
von H. Schütz, P. M. Wiedemann, W. Hennings et al. (2004), 231 Seiten
ISBN: 3-89336-350-5

46. **Grundlagen für eine nachhaltige Bewirtschaftung von Grundwasserressourcen in der Metropolregion Hamburg**
von B. Tetzlaff, R. Kunkel, R. Taugs, F. Wendland (2004), 87 Seiten
ISBN: 3-89336-352-1

47. **Die natürliche, ubiquitär überprägte Grundwasserbeschaffenheit in Deutschland**
von R. Kunkel, H.-J. Voigt, F. Wendland, S. Hannappel (2004), 207 Seiten
ISBN: 3-89336-353-X

48. **Water and Sustainable Development**
edited by H. Bogena, J.-Fr. Hake, H. Vereecken (2004), 199 pages
ISBN: 3-89336-357-2

49. **Geo- and Biodynamic Evolution during Late Silurian / Early Devonian Time (Hazro Area, SE Turkey)**
by O. Kranendonck (2004), XV, 268 pages
ISBN: 3-89336-359-9

50. **Politikszenarien für den Umweltschutz**
Untersuchungen im Auftrag des Umweltbundesamtes
Langfristszenarien und Handlungsempfehlungen ab 2012 (Politikszenarien III)
herausgegeben von P. Markewitz u. H.-J. Ziesing (2004), XVIII, 502 Seiten
ISBN: 3-89336-370-X

51. **Die Sauerstoffisotopenverhältnisse des biogenen Opals lakustriner Sedimente als mögliches Paläothermometer**
von R. Moschen (2004), XV, 130 Seiten
ISBN: 3-89336-371-8

52. **MOSYRUR: Water balance analysis in the Rur basin**
von Heye Bogena, Michael Herbst, Jürgen-Friedrich Hake, Ralf Kunkel, Carsten Montzka, Thomas Pütz, Harry Vereecken, Frank Wendland (2005), 155 Seiten
ISBN: 3-89336-385-8

53. **TRACE. Tree Rings in Archaeology, Climatology and Ecology**
Volume 3: Proceedings of the Dendrosymposium 2004,
April 22nd – 24th 2004, Birmensdorf, Switzerland
edited by Holger Gärtner, Jan Esper, Gerhard H. Schleser (2005), 176 pages
ISBN: 3-89336-386-6

54. **Risikobewertung Mobilfunk: Ergebnisse eines wissenschaftlichen Dialogs**
herausgegeben von P. M. Wiedemann, H. Schütz, A. Spangenberg (2005), ca. 380 Seiten
ISBN: 3-89336-399-8

55. **Comparison of Different Soil Water Extraction Systems for the Prognoses of Solute Transport at the Field Scale using Numerical Simulations, Field and Lysimeter Experiments**
by L. Weihermüller (2005), ca. 170 pages
ISBN: 3-89336-402-1

56. **Effect of internal leaf structures on gas exchange of leaves**
by R. Pieruschka (2005), 120 pages
ISBN: 3-89336-403-X

57. **Temporal and Spatial Patterns of Growth and Photosynthesis in Leaves of Dicotyledonous Plants Under Long-Term CO2- and O3-Exposure**
by M. M. Christ (2005), 125 pages
ISBN: 3-89336-406-4

58. **Öffentliche Kommunikation über Klimawandel und Sturmflutrisiken Bedeutungskonstruktion durch Experten, Journalisten und Bürger**
von H. P. Peters, H. Heinrichs (2005), 231 Seiten, CD
ISBN: 3-89336-415-3

59. **Umsatz verschiedener Ernterückstände in einem Bodensäulenversuchssystem – Einfluss auf die organische Bodensubstanz und den Transport zweier Xenobiotika**
von N. Drewes (2005), 221 Seiten
ISBN: 3-89336-417-X

60. **Evaluierung der CO2-Minderungsmaßnahmen im Gebäudebereich**
von M. Kleemann, P. Hansen (2005), 84 Seiten
ISBN: 3-89336-419-6

61. **TRACE. Tree Rings in Archaeology, Climatology and Ecology**
Volume 4: Proceedings of the Dendrosymposium 2005,
April 21st – 23rd 2005, Fribourg, Switzerland
edited by Ingo Heinrich, Holger Gärtner, Michel Monbaron, Gerhard Schleser
(2006), 313 pages
ISBN: 3-89336-425-0

62. **Diffuse Nitrateinträge in die Grund- und Oberflächengewässer von Rhein und Ems**
Ist-Zustands- und Maßnahmenanalysen
von R. Kunkel, F. Wendland (2006), 130 Seiten
ISBN: 3-89336-437-4

63. **Abhängigkeit des Wurzelwachstums vom Lichtregime des Sprosses und deren Modifikation durch Nährstoffe sowie im Gravitropismus**
von Kerstin A. Nagel (2006), 119 Seiten
ISBN: 3-89336-443-9

64. **Chancen und Risiken zukünftiger netzgebundener Versorgung**
Ein multi-kriterielles Verfahren zur Bewertung von Zukunftsszenarien
von C. R. Karger, W. Hennings, T. Jäger (2006), 296 Seiten
ISBN: 3-89336-445-5

65. **Die Phosphatbelastung großer Flusseinzugsgebiete aus diffusen und punktuellen Quellen**
von B. Tetzlaff (2006), 287 Seiten
ISBN: 3-89336-447-1

66. **Fate of veterinary pharmaceuticals in soil: An experimental and numerical study on the mobility, sorption and transformation of sulfadiazine**
by A. Wehrhan (2006), XXII, 134 pages
ISBN: 3-89336-448-X

67. **Biomacromolecules of Fossil Algae, Spores and Zooclasts from Selected Time Windows of Proterozoic to Mesozoic Age as Revealed by Pyrolysis-Gas Chromatography-Mass Spectrometry – A Biogeochemical Study**
by S. Dutta (2006), XVI, 139 pages
ISBN: 3-89336-455-2

Schriften des Forschungszentrums Jülich
Reihe Umwelt / Environment

68. **Bestimmung der Nicotinverteilung und anderer Stickstoffverbindungen in den Blattgeweben von *Nicotiana tabacum* unter verschiedenen Wachstumsbedingungen durch Einzelzellanalyse, Kapillarelektrophorese und der Massenspektrometrie**
von K. Wieland (2006), X, 189 Seiten
ISBN: 3-89336-458-7

69. **Systemic effects of mycorrhization on root and shoot physiology of *Lycopersicon esculentum***
by K. Klug (2006), IV, 105 Seiten
ISBN: 3-89336-463-3

70. **The impact of nutrient heterogeneity on maize plants**
by R. Rist (2006), XII, 74 Seiten
ISBN: 3-89336-464-1

71. **Optimization of Tracer Experiments to Characterize Transport Properties in Heterogeneous Aquifers Using Non-Invasive Measurement Techniques**
by K. Müller (2006), XVII, 103 Seiten
ISBN: 3-89336-465-X

72. **Measurement of Peroxy Radicals using Laser-Induced Fluorescence Technique**
by H. Fuchs (2006), VI, 140 Seiten
ISBN: 3-89336-467-6

Forschungszentrum Jülich
in der Helmholtz-Gemeinschaft

50 Jahre / Zukunft

Band/Volume 72
ISBN 3-89336-467-6

Umwelt
Environment